

UC Riverside

UC Riverside Electronic Theses and Dissertations

Title

Interpreting Intracellular Hydrogen Peroxide in Cancer Cells to Understand Cancer Susceptibility to Pharmacological Ascorbate Therapy

Permalink

<https://escholarship.org/uc/item/1f50b0bh>

Author

Erudaitius, Dieanira

Publication Date

2017

Peer reviewed|Thesis/dissertation

UNIVERSITY OF CALIFORNIA
RIVERSIDE

Interpreting Intracellular Hydrogen Peroxide in Cancer Cells to Understand Cancer
Susceptibility to Pharmacological Ascorbate Therapy

A Dissertation submitted in partial satisfaction
of the requirements for the degree of

Doctor of Philosophy

in

Bioengineering

by

Dieanira Tatyana Erudaitius

September 2017

Dissertation Committee:

Dr. Victor G. J. Rodgers, Chairperson

Dr. Devin K. Binder

Dr. Dimitrios Morikis

Dr. Kaustabh Ghosh

Copyright by
Dieanira Tatyana Erudaitius
2017

The Dissertation of Dieanira Tatyana Erudaitius is approved:

Committee Chairperson

University of California, Riverside

ACKNOWLEDGEMENTS

I, first and foremost, would like to express my sincerest gratitude to my advisor Dr. Victor G. J. Rodgers for providing me the opportunity to conduct research and accepting me as a graduate researcher in his laboratory. He has opened the door to numerous opportunities for me and without his acceptance and support I would not be the researcher I am today. In joining his lab, he allowed me the creative freedom to pursue my own research interest, which taught me to become an independent researcher and the opportunity to design my own project. I am immensely grateful for the amount of time he has invested in building my confidence and strengthening my skills as a researcher and presenter. His guidance has undoubtedly prepared me for success.

Secondly, I would like to thank Dr. Garry R. Buettner as one of the pioneers for bringing Vitamin C cancer research back to the clinical setting for patients with pancreatic cancer. His contributions as a collaborator were very insightful throughout my doctorate. I also had the opportunity to visit his lab where Dr. Claire M. Doskey and Mr. Brett Wagner took great care and time to share all of their expertise, laboratory protocols, and trained me in detail on various techniques. Their patience and kindness extended years to follow, and I am very thankful for all their help.

I would like to thank the rest of my dissertation committee: Dr. Devin K. Binder and Dr. Kaustabh Ghosh, for their insightful comments and encouragement, but also for the questions they posed which provided various perspectives to the problem. Further, I would

like to thank Dr. Devin K. Binder and Dr. Kaustabh Ghosh who both provided me access to their laboratories and research facilities without any hesitance. Special thanks to Mr. Mike Hsu, who devoted his time to train me on specific techniques.

My heartfelt appreciation goes to Dr. Dimitrios Morikis whose kind and genuine nature was more helpful than he knows. Dr. Morikis was always warm and welcoming and he also provided insightful knowledge extending the scientific realm which pertains to history, philosophy, mythology and poetry. I greatly enjoyed every encounter with Dr. Morikis, where each visit served as both inspirational and intellectually stimulating.

I wish to thank the undergraduate students who passionately devoted their time and effort in obtaining many of the results presented in this dissertation. Beginning with Andrew Huang, my first mentee, I am so grateful for the countless sleepless nights which he devoted to staying in lab until the work was completed. Andrew was always extremely determined and enthusiastic to solve problems we encountered. Next, Jacqueline Mantooth whom couldn't have arrived to our lab at any more of a perfect time. I am deeply thankful for Jacqueline's hard work, dedication, and intellect but am also privileged to have her now as a friend. Her loyalty, support and sincerity is not found often and I am grateful to have met such a precious person. I also wish to thank Jesse Soliman, for his quick devotion and attachment to the project. I greatly enjoyed his excitement to learn and entertaining personality, in addition to the personal support system he provided to get me through my final stretch. Each of you made my lab experience more enjoyable and successful. I am so

happy I got to mentor, teach and guide each of you in your own paths and goals while simultaneously learning from all you.

I would also like to acknowledge Ms. Hong Xu for her support in providing equipment and certain materials for our research. I also thank my fellow labmates and colleagues: Zied Gaieb, Nehemiah Zewde, Chris Hale, Troy Alva, Raymond Yeung, Jennifer Yang, Ryan Kozaka, Danielle Ornelas, Heran Bhakta, Alex Eastes, Rohith Mohan, Reed Harrison, Vipul Madahar, Shirin Mesbah Oskouei, Jill Clinton, Edward Cardenas, Daniel Nampe, Karen Lo and Soroush Ardekani for the stimulating discussions, work companions, and for all the fun we have had over the years. A special thanks to Andrea Cabrera for your friendship and support that has enabled me to overcome moments of hardship. I appreciate your kindness and openness, not only in your help with laboratory techniques, but also in our shared experiences.

Last but not least, I would like to thank my family and closest friends: my parents, Aramasys Erudaitius & Kathryn Willits Erudaitius, my sister, Anastassia Erudaitius, my brothers, Dimitry Erudaitius and Dylan O'Neal and my closest friends, Andrea Jimenez, Jessica Manning, Leann Fujinami & Jamie Knight for continuously supporting me throughout my entire career and life. I am extremely thankful to my parents who taught me to think objectively and self-reflect. These characteristics aided me in the drive to not become easily defeated and to surround myself by the most wonderful collection of people.

You have all helped me overcome life's struggles and are responsible in part for my success! Thank you.

The text of this dissertation, in part, is a reprint of the material as it appears in:

1. Erudaitius, D., Huang, A., Kazmi, S., Buettner, G.R. and Rodgers, V.G., 2017. Peroxiporin Expression Is an Important Factor for Cancer Cell Susceptibility to Therapeutic H₂O₂: Implications for Pharmacological Ascorbate Therapy. *PloS ONE*, 12(1), p.e0170442.

DEDICATION

I dedicate this dissertation to my parents:

Aramasys Erudaitius & Kathryn Willits Erudaitius,

whose continuous sacrifice, unconditional love, and support made it possible for me to
complete this work.

ABSTRACT OF THE DISSERTATION

Interpreting Intracellular Hydrogen Peroxide in Cancer Cells to Understand Cancer Susceptibility to Pharmacological Ascorbate Therapy

by

Dieanira Tatyana Erudaitius

Doctor of Philosophy, Graduate Program in Bioengineering
University of California, Riverside, September 2017
Dr. Victor G. J. Rodgers, Chairperson

The intravenous delivery of pharmacological ascorbate (P-AscH⁻) has recently been demonstrated to be a successful adjuvant in the treatment of some cancers. Administered as a series of infusions, P-AscH⁻ generates high fluxes of extracellular hydrogen peroxide (H₂O₂), which is toxic to certain cancer cells while not affecting normal. *In vitro* studies indicate that cancer cells have a wide range in susceptibility to P-AscH⁻ and subsequently to extracellular H₂O₂. The resulting intracellular H₂O₂ concentration is believed to accumulate differently in susceptible cancer cells as compared to non-susceptible cells. It is hypothesized that intracellular H₂O₂ concentration has a steady-state value that is significant for cell susceptibility and independent of cell type. Although this has been alluded to, this value has yet to be quantified. Further, the variations in cell parameters (i.e. membrane permeability via peroxiporins, catalase activity, etc.) for various cells are expected to be significant enough to alter intracellular H₂O₂ concentration, thereby impacting cell susceptibility. A steady-state model was developed which elucidates the

parameter contribution to intracellular H_2O_2 accumulation. The intracellular H_2O_2 concentrations during P-AscH⁻ therapy was quantified for pancreatic normal (H6c7; ascorbate non-responding), adenocarcinoma (MIA PaCa-2; ascorbate susceptible) and glioblastoma U-87 (non-responding), T98G (moderately susceptible) and LN-229 (highly susceptible) cell lines. Recognizing that MIA PaCa-2 has an enhanced expression of aquaporin-3 (AQP3) and the significance of AQP3 to plasma membrane permeability to H_2O_2 , silenced AQP3 was also investigated. Interestingly, an increase in surviving fraction was observed for the silenced cells in clonogenic studies using therapeutic H_2O_2 concentrations. These results imply that cell-susceptibility to ascorbate therapy is significantly coupled to the plasma membrane permeability to H_2O_2 , and in particular, elevated expressions of porins. Ultimately, this work provides insight to what targets are appropriate for improving P-AscH⁻ therapy. Further, our mathematical results contradict the hypothesis that a unique intracellular H_2O_2 was sufficient for a specific clonogenic response. This aligns with recent work revealing that the combination of redox-active labile iron and high intracellular H_2O_2 concentration is the necessary and sufficient condition for cellular ascorbate-susceptibility. Quantifying the relationship of this combination to the clonogenic response is the subject of future research.

Table of Contents

LIST OF FIGURES	xiv
LIST OF TABLES	xvi
CHAPTER 1. INTRODUCTION	1
1.1 Ascorbate as an adjuvant cancer	1
1.2 Ascorbate serves as a prodrug through selectively generating H ₂ O ₂	2
1.3 Transport variables influencing intracellular H ₂ O ₂ : peroxiporin expression	4
1.4 Intracellular H ₂ O ₂ : redox enzymes	5
1.5 Research Goal	8
1.6 Objective	11
CHAPTER 2. PRELIMINARY EVALUATION PERMEABILITY IS A CONTRIBUTING FACTOR TO ASCORBATE SUSCEPTIBILITY	12
2.1 Introduction to permeability variations via peroxiporin AQPs	12
2.2 Materials & Methods	13
2.2.1 Antibodies	13
2.2.2 Cells and Reagents	13
2.2.3 Immunocytochemistry Staining	14
2.2.4 Silencing AQP3 on MIA PaCa-2 Cells	15
2.2.5 Relative AQP3 Expression	16
2.2.6 Rate of H ₂ O ₂ Uptake per Cell	17
2.2.7 Clonogenic Assessment	18
2.3 Results: H ₂ O ₂ Uptake (siAQP3, inhibited catalase, pancreatic cells)	19
2.3.1 Immunocytochemistry Staining for Peroxiporins	19
2.3.2 Silencing Reduces AQP3 on the Plasma Membrane	22
2.3.3 Rate of Uptake of Extracellular H ₂ O ₂	25
2.3.4 Clonogenic Survival is Increased when AQP3 is Silenced	27
2.4 Conclusion: permeability is an additional factor to consider	31
2.5 Implications for Ascorbate Therapy	33
CHAPTER 3. DEVELOPMENT OF MATHEMATICAL MODEL FOR INTRACELLULAR H ₂ O ₂ QUANTIFICATION	34
3.1 Overview	34
3.2 Introduction	35

3.3 Mathematical Methods	41
3.3.1 Governing Equations	41
3.3.2 Steady-state Model for intracellular H ₂ O ₂ concentration (θ_{ss})	45
3.3.3 Sensitivity of Intracellular H ₂ O ₂ concentration to variations in cell properties.....	46
3.4 Validity of Lumped Parameter Model	47
3.4.1 Significance of spatial dependency in the cytosol region	47
3.4.2 Pseudo steady-state assumption	59
3.4.3 Estimation of average external H ₂ O ₂ for clonogenic assay.....	60
CHAPTER 4. EXPERIMENTAL APPROACH FOR DETERMINING INTRACELLULAR H ₂ O ₂ DURING THERAPY	61
4.1 Determining appropriate parameters to calculate θ_{ss}	61
4.2 Materials and Methods	62
4.2.1 Cells and Reagents	62
4.2.2 Clonogenic Assessment	63
4.2.3 Confocal Imaging: peroxisomes and cell nucleus	64
4.2.4 Determining catalase concentration	67
4.2.5 Peroxisome isolation	68
4.2.6 Determining peroxisome membrane permeability.....	70
4.2.7 H ₂ O ₂ uptake study (whole cell intact): to regress for <i>mplm</i>	72
CHAPTER 5. CELL-SPECIFIC PARAMETERS AND RESULTING INTRACELLUAR H ₂ O ₂	74
5.1 Parameters used for determining θ_{ss}	74
5.2 θ_{ss} and its validation of lumped parameter assumption	79
5.3 Extracellular concentration during dosing	82
5.4 Calculated θ_{ss} and C_{in}	84
5.5 Sensitivity of internal H ₂ O ₂ to each parameter	87
5.6 Clonogenic response vs. extracellular H ₂ O ₂ concentration	96
5.7 Clonogenic response vs. intracellular concentration	99
5.8 Clonogenic response vs. catalase concentration	101
5.9 Clonogenic response vs. plasma membrane permeability	104
5.10 Clonogenic response vs. peroxisome membrane permeability.....	107
5.12 Conclusion	110

CHAPTER 6. ON CATALASE LATENCY: A MATHEMATICAL INTERPRETATION.....	111
6.1 Introduction.....	111
6.2 Mathematical Methods	113
6.2.1 Latency in the peroxisome	113
6.2.2 Latency.....	130
6.3 Conclusion	135
CHAPTER 7. CONCLUSION AND IMPACT	136
APPENDIX I: EXAMPLE IMMUNOCYTOCHEMISTRY STAINING FOR AQP3...142	
APPENDIX II: CODE FOR REGRESSION OF PEROXISOME MEMBRANE PERMEABILITY m_p	143
Codes for regression for peroxisome membrane permeability	143
Results for pancreatic peroxisome membrane mass transfer coefficient (m_p)	146
Results for glioblastoma peroxisome membrane mass transfer coefficient (m_p)	146
APPENDIX III: CODE FOR REGRESSION OF PLASMA MEMBRANE PERMEABILITY m_{plm}	148
Codes for regression for plasma membrane permeability	148
Results for pancreatic plasma membrane mass transfer coefficient (m_{plm})	151
Results for glioblastoma plasma membrane mass transfer coefficient (m_{plm})	152
APPENDIX IV: EXAMPLE CALCULATION FOR \bar{c}_{ext}	153
Overview.....	153
Code for generating external H_2O_2 during clonogenic study	153
Example results.....	154
APPENDIX V: PEROXIPORIN EXPRESSION	157
REFERENCES	162

LIST OF FIGURES

Figure 1.1 Diagram of ascorbic acid and related species from the blood to the cell	9
Figure 2.1 Peroxiporin signal intensity per pancreatic cell line.....	21
Figure 2.2 Verification of siAQP3 using flow cytometry.....	23
Figure 2.3 Rate of H ₂ O ₂ uptake per cell	26
Figure 2.4 A & B Clonogenic response of normal pancreatic cells.....	28
Figure 2.5 C & D Clonogenic response of unmodified and siAQP3 cancer cells	29
Figure 3.1 Illustration of proposed dominant mechanisms for ascorbate-susceptibility ...	38
Figure 3.2 Illustration of proposed modeling approach.....	43
Figure 3.3 Illustration for model used to examine spatial dependency	49
Figure 4.1 Example confocal image for peroxisome counting	66
Figure 5.1 Spatial dependency plots per cell line	80
Figure 5.2 H ₂ O ₂ concentration per cell vs average external H ₂ O ₂ concentration.....	83
Figure 5.3 Sensitivity surface plots.....	89
Figure 5.4 Glioblastoma clonogenic response to therapeutic H ₂ O ₂ dosing	97
Figure 5.5 Surviving fraction vs. intracellular H ₂ O ₂ concentration per cell line	100
Figure 5.6 Surviving fraction vs. catalase concentration per cell line	102
Figure 5.7 Surviving fraction vs. plasma membrane permeability per cell line	105
Figure 5.8 Surviving fraction vs. peroxisome membrane permeability per cell line.....	108
Figure 6.1 Illustration of latency of catalase in the peroxisome	115
Figure 6.2 Overall calculated latency relating Bi_p and ϕ_p	133

Figure Appendix I Example immunocytochemistry staining for the presences of AQP3	142
Figure Appendix V.1 Peroxiporin AQP3 expression on glioblastoma cells	158
Figure Appendix V.2 Peroxiporin AQP8 expression on glioblastoma cells	160

LIST OF TABLES

Table 5.1 Summary of cellular parameters by cell type	77
Table 5.1 Continued.....	78
Table 5.2 P-value significance between cell type for reported m_{plm}	79
Table 5.3 Parameters used to verify spatial dependency of θ_{ss}	79
Table 5.4 Cell specific C_{ext} , \bar{C}_{ext} , θ_{ss} , C_{in} & clonogenic response	85
Table 5.5 Localized sensitivity values for each cell line	87
Table 6.1 Parameters used for calculating the cell Thiele modulus	129
Table 6.2 Calculated peroxisome effectiveness factor and latency	132
Table Appendix II Results for pancreatic peroxisome permeability	146
Table Appendix II Results for glioblastoma peroxisome permeability	147
Table Appendix III Results for pancreatic plasma permeability	151
Table Appendix III Results for glioblastoma plasma permeability	152
Table Appendix V Results from MATLAB for calculating \bar{C}_{ext}	154
Table Appendix V Calculating \bar{C}_{ext} from MATLAB results	156

CHAPTER 1. INTRODUCTION

1.1 Ascorbate as an adjuvant cancer

Pharmacological ascorbate (P-AscH⁻), administered as a series of bolus injections, is currently in progress of investigation to serve as an adjuvant in the treatment of various cancers during clinical trials conducted by the School of Medicine at the University of Iowa [1-8]. Acknowledging the long-held controversy to the benefits of ascorbate and its use in cancer treatment [9-11], recent breakthroughs have led to the heightened belief that intravenously delivered P-AscH⁻ can serve as an advancing therapy adjuvant to reduce certain tumors. Most of the controversy revolves around the focus of Mayo Clinic exploring high concentrations of oral delivery of vitamin C (ascorbate) but not the intravenous delivery; this greatly hindered the progression of research in this field [10, 11]. It is now accepted that intravenous injection of P-AscH⁻ allows for high plasma concentrations which are not achievable through oral ingestion; due to regulation of the digestive system [9]. Further, this treatment has been determined to be safe and patients were observed to have increased lifespans [1-3].

While P-AscH⁻ has promise for improving outcomes for certain cancer patients, such as pancreatic cancer, its broad application for other types of cancer has yet to be realized. The hesitancy in advancing forward with P-AscH⁻ therapy for patients with other types of cancer is due, in part, to observations in a recent *in vitro* study by Chen *et al.* (2008) [12]. There, they reported that while normal cells remain virtually unaffected to P-AscH⁻, cancer

cell lines exhibit a variety of susceptibilities as seen by rates of clonogenic survival. Therefore, it is of great interest to understand why certain cancer cells are more responsive to P-AscH⁻ and thereby guide the use of P-AscH⁻ as an adjuvant to cancer therapy.

1.2 Ascorbate serves as a prodrug through selectively generating hydrogen peroxide (H₂O₂)

In order to isolate the species of interest, a short discussion is required on the chemistry behind ascorbate once it is introduced into the body, Fig 1.1. The mechanism behind ascorbate-mediated cell death is being extensively studied [1-16]. This work developed from understanding the unique nature of ascorbate and its ability to serve as an anti-oxidant (at low physiological concentrations) compared to its pro-oxidant behavior (at pharmacological concentrations) [12, 17]. At physiological pH, vitamin C converts to ascorbate (AscH⁻) which can then transport across the blood vessel through sodium dependent channels, resulting in a cascade of reactions, Fig 1.1. Once AscH⁻ has transported across the blood vessel, it undergoes oxidation resulting in dehydroascorbic acid (DHA) [17], Fig 1.1 displayed in green. In addition, ascorbate readily forms free radicals within the body, which are capable of reducing to hydrogen peroxide (H₂O₂), Fig 1.1; which is toxic to cells if not properly removed. DHA can permeate the cell via GLUT receptors and continue to react to form intracellular H₂O₂; whereas, extracellular H₂O₂ permeates the cell via specific AQPs. Irrespective of the mechanism, a critical factor in determining the redox environment of a cell is H₂O₂ which must be regulated by enzymes (purple), Fig 1.1, to maintain a suitable concentration, extracellularly and intracellularly.

The mechanism behind ascorbate mediated cell death has been extensively studied and shows that the cytotoxicity is due to extracellular and not intracellular ascorbate [23]. Furthermore, the extracellular ascorbate exhibited similar cytotoxicity as cells exposed to extracellular H_2O_2 [23]. Lastly, tumor reduction in mice models did not occur when exposed to DHA [18]; thus, eliminating the need to investigate further the mechanism of DHA permeating the cell through GLUT receptors. Extracellular H_2O_2 produced by pharmacological ascorbate results in cytotoxicity whereas neither extracellular DHA [18] nor intracellular ascorbate achieve the same result. Therefore, extracellular H_2O_2 is the main interest as its production directly affects the reproducibility of cells and explains the reduction seen by tumor cells. The series of possible intracellular reactions resulting from H_2O_2 and DHA permeation is displayed; however, we know toxicity via P-AscH⁻ is directly related to the flux of H_2O_2 where as DHA permeation is irrelevant. H_2O_2 , shown in green, is toxic to cells if not properly removed by consumption enzymes (shown in purple). At high H_2O_2 concentrations resulting from P-AscH⁻, catalase (purple) is the only enzyme proficient in consuming H_2O_2 . The GPx/GSH recycling system becomes shunted [38], where similarly other H_2O_2 removal enzymes are not efficient in consuming the high concentrations of H_2O_2 .

It is now clear that at higher concentrations, ascorbate undergoes autoxidation and readily forms H_2O_2 . This extracellular H_2O_2 is unable to maintain a sustainable concentration within the plasma [19] and instead is selectively generated in the extracellular space. The

former is ideal as high levels of H_2O_2 in the blood stream can lead to complications in sufficient blood flow delivered to organs and consequently patient survival.

Furthermore, the presence of catalytic metals (i.e. iron) serves to accelerate this process [20]. In addition to the biochemical nature of ascorbate, a tremendous amount of work has been directed into discovering the variation in enzymatic activity of ascorbate-susceptible cells [17, 21]. In order to unveil the mechanism of ascorbate-mediated cell death, a significant amount of research has worked on understanding the type of cell death induced (apoptosis, autophagy, etc.) [17, 22] and the intracellular damage (metabolic, nuclear, etc.) [21] occurring. It was further confirmed that cytotoxicity was a result of extracellular and not intracellular ascorbate [19, 23]. Furthermore, numerous *in vivo* and *in vitro* studies have displayed a range of susceptibility to P-AscH⁻ across different types of cancer [1, 12, 22-32], and intracellular H_2O_2 , being the byproduct of P-AscH⁻ oxidation, has been identified as the primary factor for cellular cytotoxicity. Thus, ascorbate is categorized as a pro-drug due to its ability to generate high concentrations of extracellular hydrogen peroxide (H_2O_2) that permeates into the intracellular space [4, 17, 19, 23].

1.3 Transport variables influencing intracellular H_2O_2 : peroxiporin expression

The variability in the plasma membrane permeability to H_2O_2 may be another factor that contributes to the fate of cells upon exposure to P-AscH⁻. Interestingly, plasma membrane permeability to H_2O_2 also exhibits significant variability across cell lines *via* the wide range of expression levels of peroxiporins. Peroxiporins are aquaporins (AQPs) that facilitate the flux of H_2O_2 across the plasma membrane [33, 34]. The AQP isoforms currently identified

that allow passive diffusion of H_2O_2 are AQP1, AQP3, and AQP8 [33, 35]. AQPs are heavily expressed in many types of tumors [36], especially those considered aggressive [37]. Thus, it is hypothesized that increased plasma membrane permeability to extracellular H_2O_2 (*i.e.*, *via* enhanced expression of peroxiporins) can further increase the efficacy of P-AscH⁻ therapy.

We believe this elevated AQP expression, specifically of peroxiporins, to be the principal pathway for the entry of H_2O_2 into tumor cells. Thus, cells susceptible to ascorbate therapy, *i.e.* pancreatic adenocarcinoma cells, are suspected to exhibit elevated peroxiporin expression; therefore, contributing to cell death due to an increased intracellular accumulation of H_2O_2 produced by pharmacological ascorbate.

1.4 Intracellular H_2O_2 : redox enzymes

In addition to transport issues, there exist differences in concentrations of intracellular enzymes that aid in the removal of H_2O_2 . At the cellular level, a family of intracellular enzymes exist to finely control the intracellular levels of H_2O_2 , which normally exists around the 10 nM range [9]. Among them are the six peroxiredoxin enzymes, the glutathione peroxidase (GPx)/glutathione (GSH) system and catalase [38]. Catalase, in contrast to the other removal enzymes, is responsible for irreversibly consuming intracellular H_2O_2 when in the presence of high concentrations [21, 25].

Among the various scavenging enzymes that control the intracellular H_2O_2 concentration at physiological conditions [17], catalase appears to be the primary enzyme contributing to the removal of the H_2O_2 generated by P-AscH⁻ [17, 21, 38-40]. Interestingly, catalase exhibits higher activity in normal cells where its expression can range on the order of 10- to 100-fold greater than in some tumor cells [41]. This difference in catalase activity amongst cells can greatly affect the rate of intracellular removal of H_2O_2 generated by P-AscH⁻. It is believed that the high catalase activity of normal cells reduces the intracellular H_2O_2 concentrations to levels that are non-toxic. Conversely, tumor cells with relatively low catalase activity are expected to be more susceptible to ascorbate-mediated cell-death.

It has been demonstrated that the effects of P-AscH⁻ are reversible with the introduction of specific H_2O_2 scavenging enzymes [42], further supporting the argument that extracellular H_2O_2 is the primary factor in cytotoxicity via P-AscH⁻. More specifically, the effect of P-AscH⁻ on pancreatic cancer cells was found to be mitigated when co-cultured with catalase (the primary scavenging enzyme in the presence of high H_2O_2 concentrations) [12, 21]. Doskey et al. (2016) [21] demonstrate that H_2O_2 is involved in the mechanism of P-AscH⁻ toxicity to cancer cells and that the removal of H_2O_2 via catalase is an important factor. It has further been suggested that catalase may serve as a potential predictor in the ascorbate-susceptibility [43].

The extracellular H_2O_2 generated by ascorbate ultimately permeates across the plasma membrane. This, in turn, is expected to increase the intracellular H_2O_2 [42] to substantially higher levels than physiological concentrations. Extracellular P-AscH⁻ has also been shown to induce DNA damage (mitochondrial and nuclear) in addition to ATP depletion via H_2O_2 [1, 2, 22, 23, 30-32, 44, 45]. Again, introducing extracellular catalase to the P-AscH⁻ culture prevented ATP depletion which supports the hypothesis that ascorbate-mediated ATP depletion is via the extracellular H_2O_2 produced that permeates the cell. At these elevated concentrations, in addition to the DNA damage and ATP level effects that occur, it has also been suggested that intracellular H_2O_2 is activated in the presence of catalytic transition metals generating significant hydroxyl radical (HO[•]) [46]. Ultimately, this high flux of HO[•] substantially increases DNA damage, which is believed to be the primary factor in inhibiting cellular reproduction. Doskey et al. (2016) [21] show that the ED₅₀ results for clonogenic exposure to P-AscH⁻ is directly coupled to the rate of H_2O_2 uptake per cell. This finding confirms that H_2O_2 is a primary factor in DNA damage as well as in compromising ATP levels during P-AscH⁻.

1.5 Research Goal

Recognizing the complexity of the factors that can contribute to selective cell susceptibility, a quantitative systems understanding of the variations in the reaction and transport rates for H_2O_2 is necessary to elucidate the mechanism for a successful pharmacological ascorbate therapy. It is hypothesized that internal H_2O_2 concentration has a steady-state value that is significant for cell susceptibility and is independent of cell type. Although this has been alluded to, this value has yet to be quantified. Further, the variations in peroxiporins and catalase rates for various cells types are significant enough to alter the internal H_2O_2 concentration during ascorbate therapy, thereby impacting the cell susceptibility. We use a systematic approach to ultimately determine the intracellular H_2O_2 concentration of specific cell lines to explain whether there exists a critical threshold needed to be reached for cell susceptibility.

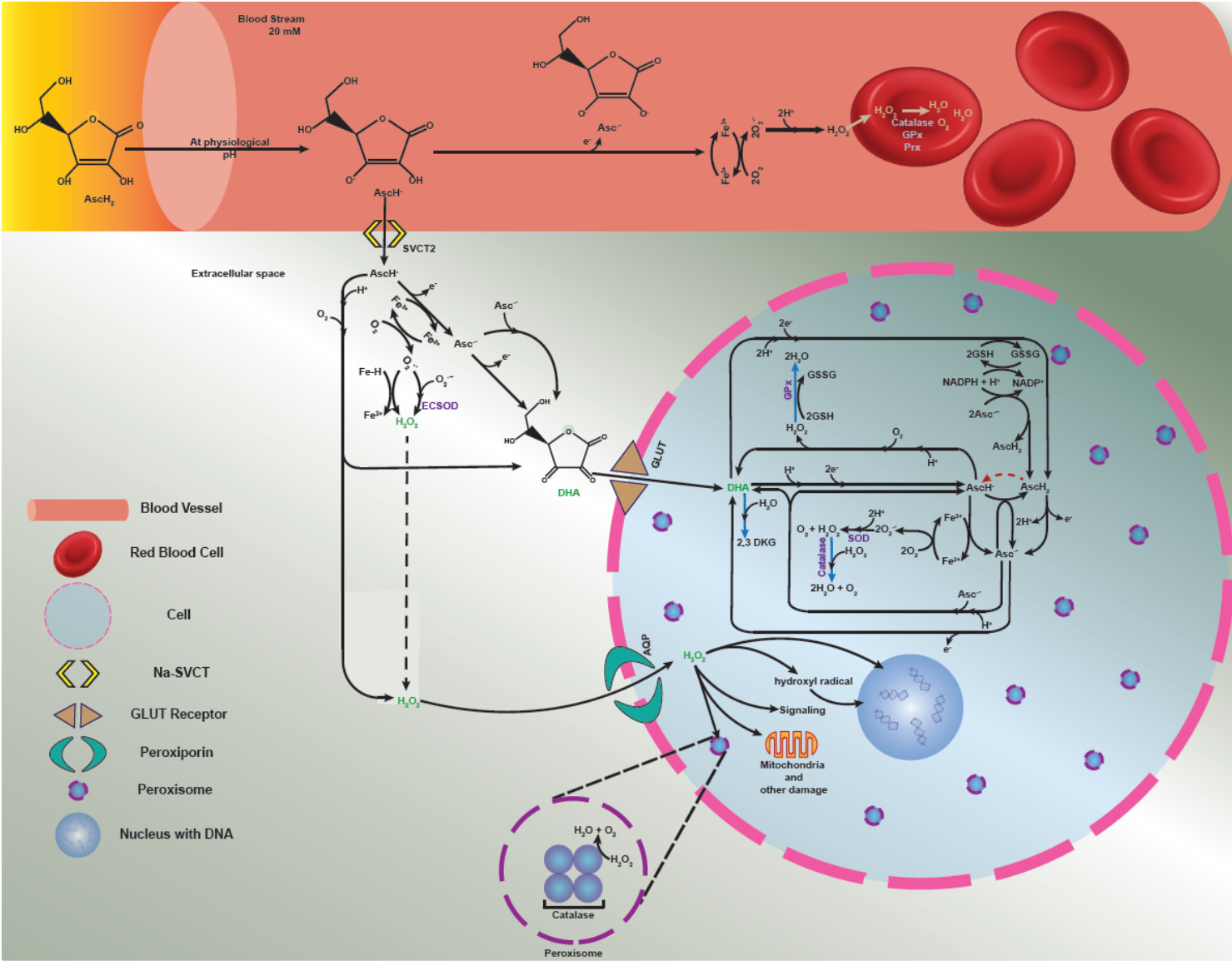


Fig 1.1 Diagram of ascorbic acid and related species from the blood to the cell

Pharmacological concentrations (~20 mM) of ascorbic acid (AscH_2 , vitamin C) are intravenously introduced, top left. Once inside the blood stream, AscH_2 converts to ascorbate (AscH^-) as this is the dominant form at physiological pH. AscH^- can either further reduce resulting in the ascorbate radical ($\text{Asc}^{\bullet-}$) and H_2O_2 , or can transverse the epithelial layer via sodium dependent ascorbate transporters (Na-SVCT). Fortunately, H_2O_2 is unable to maintain a sustainable concentration within the plasma [47] and thus AscH^- transport through SVCT is favored. Once AscH^- enters the extracellular space, it further reduces into two permeable species (green), dehydroascorbic acid (DHA) and H_2O_2 . DHA is permeable through active GLUT transporters where H_2O_2 passively diffuses through peroxiporins. The mechanism behind ascorbate mediated cell death has been extensively studied and shows that the cytotoxicity is due to extracellular and not intracellular ascorbate [23]. Furthermore, extracellular H_2O_2 produced by P- AscH^- results in cytotoxicity whereas neither extracellular DHA [18] nor intracellular ascorbate achieve the same result. The series of possible intracellular reactions resulting from H_2O_2 and DHA permeation is displayed; however, toxicity via P- AscH^- is directly related to the flux of H_2O_2 where as DHA permeation is irrelevant. H_2O_2 (green) is toxic to cells if not properly removed by consumption enzymes (purple), again catalase is the primary removal enzyme. Intracellular H_2O_2 has a variety of pathways and targets; while it is commonly known to serve as a signaling molecule [34, 61] it can also induce DNA damage (mitochondrial and nuclear)/deplete ATP [1, 2, 22, 23, 30-32, 48, 49], and/or produce the hydroxyl radical in the presence of iron [56] which is known to result in detrimental cellular damage. This schematic provides a holistic view of the reactions and transport associated with ascorbate which allows us to narrow the focus to extracellular H_2O_2 permeation via peroxiporins and the desire to quantify resulting intracellular H_2O_2 during therapy.

1.6 Objective

The objective of this work develops a quantitative systems understanding to the variations in the reaction and transport rates for H_2O_2 to: 1) elucidate the mechanism of successful pharmacological ascorbate therapy, *in vitro*, and 2) quantify the critical intracellular H_2O_2 concentration for successful P-AscH⁻ therapy. Within the framework of this study, the following cell lines were addressed based on their degree of susceptibility: normal pancreatic cells (non-responding, H6c7), pancreatic adenocarcinoma cells (susceptible, MIA PaCa-2), glioblastoma (non-responding, U-87 MG), glioblastoma (moderately susceptible, T98G), and glioblastoma (susceptible, LN-229).

Our goal is to compare a variety of tumor and normal cells by specifically addressing the transport and reaction variations to ultimately unveil the critical intracellular H_2O_2 concentration which prevents cells from remaining viable. This research is significant because it reveals the characteristics that need to be exhibited by various cells types for P-AscH⁻ therapy to be used successfully as well as allowing for the possibility of this therapy to be adjusted to cellular targets expressed by the specific cells.

CHAPTER 2. PRELIMINARY EVALUATION

PERMEABILITY IS A CONTRIBUTING FACTOR TO ASCORBATE SUSCEPTIBILITY

2.1 Introduction to permeability variations via porixporin AQPs

In this work, we investigate the significance of plasma membrane H₂O₂ permeability to *in vitro* cell susceptibility to therapeutic extracellular H₂O₂ concentrations. In particular, the clonogenic surviving fraction response for the pancreatic cancer cell line MIA PaCa-2 with modified porixporin expression is evaluated. Initially the expression of AQP1, AQP3, and AQP8 of MIA PaCa-2 are qualitatively screened against the normal pancreatic tissue cell line H6c7 using an immunocytochemistry assay. Recognizing that AQP3 is substantially overexpressed in MIA PaCa-2, the study focuses on silencing AQP3 (siAQP3 MIA PaCa-2). Next the relative expression levels of AQP3 for both siAQP3 MIA PaCa-2 and unmodified MIA PaCa-2 using flow cytometry is verified. In addition, the rate of H₂O₂ uptake and cell susceptibility between the two cell lines are compared. Finally, the clonogenic surviving fraction for exposure to therapeutic H₂O₂ concentrations is evaluated for siAQP3 MIA PaCa-2 and unmodified MIA PaCa-2. The results of this study show that AQP3 expression is significant in the clonogenic surviving fraction response for MIA PaCa-2 for *in vitro* therapeutic exposure to H₂O₂. These results emphasize the importance of considering plasma membrane permeability to H₂O₂ when elucidating cellular properties that can impact the response of cells to exposure to extracellular H₂O₂ and the success of P-AscH⁻ as an adjuvant to cancer therapies.

2.2 Materials & Methods

2.2.1 Antibodies

The following antibodies were used in this study for immunocytochemistry and flow cytometry: rabbit anti-AQP1 antibody (SAB5200109; Sigma Aldrich, St. Louis, MO, USA), rabbit anti-AQP3 antibody (SAB5200111; Sigma Aldrich, St. Louis, MO, USA), mouse anti-AQP8 antibody (SAB1403559; Sigma Aldrich, St. Louis, MO), goat anti-rabbit IgG (A11008; Life Technologies, Carlsbad, CA, USA), goat anti-mouse IgG (A11005; Life Technologies, Carlsbad, CA, USA).

2.2.2 Cells and Reagents

Pancreatic H6c7 cells (HPV16-E6E7) [50] were established by transduction of HPV16-E6E7 genes into a primary culture of normal pancreatic duct epithelial cells and cultured in keratinocyte SFM (KSFM, Invitrogen, Carlsbad, CA) with supplements: human recombinant epidermal growth factor and bovine pituitary extract (Life Technologies, Carlsbad, CA, USA), in addition to 1% antibiotics. Pancreatic adenocarcinoma MIA PaCa-2 cells (American Type Culture Collection Manassas, VA) were cultured in Dulbecco's Modified Eagle's Medium (DMEM, Life Technologies, Carlsbad, CA, USA) with 10% fetal bovine serum (FBS, Life Technologies, Carlsbad, CA, USA) and 1% antibiotic. All cells were maintained at incubation of 37°C and supplied with 5% CO₂ and 1% penicillin streptomycin (Life Technologies, Carlsbad, CA, USA).

2.2.3 Immunocytochemistry Staining

Cells were seeded on glass cover slips (ThermoFisher Scientific, Lafayette, CO, USA) 48 h before fixing with paraformaldehyde (4% PFA) for 15 min. PFA was removed by three 5-min 1x PBS washes. Normal goat serum (5% NGS) diluted in 1x PBS was added to cells for 1 h at room temperature (RT) on a shaker to block non-specific binding. Primary antibodies diluted 1:200 in 0.3% Triton X 100 (in PBS) were added to cells and left to gently shake for 12 h in 4°C. Primary antibodies were removed *via* three 5-min 1x PBS washes. Secondary antibodies diluted 1:100 in NGS were added to cells and placed on shaker for 2 h RT. Secondary antibodies were removed by three 5-min 1x PBS washes and glass coverslips containing stained cells were mounted on microscope slides (ThermoFisher Scientific, Lafayette, CO, USA). NucBlue Live Cell Stain ReadyProbes reagent (R37605; Life Technologies, Carlsbad, CA, USA) was added to stain the nucleus of cells. Images were taken with the Lecia SP5 confocal microscope (Lecia, Solms, Germany) and analyzed using ImageJ (NIH). AQP 1, 3 or 8 was determined by measuring target fluorescence intensity (from 10 images) per cell area for H6c7 and MIA PaCa-2 cells. Statistical significance between protein expression (AQP 1, 3 or 8) and each cell type was determined through ANOVA (Single Factor). P-values less than 0.05 were accepted as indicating a statistical significant difference. Error bars represent standard error (SE). Data were analyzed and plotted using Excel-2007 (Microsoft; Redmond, WA), and SigmaPlot (Systat Software Inc; San Jose, CA, USA) software.

2.2.4 Silencing AQP3 on MIA PaCa-2 Cells

Silencing was accomplished through reverse transfection using double stranded siRNA, siRNA AQP3 (s1523; Invitrogen, Carlsbad, CA). The protocol provided by Invitrogen was adjusted appropriately. A total of 6 pmol siRNA AQP3 (20 μ L or 500 μ L) were diluted in Opti-MEM I Reduced Serum Medium (31985-062; Life Technologies, Carlsbad, CA, USA) then added and evenly spread in wells. Following with the addition of Lipofectamine RNAiMAX (133778-150; Life Technologies, Carlsbad, CA, USA) (0.3 μ L or 5 μ L) and thoroughly mixed to each, 96- or 6-well plates, containing the diluted siRNA molecules. The siRNA and Lipofectamine were allowed to interact 10-20 min at RT to allow siRNA-lipid complex formation. Cells were diluted in appropriate complete growth medium and cell density reached 30-50% confluency 24 h after plating. Plates were gently mixed. Plates were incubated for 48 h at 37 °C with 5% CO₂ supplied. The transfection efficiency was obtained for MIA PaCa-2 using siRNA Cy-3 GAPDH (Life Technologies, Carlsbad, CA, USA) in place of siAQP3 strands and serves as a positive control for the method of silencing. Successfully transfected cells were visualized using ArcturusXT LCM System (ThermoFisher Scientific, Lafayette, CO, USA) and counted using disposable hemocytometers (INCYTO, Covington, GA, USA). Scrambled siRNA AQP3 (4390843; Life Technologies, Carlsbad, CA, USA) sequences were used for the negative control of each experimental set up to ensure that the silencing procedure was not affecting results. The scrambled siRNA sequences were delivered to the cells in an identical manner as the siRNA AQP3 with the same concentrations of each component and identical cell plating number.

2.2.5 Relative AQP3 Expression

Flow cytometric analysis was performed to obtain quantification in fluorescent signal reduction for AQP3 between MIA PaCa-2 unmodified and siAQP3 MIA PaCa-2 cells. Cells were harvested using accutase (A6964; Sigma Aldrich, St. Louis, MO, USA) and quenched using cell culture medium consisting of DMEM (Life Technologies, Carlsbad, CA, USA) with 10% FBS (Life Technologies, Carlsbad, CA, USA) and 1% antibiotic. Cells were centrifuged (1000 rpm) (Marathon 8K centrifuge; Beckman Coulter, Indianapolis, IN, USA) for 5 min at RT. Following centrifugation, cells were re-suspended in ice-cold FACS Buffer (5 mL) containing D-PBS (14190250; ThermoFisher Scientific, Lafayette, CO, USA), BSA (0.5% w/v final) (A7906; Sigma Aldrich, St. Louis, MO, USA), and 2 mM EDTA (15575020; ThermoFisher Scientific, Lafayette, CO, USA) and centrifuged (1000 rpm) (Eppendorf centrifuge 5415R, Hauppauge, NY, USA) for 5 min at RT. Subsequently, cells were re-suspended in ice-cold FACS Buffer (100 μ L) and further labelled with rabbit anti-AQP3 antibody (1:25 dilution), gently mixed, and incubated for 20 min at 4 °C . Cells were then centrifuged (1000 rpm) (Eppendorf centrifuge 5415R, Hauppauge, NY, USA) twice for 4 min at RT with a 1 mL ice-cold FACS buffer wash in between. A fluorescence labeled anti-rabbit IgG (DI-1488; Vector Laboratories) was added (1:100 dilution), mixed gently, and incubated for 15 min at 4 °C. Cells were then centrifuged (1000 rpm) (Eppendorf centrifuge 5415R, Hauppauge, NY, USA) twice for 4 min at RT with a wash using FACS buffer in between the spins. Subsequently, cells were fixed with 1% PFA and detected by a Cell Lab Quanta SC flow cytometer (Beckman

Coulter, Brea, CA, USA). Data was analyzed and plotted with FlowJo (Treestar, Inc., Ashland, OR, USA).

2.2.6 Rate of H₂O₂ Uptake per Cell

The rate of H₂O₂ uptake for unmodified MIA PaCa-2 and siAQP3 MIA PaCa-2 cell lines were measured, in the same manner as described previously by Wagner *et al.* [51]. This assay provides an exogenous H₂O₂ removal rate, on a per cell basis. The assay measures the change in extracellular H₂O₂ over time, which decays exponentially representing a pseudo-first order behavior of the intracellular catalase reaction. The technique is a highly sensitive fluorescent method capable of detecting low concentrations of H₂O₂, below 0.5 μM. Briefly, cells were seeded in 96-well culture (Corning, Union City, CA, USA) treated dishes and incubated 48 h prior to the assay at 37 °C, 5 % CO₂; 90% confluency was reached. An extracellular bolus of 20 μM H₂O₂ (Sigma, St. Louis, MO, USA) was introduced in 5 min intervals to defined wells containing cells. A quenching solution comprised of 20 mL 1x HBSS (ThermoFisher Scientific, Lafayette, CO, USA), 20 μL 1M 4(-2-hydroxyethyl)-1-piperazineethansulfonic acid (HEPES) (pH 7.2 – 7.5) (ThermoFisher Scientific, Lafayette, CO, USA), 10 mg NaHCO₃ (3mM) (ThermoFisher Scientific, Lafayette, CO, USA), 5 mg 4-hydroxyphenylacetic acid (*p*HPA) (Sigma, St. Louis, MO, USA), and 2 mg HRP (horse radish peroxidase Type 1) (Sigma, St. Louis, MO, USA) was used to terminate the assay. The quenching solution prevents any remaining H₂O₂ from entering the cell as H₂O₂ instead activates HRP which in turn oxidizes *p*HPA resulting in the fluorescent *p*HPA dimer. The fluorescent signal is representative of the H₂O₂

concentration in each well and is further detected via the Tecan F200 (Tecan US, Morrisville, NC) plate reader with an excitation at 340 nm (bandwidth 20 nm) and monitoring an emission at 430 nm (bandwidth 20 nm) from above the wells. Wells containing cells were trypsinized and the number of cells were determined using a Moxi Z Mini Automated Cell Counter (ORFLO Technologies, Ketchum, ID, USA). The capacity of the cells to remove extracellular H₂O₂ (k_{cell}) is calculated from the number of cells, concentration of H₂O₂ remaining, total volume of media, and the observed rate of extracellular H₂O₂ removal (k_{obs}). Statistical significance between k_{cell} was determined through ANOVA (Single Factor) and the presented errors were propagated. Since k_{cell} has two associated errors, k_{obs} (obtained through linear regression) and the number of cells, the errors in k_{cell} were propagated. Cells were counted at the end of the experiment. P-values less than 0.05 were accepted as indicating a statistical significant difference. Data were analyzed and plotted using Excel-2007 (Microsoft; Redmond, WA), and SigmaPlot (Systat Software Inc; San Jose, CA, USA) software.

2.2.7 Clonogenic Assessment

Cells (2×10^5) were seeded in 6-well culture (Corning, Union City, CA, USA) treated dishes and exposed to appropriate H₂O₂ doses 48 h later. H₂O₂ exposures of (0 nmol cell⁻¹ - 0.30 nmol cell⁻¹; representative of 0, 50, 60, 70, 80 and 90 μ M) [52] were diluted in the appropriate culture media and cells were exposed for 1 h at 37 °C. After exposure, the diluted media was removed, cells were trypsinized and counted with a Moxi Z Mini Automated Cell Counter (ORFLO Technologies, Ketchum, ID, USA) and re-plated at 300

cells mL⁻¹ in triplicates with appropriate media in 6-well culture (Corning, Union City, CA, USA) treated dishes. Plates were incubated for two weeks at 37 °C, 5% CO₂ and colonies formed between 10 to 14 d at 37 °C. Following a two-week incubation period, the colonies were fixed with 70% ethanol and stained with Coomassie Brilliant Blue R-250 (1610436; BioRad, Hercules, CA). Colonies with more than 50 cells were counted using a Counter-Pen (3133; Traceable Products, Webster, TX). The plating efficiency (PE) and surviving fraction (SF) were determined; PE = (colonies counted/cells plated) x 100 and SF = (PE of treated sample/PE of control) x 100 [53, 54]. Statistical significance between each H₂O₂ exposure dose and cell types or cell modification was determined through ANOVA (Single Factor). P-values less than 0.05 were accepted as indicating a statistical significant difference. Error bars displayed represent the standard error (SE). Data were analyzed and plotted using Excel-2007 (Microsoft; Redmond, WA), and SigmaPlot (Systat Software Inc; San Jose, CA, USA) software. Plots of H₂O₂ exposure doses are represented in the nmol cell⁻¹ instead of concentrations because it serves as a more informative dosing metric for cell culture, as often times variations seen in experimental results arise as these systems are cell density dependent [52].

2.3 Results: H₂O₂ Uptake (siAQP3, inhibited catalase, pancreatic cells)

2.3.1 Immunocytochemistry Staining for Peroxiporins

We conducted immunocytochemistry (ICC) staining to verify the presence of peroxiporins AQP1, AQP3, and AQP8 for MIA PaCa-2 and H6c7 cells (example ICC in Appendix I). In addition to verifying the presence of these peroxiporins, the signal intensities evaluated

from immunocytochemistry also allowed for a qualitative measurement for the relative expression levels for each aquaporin on both cell types. Elevated signal intensities indicate greater presence of these proteins and therefore elevated expression. Images of the immunocytochemistry staining for AQP1, AQP3, and AQP8 in H6c7 and MIA PaCa-2 cell, allow qualitative assessment for AQP expression of each cell type. Quantification shows the variation in expression of each of the AQPs between the two cell-types providing insight as to which aquaporin is more highly expressed by MIA PaCa-2 cancer cells, Fig 2.1. Differences in expression of aquaporin AQP1, is not apparent between H6c7 and MIA cells. Although AQP8 has a higher expression in MIA PaCa-2 compared to H6c7 cells, it is clear that AQP3 is significantly more elevated in MIA PaCa-2 cells compared to H6c7 cells. This study therefore focuses on the significance of AQP3.

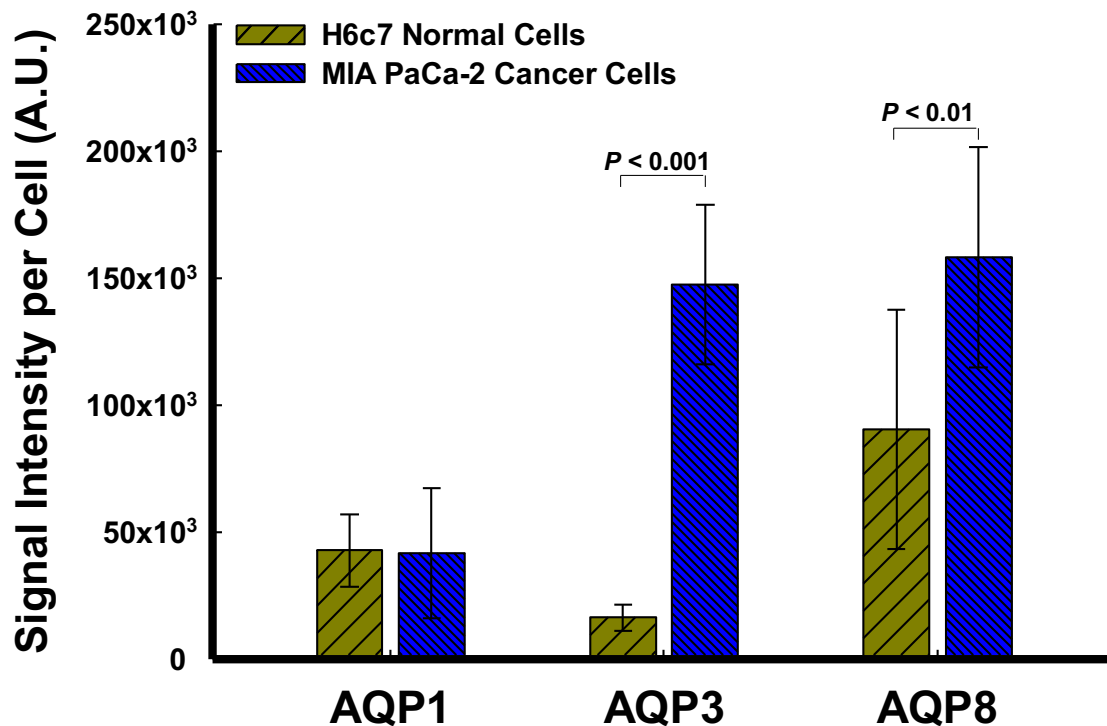


Fig 2.1. Pancreatic cancer cells exhibit elevated peroxiporin (AQP3 and AQP8) expression compared to normal cells. The green fluorescence signal intensity from immunocytochemistry staining for the presence of peroxiporins images were analyzed per cell using ImageJ (NIH). Elevated signal intensities indicate a greater presence of a protein and therefore elevated expression. Elevated expression of peroxiporin AQP1 is not apparent between H6c7 and MIA PaCa-2 cells. However, both peroxiporin AQP3 and AQP8 show a significant difference between MIA PaCa-2 and H6c7 cells ($P < 0.001$ and $P < 0.01$, respectively, $n = 3$ in both cases). P-values are obtained through ANOVA. Error bars represent standard error (SE). A.U. = arbitrary units.

2.3.2 Silencing Reduces AQP3 on the Plasma Membrane

To examine the role of AQP3 in modulating the rate of uptake of extracellular H₂O₂ by MIA PaCa-2 cells we used siAQP3 as a tool to modulate AQP3 expression. Flow cytometric analysis was used to verify the silencing of aquaporin AQP3 on the plasma membrane. We were able to confirm a factor of 10 relative decrease in aquaporin AQP3 expression for the silenced cells by obtaining AQP3 specific signals for wild-type unmodified MIA PaCa-2 vs. silenced AQP3. Fig 2.2 shows a positive AQP3 signal frequency of 91.7 (orange curve) for the unmodified MIA PaCa-2 cancer cells sampled (8,036 cells). After silencing AQP3 for MIA PaCa-2, the signal shifts to display a positive signal frequency of 59.8 (red curve) for the silenced MIA PaCa-2 sampled cells (siAQP3 MIA PaCa-2, 8,067 cells). The shift in fluorescence between MIA PaCa-2 (orange) and siAQP3 MIA PaCa-2 cells (red) demonstrates a decrease in AQP3 expression for siAQP3 MIA PaCa-2 cells by a factor of 10, when comparing the average displayed by the peaks of each curve.

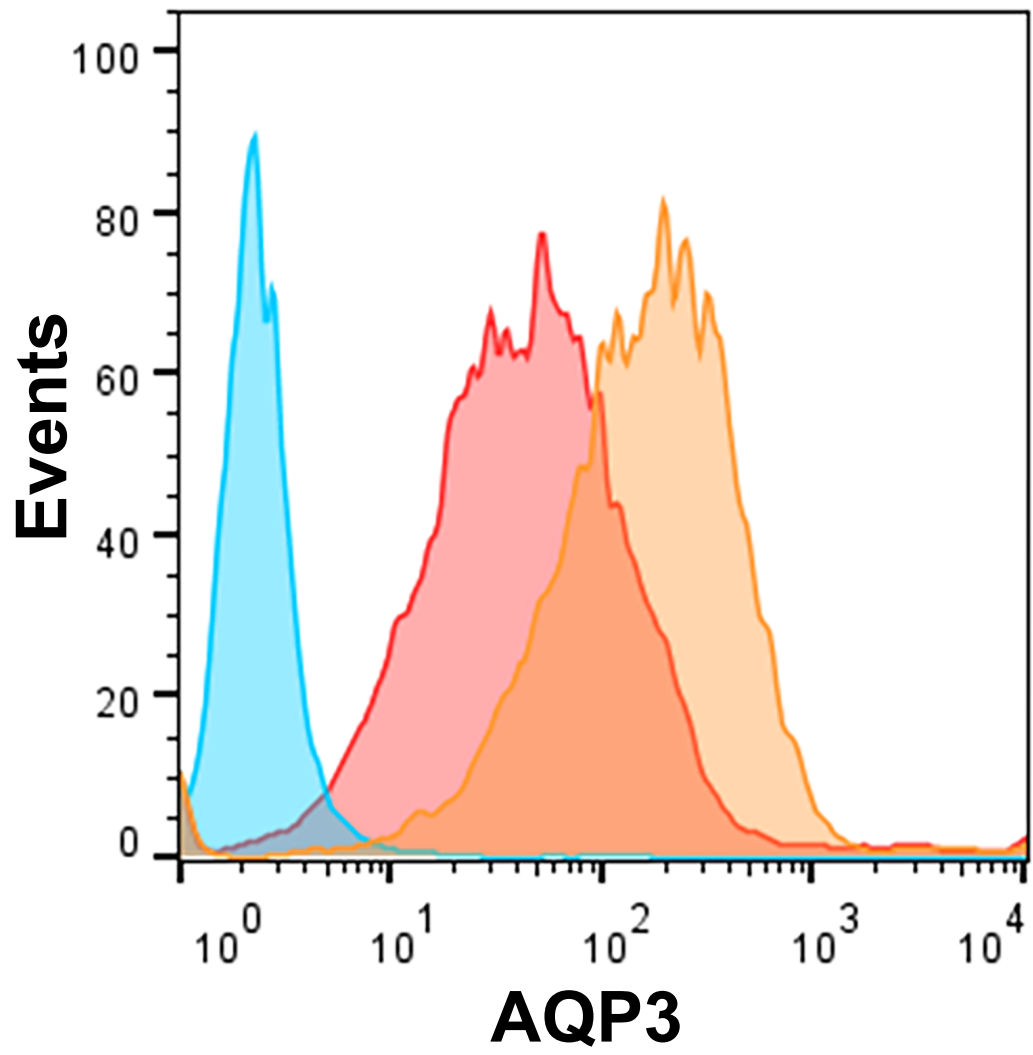


Fig 2.2 Silencing AQP3 with siRNA reduces AQP expression by a factor of 10 for MIA PaCa-2 cells. Verification for silencing of aquaporin AQP3 on the plasma membrane of cancer cells is confirmed by the observed shift in the AQP3 apparent signal. An AQP3 specific signal is shown to exhibit a positive frequency of 91.7 (orange curve) for the unmodified MIA PaCa-2 cancer cells sampled (8,036 cells). After silencing AQP3 for MIA PaCa-2 cancer cells (siAQP3 MIA PaCa-2), the signal shifts to display a positive signal frequency of 59.8 (red curve) for sampled cells (8,067 cells). The peak of the unmodified MIA PaCa-2 cells (orange) displays an average positive signal around 200 whereas the siAQP3 MIA PaCa-2 cells (red) displays an average around 20. This shift in AQP3 signal demonstrates a decrease by a factor of 10 in AQP expression for the silenced MIA PaCa-2 cells when compared to unmodified MIA PaCa-2. The blue curve is the negative IgG control. Data were generated by immunofluorescence tagging, detection through flow cytometry, and analyzed through FlowJo (Treestar, Inc., Ashland, OR, USA).

2.3.3 Rate of Uptake of Extracellular H₂O₂

The rate of exogenous H₂O₂ uptake was determined for MIA PaCa-2 and siAQP3 MIA PaCa-2 cells using a kinetic assay described previously [51]. The rate constant for the uptake of extracellular H₂O₂ per cell is significantly decreased for siAQP3 MIA PaCa-2 as compared to MIA PaCa-2 cells ($P = 0.002$, $n = 4$), Fig 2.3. This confirms that AQP3 is an important factor in controlling the flux of H₂O₂ through the plasma membrane. Scrambled siRNA for AQP3 (negative control) displayed no significant difference for the rate of H₂O₂ uptake when compared to MIA PaCa-2 unmodified cells ($P = 0.41$, $n = 4$).

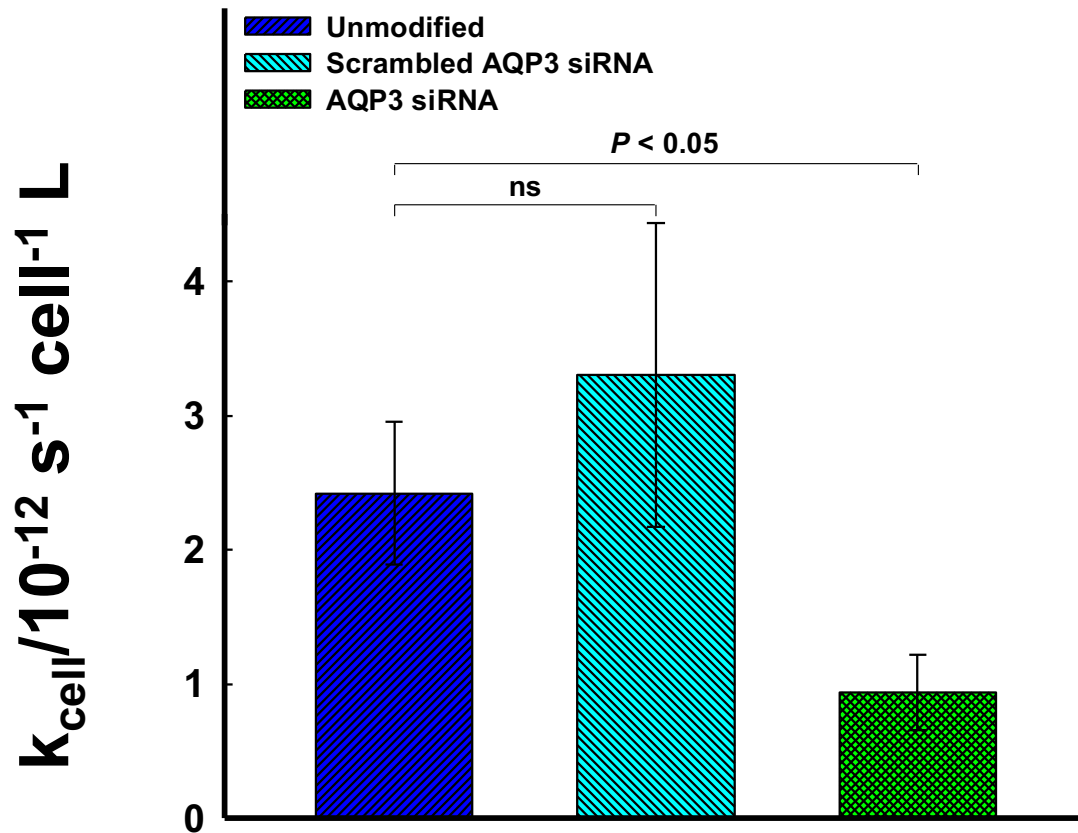
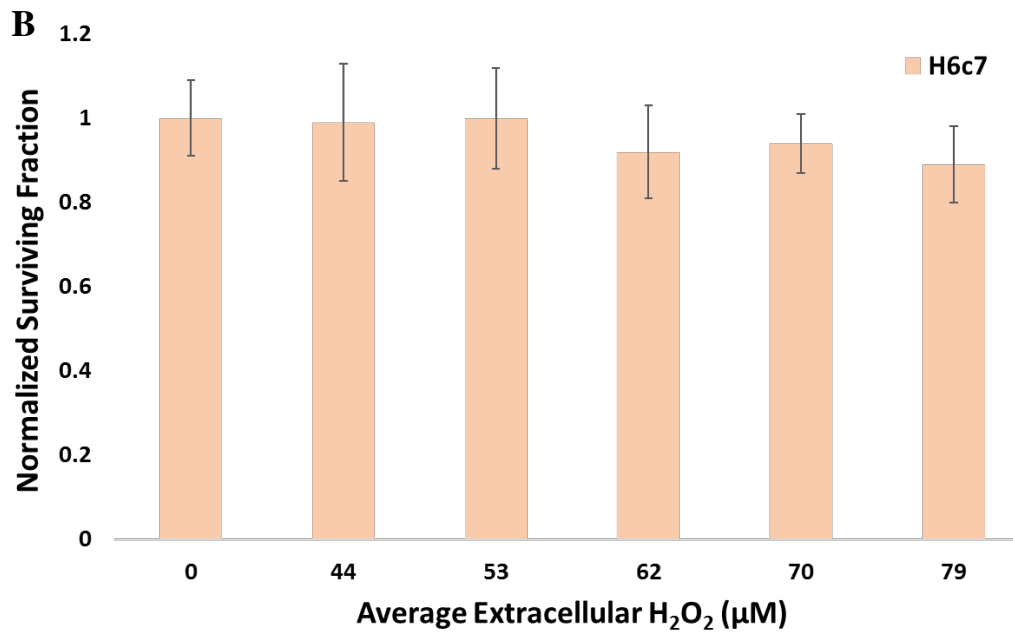
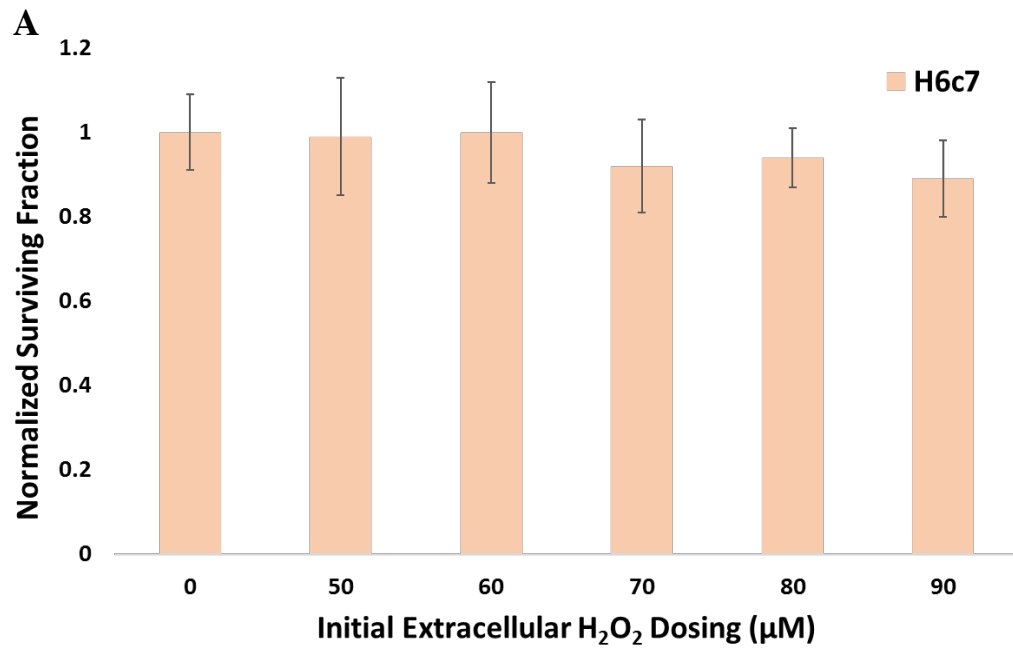


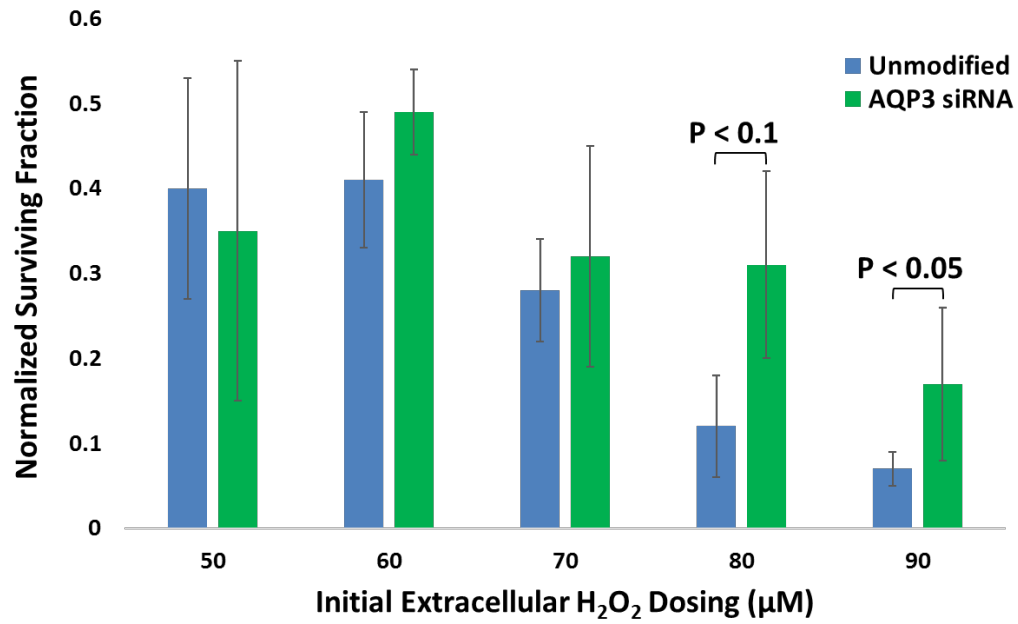
Fig 2.3. Silencing AQP3 on MIA PaCa-2 cancer cells decreases the rate of H₂O₂ uptake per cell. The rate of H₂O₂ uptake by per cell is displayed for MIA PaCa-2 (blue) and siAQP3 MIA PaCa-2 (green). There is a significant decrease in rate between MIA PaCa-2 and siAQP3 MIA PaCa-2 cells ($P = 0.002$, $n = 4$). The rate of H₂O₂ uptake for the negative control (scrambled MIA PaCa-2, cyan) is not significantly different from MIA PaCa-2 ($P = 0.41$, $n = 4$) confirming that the silencing method is not affecting the results. P-values are displayed for cases that are significantly different and are determined through ANOVA analysis. Error bars displayed represent the propagated error.

2.3.4 Clonogenic Survival is Increased when AQP3 is Silenced

Assays designed to determine the clonogenic survival of cells upon exposure to a bolus of H₂O₂ up to 0.30 nmol cell⁻¹ (corresponding to a concentration of 90 μM) reveal the dose-response for the three cell lines, Fig 2.4A and 2.4B. H6c7 cells (Fig 2.4A) were unaffected by exposure to bolus addition of extracellular H₂O₂. MIA PaCa-2 and siAQP3 MIA PaCa-2 cells both demonstrated significant decrease in their surviving fraction when exposed to increased concentrations of H₂O₂ compared to their controls, Fig 2.4B. However, siAQP3 MIA PaCa-2 cells showed an increase in surviving fraction compared to MIA PaCa-2 cells upon exposure to therapeutic ranges of H₂O₂ at 0.27 nmol cell⁻¹ (80 μM) ($P = 0.08$, $n = 3$) and 0.30 nmol cell⁻¹ (90 μM) ($P = 0.02$, $n = 3$). These results indicate that the AQP3, which facilitates the permeability of H₂O₂ across the plasma membrane, is an important determinant of the toxicity of H₂O₂; AQP3 expression appears to be a significant factor in the outcome of ascorbate therapy.



C



D

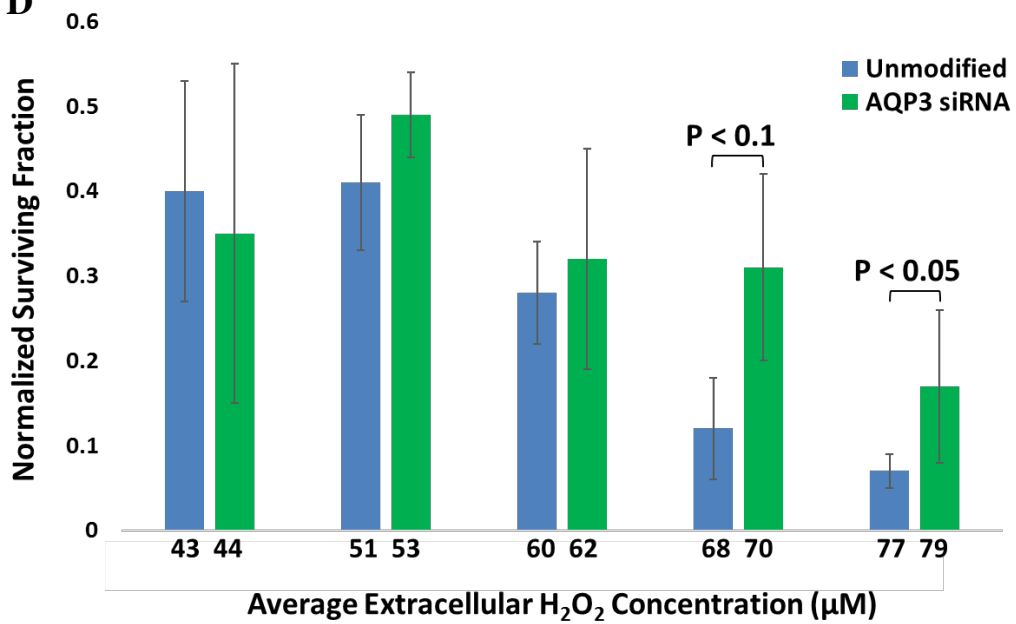


Fig 2.4. Silencing AQP3 increases the surviving fraction of pancreatic cancer cells at therapeutic H₂O₂ concentrations. A & B) Surviving fraction, relative to 0 μM H₂O₂, of H6c7 cells are not significantly affected for dosing shown. C & D) Surviving fraction, relative to 0 μM H₂O₂, is significantly increased for siAQP3 MIA PaCa-2 as compared to unmodified MIA PaCa-2 for therapeutic initial dosing of 80 μM and 90 μM H₂O₂ ($P = 0.08$ and 0.02 , respectively and $n = 3$ for both). Surviving fraction of H6c7 cells are not significantly affected for dosing shown. These results imply that plasma membrane permeability to H₂O₂ *via* AQP3 is an important factor in the surviving fraction outcomes for MIA PaCa-2. B & D) Representation using the average extracellular H₂O₂ concentration dosing is explained later (section 2.4.3). Statistical significance was determined through ANOVA. Error bars displayed represent the standard error (SE).

2.4 Conclusion: permeability is an additional factor to consider

While pancreatic cancer cells exhibit significantly reduced proliferation in the presence of extracellular P-AscH⁻ [1], and normal cells remain unaffected, other cancer cells exhibit a wide variation in susceptibility. Previously, a focus for the underlying differences in susceptibility to P-AscH⁻ has been on the varying catalase activity across cell types [1, 17]. Catalase serves as an intracellular sink for the H₂O₂ generated by P-AscH⁻. Our results show that AQP3 acts as a conduit for the flux of H₂O₂ into the cell [17]. However, a more complete analysis is required for understanding overall flux contributions from variation in permeability to H₂O₂ as well as catalase activity.

The overall intracellular concentration of H₂O₂ in normal cells is likely to be substantially less than in pancreatic cancer tumor cells during therapy with P-AscH⁻. Thus, the removal rate of H₂O₂ is likely to be substantially higher for H6c7 cells as opposed to MIA PaCa-2 once it has crossed the plasma membrane. But, in addition, the results from Fig 2.1 imply that the permeability of H₂O₂, at least through the available peroxiporins, is also substantially reduced for H6c7 cells as compared to MIA PaCa-2. This further suggests that the expression of peroxiporins may be also linked to the susceptibility of cells to the H₂O₂ generated by P-AscH⁻. Thus, those cancer cells that are most susceptible may have an increased expression of peroxiporin in addition to a lower relative catalase activity compared to normal cells.

We show that silencing a peroxiporin, specifically AQP3, inhibits the passage of H₂O₂ into the cell. Additionally, and more importantly, the silencing of peroxiporin AQP3 on pancreatic cancer cells suggests that accumulation of lethal intracellular H₂O₂ concentrations is prevented; consequently, allowing for an increase in clonogenic response. Silencing peroxiporin AQP3 resulted in an increase in surviving fraction of siAQP3 MIA PaCa-2 cells in a clonogenic assay using pharmacological H₂O₂ concentrations of 0.30 nmol cell⁻¹ (90 μM) in comparison to MIA PaCa-2 (*P* = 0.02). This implies that cell-susceptibility to ascorbate therapy is significantly coupled to the permeability of the cell's plasma membrane to H₂O₂, and in particular, elevated expressions of peroxiporins.

Susceptibility to P-AscH⁻ is mirrored in clonogenic assays in response to therapeutic H₂O₂ *in vitro* [1]. Therapeutic H₂O₂ levels range between 0.27 nmol cell⁻¹ to 0.30 nmol cell⁻¹ (80 μM to 90 μM) and is representative of extracellular H₂O₂ produced upon delivery of P-AscH⁻. In a murine model when P-AscH⁻ is given intravenously, concentrations on the order of 20 μM of extracellular H₂O₂ can be achieved [2]. Thus, clonogenic assays are appropriate assessment in this work. The therapeutic range of H₂O₂ for the clonogenic studies was between 80 μM and 90 μM. This is consistent with 87 μM of extracellular H₂O₂ achieved following intravenous P-AscH⁻ infusions [23]. In that study the extracellular ascorbate reached 34 mM.

Overall, this work demonstrates that the permeability of the plasma membrane to H₂O₂ is an important factor when addressing the efficacy of P-AscH⁻ as an adjuvant to cancer

therapy. Although extensive research would be required, modulating membrane peroxiporin expression may increase the efficacy of P-AscH⁻ as an adjuvant for other types of cancer. As a side note, some drugs, such as gemcitabine used for pancreatic cancer, are known to elevate peroxiporin, specifically AQP3, expression in cancer cells [3, 55]. This additional factor may be significant for expanding the use of P-AscH⁻ therapy for other forms of cancer.

2.5 Implications for Ascorbate Therapy

Extracellularly, ascorbate generates H₂O₂ that ultimately permeates across the plasma membrane. This H₂O₂, if not adequately removed by the cell, may result in intracellular H₂O₂ accumulation that prevents the cell from remaining viable. The work presented here, demonstrates that peroxiporin expression is potentially an additional and important factor in determining the success of pharmacological ascorbate therapy. It is suggested that cancer cells with elevated peroxiporins on the plasma membrane could provide increased routes of entry for H₂O₂ which could potentially contribute to intracellular H₂O₂ accumulation. Since many cancer tissues and cells have elevated expressions of AQPs, further investigation of the significance of peroxiporin expression as a factor in P-AscH⁻ therapy is warranted.

CHAPTER 3. DEVELOPMENT OF MATHEMATICAL MODEL FOR INTRACELLULAR H₂O₂ QUANTIFICATION

3.1 Overview

The high extracellular hydrogen peroxide (H₂O₂) concentrations generated during pharmacological ascorbate (P-AscH⁻) therapy has been shown to exhibit a high flux into susceptible cancer cells leading to a decrease in clonogenic survival; where normal cells remain unaffected. The resulting intracellular H₂O₂ concentration is a function of a number of factors that vary across cell lines including catalase activity, and, as determined more recently, peroxiporin expression. Using a mathematical modeling approach coupled with experimentally determined parameters, a relationship between intracellular H₂O₂ and potentially variable cellular properties such as catalase activity and plasma membrane permeability to H₂O₂ is provided. The resulting estimates are correlated with the clonogenic response for normal pancreatic cells (H6c7), and the glioblastoma cell lines, LN-229, T98G, and U-87. The results show that even when the intracellular H₂O₂ concentrations was estimated to be the same, the non-cancerous H6c7 cells has a significantly higher surviving fraction than any of the cancer cells. This is consistent with the recent analysis that the intracellular H₂O₂, while critical during P-AscH⁻ therapy, is not the only factor in predicting pharmacological ascorbate therapy success. The presented mathematical model provides a rapid quantitative assessment of intracellular H₂O₂ during high P-AscH⁻ that can be used in the continued effort to understand the efficacy of pharmacological ascorbate therapy.

3.2 Introduction

Pharmacological ascorbate (P-AscH⁻) has demonstrated tremendous promise as an adjuvant in patients with pancreatic ductal adenocarcinoma [1-4]. The current understanding of this phenomena is that P-AscH⁻ serves as a pro-drug by its ability to generate high concentrations of extracellular hydrogen peroxide (H₂O₂) [4, 12, 17, 19, 23]. The extracellular H₂O₂ permeates the plasma membrane and, potentially, elevates the intracellular hydrogen peroxide concentration. Left unimpeded, the high intracellular H₂O₂ reacts with labile iron that ultimately produce the highly reactive hydroxyl radicals (\cdot OH) [56]. The hydroxyl radical, in the vicinity of the nucleus, can generate cellular oxidative damage, especially to the DNA in cells and cytotoxicity [1, 2, 23, 22, 30-32, 44, 45, 57].

Normal tissues have a relatively high catalase activity and it is believed that the intracellular H₂O₂ levels are below the toxicity range during P-AscH⁻ therapy. A family of intracellular enzymes exist to finely control the intracellular levels of H₂O₂, which normally exists around the 10 nM range [9]. However, catalase is the dominant mechanism for irreversibly consuming intracellular H₂O₂ when intracellular H₂O₂ concentrations are high, such as during pharmacological dosing associated with P-AscH⁻ therapy [17, 19, 38]

But, while P-AscH⁻ therapy is successful for some cancers, numerous *in vivo* and *in vitro* studies have demonstrated a range of susceptibility to P-AscH⁻ therapy across different types of cancers [1, 22-32]. The reason why some cancer cell lines are responsive to P-AscH⁻ therapy while others are not remains elusive. However, at least two factors have

been identified as to having a direct impact on the intracellular H_2O_2 concentration during P-AscH⁻ therapy. These are; i) overall catalase activity and, ii) permeability of the plasma membrane to the flux of H_2O_2 .

Catalase activity vary widely across cell lines. Catalase activity is known to exhibit lower activity in tumor cells; where catalase expression ranges on the order of 10-100 fold times more for normal cells when compared to tumor cells [41]. Other empirical studies have shown more than a 50% decrease in steady-state catalase activity for tumor cells [12]. This variation in catalase activity across cell lines could significantly affect the removal of H_2O_2 , making tumor cells more susceptible to ascorbate mediated cell-death, as their capability to remove H_2O_2 is greatly hindered.

In addition to catalase activity, it has been recently shown that H_2O_2 permeability of the plasma membrane is significant factor in cell susceptibility to extracellular H_2O_2 [58]. Peroxiporins (aquaporins that allow transport of H_2O_2 across the plasma membranes), specifically AQP1, AQP3 and AQP8, are thought to be the principal pathways for the entry of H_2O_2 across the plasma membrane and that the flux of H_2O_2 across the plasma membrane is dominated by passive diffusion through these peroxiporins [37, 59, 60]. Many aquaporins are overexpressed in tumor cells of different origins, especially in aggressive tumors [37] and it has recently been shown that pancreatic adenocarcinoma cells are believed to exhibit elevated AQP8 expression [37]. AQP3 has been found to increase by

as much as eight-fold in cancer cells when treated with nucleoside analogs such as gemcitabine [55].

In our previous work [58], AQP3 was silenced in the MIA PaCa-2 pancreatic cancer cell line (AQP3 siRNA MIA PaCa-2) and its clonogenic response was compared to unmodified MIA PaCa-2 for exposure to extracellular H₂O₂ concentrations equivalent to that generated during P-AscH⁻ therapy dosing. The results showed over twice the clonogenic surviving fraction for the AQP3 siRNA MIA PaCa-2 when compared to MIA PaCa-2. Thus, it is hypothesized the plasma membrane permeability differences, possibility due to the variability of peroxiporin expression across cell lines, can contribute to the variability of cell susceptibility to P-AscH⁻ therapy. Figure 3.1 illustrates how the variations in catalase activity and peroxiporin expression might influence the cell susceptibility to ascorbate therapy.

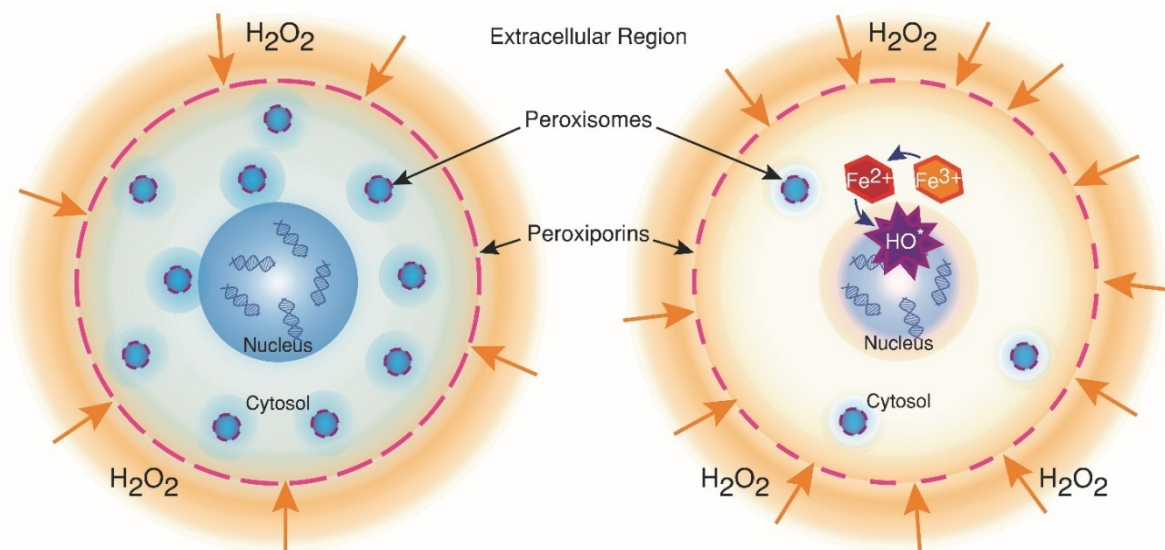


Fig 3.1. Illustration of the proposed dominant mechanisms for cellular susceptibility to ascorbate therapy. Ascorbate is introduced into the extracellular region by intravenous dosing that generates extracellular H_2O_2 . The extracellular H_2O_2 enters the cell via its available peroxiporins at a rate consistent with the plasma membrane permeability and the effective catalase activity. In the figure to the left, it is proposed that normal cells and ascorbate-resistant cancer cells have either the ability to minimize peroxide permeability, rapidly catalyze intracellular hydrogen peroxide (via peroxisomes) and/or have limited labile iron present. The figure to the right illustrates susceptible cells which may have increased plasma membrane permeability to peroxide, reduced catalase activity and/or increased labile iron. The consequence of the chemical conditions in the susceptible cell is the generation of hydroxyl radicals near DNA that can result in damage and, ultimately, reduced clonogenic survival. This study focuses on quantifying the intracellular H_2O_2 during P-AscH⁻ therapy and determining its relationship and sensitivity to variations in catalase activity and plasma membrane permeability, both which have been found to vary across cell lines.

The overarching goal of this work is to elucidate why there is a variation in susceptibility to P-AscH⁻ therapy dosing across cell lines. Under this framework, the goal of this work is to provide a quantitative assessment of the intracellular H₂O₂ concentration during P-AscH⁻ therapy for varying cell lines and determine if there is a correlation between the intracellular concentration and the clonogenic response that is independent of cell line. Other researchers have mathematically modeled the intracellular concentration of H₂O₂ primarily because of its critical significance in the homeostasis of the cellular redox environment [38, 61-63]. The seminal work of Antunes and Cadenas (2000) provided a diffusion model based on latency of catalase. In addition, their diffusion model used a model representative of active diffusion. As mentioned above, it is now recognized that peroxiporins act as passive diffusion vessels to the exchange of H₂O₂ across the plasma membrane. Ng et al. (2007) evaluated the range of H₂O₂ likely present during the GPx/GSH process during physiological conditions, but did not address the role of catalase [38]. Lim et al. (2015) developed a mathematical model for H₂O₂ in the cytosol under physiological conditions using a reduced kinetic model but did not consider catalase or membrane permeability [63]. This work is the first to quantify intracellular H₂O₂ relevant to P-AscH⁻ therapy. Further, this work examines the significant parameters associated with the intracellular H₂O₂ concentration and addresses whether their variability across cell lines are key factors. The critical issues to be addressed are; 1) the sensitivity of the intracellular H₂O₂ concentration to cellular variations in catalase activity and plasma membrane permeability, and, 2) the relationship between the intracellular H₂O₂ concentration and the clonogenic response of normal and cancer cell lines. This work will focus on the pancreatic

cell lines H6c7, MIA PaCa-2, and modified AQP3 siRNA MIA PaCa-2, and the glioblastoma cell lines, LN-229, T98G, and U-87. These glioblastoma cell lines have been found to range in susceptibility to ascorbate *in vitro* with LN-229 being highly susceptible, T98G being moderately susceptible and U-87 being insensitive [23].

This work has three parts. The first part of this work discusses the development of the mathematical model used to estimate intracellular H_2O_2 . In this development, measurable parameters associated with specific cell lines will be identified and the expected sensitivity of these parameters on the intracellular H_2O_2 concentration will be accessed. In the second part of this work, experimental and modeling methods will be combined to obtain the parameters needed to model the intracellular H_2O_2 concentration for the cells lines reviewed in this work. Finally, the intracellular H_2O_2 concentration will be calculated for each cell line during dosing with the equivalent extracellular H_2O_2 concentration that is present during P-AscH⁺ therapy. The overall calculated intracellular H_2O_2 will be plotted against the resulting surviving fraction determined from the clonogenic study to determine whether intracellular H_2O_2 is the fundamental factor in dictating the cellular response to therapeutic levels of H_2O_2 .

3.3 Mathematical Methods

3.3.1 Governing Equations

The generalized mathematical model for the conservation of mass of species i in a given closed mathematical volume, V , with surface area, A , can be expressed as

$$\frac{d}{dt} \int_V C_i dv = - \int_A \vec{n} \cdot \vec{N}_i da + \int_V R_i dv \quad (3.1)$$

where C_i is the molar concentration of species i in the volume, t is time, and $\frac{d}{dt} \int_V C_i dv$ is the rate of molar accumulation of species i in the prescribed volume. \vec{N}_i is the flux of species i (moles of species i per area per time) and the integral $-\int_A \vec{n} \cdot \vec{N}_i da$ is the molar rate of species i entering into the volume across the surface area, A . The negative sign is to account for the direction of the outward bound normal \vec{n} that is used to define the orientation of the surface. R_i is the net molar rate of formation of species i per volume in the volume so $\int_V R_i dV$ is the rate of the moles of species i that is generated in the volume due to its production from reactions. Because this model is the integral of the concentration in differential volumes (dv), it captures the variation in the concentration of species i in both time and space. Nevertheless, this form of the conservation of mass is advantageous as it provides the foundation for the assumptions of the idealized model used in this work.

In particular, the idealized model assumes that the concentrations in all of the volumes in question are relatively independent of spatial variations and, thus, the conservation of species i is a function of only time (lumped parameter model or well-mixed assumption).

Under this assumption, Eqn 3.1 can be integrated to the entire volume and becomes

$$V \frac{dC_i}{dt} = N_i |_A A + R_i V. \quad (3.2)$$

Here we expressed the molar flux of species i in its scalar form and allow A to represent the area of the volume in which species i enters the volume.

For the analysis of intracellular H_2O_2 (in the cytosol) during ascorbate therapy, we consider three volumes, the volume of the extracellular compartment, V_{ext} , the volume of the cytosol, V_{in} , and the volume of the peroxisomes, V_p , where cytosolic H_2O_2 permeates and is consumed via catalase. Thus, three equations are necessary to capture the overall mass balance of H_2O_2 in this system. Fig 3.2 illustrates the selected system used in this analysis. The corresponding concentrations of H_2O_2 in the extracellular region, the cytosol, and in the peroxisomes are, C_{ext} , C_{in} , and C_p , respectively.

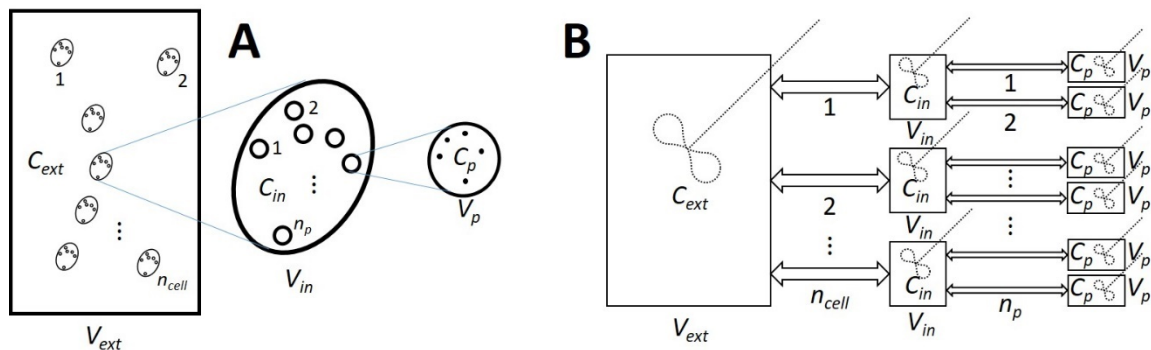


Fig 3.2. Illustration of the proposed modeling approach. In Fig 3.2A, the external H₂O₂ (concentration C_{ext}) permeates into each of the n_{cell} cells via diffusion. The resulting intercellular H₂O₂ (concentration C_{in}) can, subsequently, diffuse across the peroxisome membranes into the n_p peroxisomes per cell where it is further consumed by catalase. The concentration of H₂O₂ in the peroxisomes is denoted by C_p . The volumes for the chambers are V_{ext} , V_{in} , and V_p , for the extracellular, intracellular (cytosolic) and the peroxisomes, respectively. Fig 3.2B is the idealized lump parameter model for the system. Here concentration is assumed to be spatially independent in all compartments (illustrated by the well-mixed impeller symbol). The flux of H₂O₂ across chambers is denoted by the double arrows. In this modeling effort, the flux is modeled using membrane permeability with concentration difference across chambers as the driving force.

The transport mechanism of H₂O₂ across the plasma membrane and through peroxiporins is via diffusion and, thus, the driving force is the concentration gradient at the interface area between volumes. To eliminate spatial dependency, the flux is represented by the concentration differences in each volume at the interface and a membrane permeability. Thus, assuming a dilute solution, the Fickian model for N_i can be described as

$$N_i|_A = -D_{ij}\nabla C_i|_{interface} \approx m_k(C_{i,V_{k+1}} - \varphi_k C_{i,V_k}) \quad (3.3)$$

where D_{ij} is the Fickian diffusion coefficient of species i in solvent j , $\nabla C_i|_{interface}$ is the concentration gradient at the interface of the adjacent volumes (for one-dimensional radial direction $\nabla C_i|_{interface} = \frac{\partial C_i}{\partial r}|_{r=R}$), m_k is the membrane permeability associated with the area interface for the k^{th} volume, V_k , and V_{k+1} in the adjacent volume at the transport interface. The partition coefficient, φ_k , is used to correct for thermodynamic equilibrium for concentrations across interfaces. Note that the membrane permeability represents the diffusivity of the species divided by a characteristic length of the system. The approximation on the right-hand side of Eqn (3.3) uses the concentration difference across the interface which is indicative for passive diffusion and is equivalent to the numerical approximation for diffusive flux. This form of expression for passive diffusive flux differs from that proposed previously by Antunes and Cadenas (2000) and others which was representative of active transport, and, thus, a function of only one concentration at the interface [61, 62]. The current model allows flux to reduce and establish equilibrium with non-zero species i concentrations. Letting species i be H₂O₂, Eqns. (3.2) and (3.3) can be combined to provide the idealized lumped parameter for H₂O₂ in this study.

Assuming a dilute concentration of H_2O_2 , Eqns (3.1 – 3.3) is used for all compartments to obtain,

$$V_{ext} \frac{dC_{ext}}{dt} = M_{in} \delta(t) - m_{plm} A_{cell} n_{cell} (\varphi_{plm} C_{ext} - C_{in}) \quad (3.4)$$

$$V_{in} \frac{dC_{in}}{dt} = m_{plm} A_{cell} (\varphi_{plm} C_{ext} - C_{in}) - m_p A_p n_p (\varphi_p C_{in} - C_p) \quad (3.5)$$

$$V_p \frac{dC_p}{dt} = m_p A_p (\varphi_p C_{in} - C_p) - k_2 C_{cat_p} C_p V_p. \quad (3.6)$$

Here, m_{plm} and m_p , represent the plasma membrane permeability and the peroxisome membrane permeability, respectively. The parameters φ_{plm} and φ_p are the partition coefficients of the plasma membrane and peroxisome membrane, respectively. For this study, these values are assumed to be unity. The initial moles of H_2O_2 added in the extracellular compartment is denoted as $M_{in} \delta(t)$, A_{cell} is the area of a cell, n_{cell} is the number of cells in the external volume, V_{ext} . No reaction is assumed to take place in the extracellular or cytosolic volume. The catalase reaction of H_2O_2 is assumed to occur within the peroxisomes, and, here, $R_i = -k_2 C_{cat_p} C_p$. Here k_2 is the effective second order reaction rate of H_2O_2 decomposition by catalase, and C_{cat_p} is the concentration of catalase inside each peroxisome [64].

3.3.2 Steady-state Model for intracellular H_2O_2 concentration (θ_{ss})

The steady-state intracellular H_2O_2 concentration that corresponds to the extracellular concentration can be obtained by setting the time derivatives of Eqn (3.5) and (3.6) to zero while assuming C_{ext} is constant. The resulting H_2O_2 ratio is

$$\theta_{ss} = \frac{m_{plm}A_{cell}\varphi_{plm}(m_pA_p+k_2C_{cat_p}V_p)}{m_{plm}A_{cell}(m_pA_p+k_2C_{cat_p}V_p)+m_pA_p n_p \varphi_p k_2 C_{cat_p} V_p} \quad (3.7)$$

where $\theta_{ss} = \frac{C_{in}}{\varphi_{plm}C_{ext}}$. From a practical perspective, the concentration of catalase extracted per cell, $C_{cat_{cell}}$ can be used giving

$$\theta_{ss} = \frac{m_{plm}A_{cell}\varphi_{plm}\left(m_pA_p+k_2\frac{C_{cat_{cell}}V_{cell}}{n_p}\right)}{m_{plm}A_{cell}\left(m_pA_p+k_2\frac{C_{cat_{cell}}V_{cell}}{n_p}\right)+m_pA_p n_p \varphi_p k_2 \frac{C_{cat_{cell}}V_{cell}}{n_p}} \quad (3.8)$$

It is instructive to note that the above models satisfy the asymptotic limits for θ_{ss} . If no catalase activity, then $k_2C_{cat_p} \rightarrow 0$ and the solution to Eqn (3.7) approaches 1. In addition, at high catalase where $k_2C_{cat_p} \gg \frac{m_pA_p}{V_p}$, then $\theta_{ss} \rightarrow 0$. This model provides a convenient format for addressing the dependency of the steady-state intracellular H_2O_2 concentration on various parameters as well as provides a convenient format for sensitivity analysis.

3.3.3 Sensitivity of Intracellular H_2O_2 concentration to variations in cell properties

Catalase activity and plasma membrane permeability have been identified as two parameters that vary across cell lines and could, subsequently, impact the intracellular H_2O_2 concentration during ascorbate therapy. Local sensitivity analysis is used to estimate the impact of these parameters on θ_{ss} . Using the dimensionless sensitivity parameter $s_{\theta,j}$ defined as the local derivative of θ_{ss} with respect to the j^{th} normalized parameter [65], we obtain the following sensitivity for each parameter,

$$S_{\theta, m_{plm}} = \frac{A_{cell} k_2 C_{cat_p} m_p n_p A_p \varphi_p \varphi_{plm} V_p (m_p A_p + k_2 C_{cat_p} V_p) m_{plm}}{[m_{plm} A_{cell} (m_p A_p + k_2 C_{cat_p} V_p) + k_2 C_{cat_p} V_p m_p n_p A_p \varphi_p]^2} \quad (3.9)$$

$$S_{\theta, C_{cat_p}} = \frac{-m_{plm} A_{cell} (m_p)^2 n_p (A_p)^2 k_2 \varphi_p \varphi_{plm} V_p C_{cat_p}}{[m_{plm} A_{cell} (m_p A_p + k_2 C_{cat_p} V_p) + k_2 C_{cat_p} V_p m_p n_p A_p \varphi_p]^2} \quad (3.10)$$

$$S_{\theta, m_p} = \frac{-m_{plm} (C_{cat_p})^2 A_{cell} (k_2)^2 n_p A_p \varphi_p (V_p)^2 \varphi_{plm} m_p}{[m_{plm} A_{cell} (m_p A_p + k_2 C_{cat_p} V_p) + k_2 C_{cat_p} V_p m_p n_p A_p \varphi_p]^2} \quad (3.11)$$

$$S_{\theta, A_{cell}} = \frac{m_{plm} C_{cat_p} k_2 m_p n_p A_p \varphi_p V_p \varphi_{plm} (m_p A_p + k_2 C_{cat_p} V_p) A_{cell}}{[m_{plm} A_{cell} (m_p A_p + k_2 C_{cat_p} V_p) + k_2 C_{cat_p} V_p m_p n_p A_p \varphi_p]^2} \quad (3.12)$$

$$S_{\theta, A_p} = \frac{-m_{plm} (C_{cat_p})^2 A_{cell} (k_2)^2 m_p n_p \varphi_p (V_p)^2 \varphi_{plm} A_p}{[m_{plm} A_{cell} (m_p A_p + k_2 C_{cat_p} V_p) + k_2 C_{cat_p} V_p m_p n_p A_p \varphi_p]^2} \quad (3.13)$$

$$S_{\theta, V_p} = \frac{-m_{plm} C_{cat_p} A_{cell} k_2 (m_p)^2 n_p (A_p)^2 \varphi_p \varphi_{plm} V_p}{[m_{plm} A_{cell} (m_p A_p + k_2 C_{cat_p} V_p) + k_2 C_{cat_p} V_p m_p n_p A_p \varphi_p]^2} \quad (3.14)$$

$$S_{\theta, n_p} = \frac{-m_{plm} C_{cat_p} A_{cell} k_2 m_p A_p \varphi_p \varphi_{plm} V_p (m_p A_p + k_2 C_{cat_p} V_p) n_p}{[m_{plm} A_{cell} m_p A_p + k_2 C_{cat_p} (m_{plm} A_{cell} + m_p n_p A_p \varphi_p) V_p]^2} \quad (3.15)$$

$$S_{\theta, V_{cell}} = \frac{-m_{plm} C_{cat_{cell}} A_{cell} k_2 (m_p)^2 (n_p)^2 (A_p)^2 \varphi_p \varphi_{plm}}{[m_p n_p A_p k_2 C_{cat_{cell}} \varphi_p V_{cell} + m_{plm} A_{cell} (m_p n_p A_p + k_2 C_{cat_{cell}} V_{cell})]^2} \quad (3.16)$$

3.4 Validity of Lumped Parameter Model

3.4.1 Significance of spatial dependency in the cytosol region

Eqn (3.7) provides a simple approach to estimating the intracellular H_2O_2 concentration during P-AscH⁺ therapy. However, this method has several limitations that must be addressed when determining the validity of the solution. To begin, the lumped parameter

model assumes the H_2O_2 concentrations are spatially independent. To check the validity of this approximation for the cytosol, we begin by looking at the potential for concentration gradients to exist by modeling this volume using a steady-state diffusion problem with a pseudo-homogeneous reaction. The pseudo-homogenous reaction model assumes that the peroxisomes are well distributed and the catalase-related reaction is carried out throughout the volume. For this approach, the cell is assumed to be spherical with a radius of r_c and the nucleus has a radius of r_n . Figure 3.3 illustrates the geometry for this model. The dashed enclosed lines in Fig 3.3 in the intracellular volume illustrates the control volume concept under consideration. In this approach, the control volume is sufficiently large to contain the peroxisomes but assumed to be small enough to apply the continuum model for the conservation of mass. Using Eqn (3.1) and converting the area integral to a volume integral and assuming spherical coordinates we obtain,

$$\frac{\partial C_{in}}{\partial t} = D_{ij} \frac{1}{r^2} \frac{\partial}{\partial r} \left(r^2 \frac{\partial C_{in}}{\partial r} \right) + R_i \quad (3.17)$$

The peroxisomes are present in the region $r_c \geq r > r_n$ and $R_i = -k_2^* \rho_p C_{in}$ where ρ_p is the number density of peroxisomes in the volume, and k_2^* is the effective second-order reaction rate constant for the observed reaction. The parameter k_2^* is specific to each cell line and absorbs variations in latency, and catalase activity.

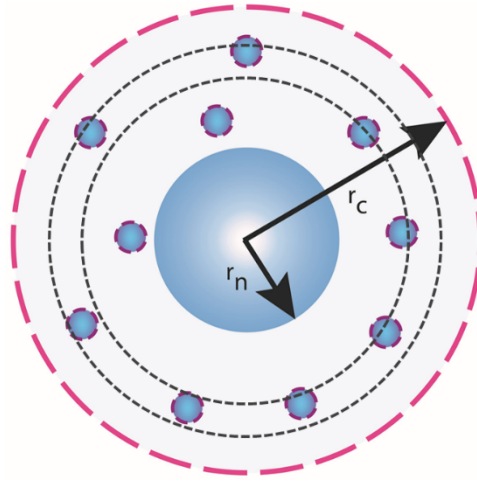


Fig 3.3. Illustration of the model used to examine the spatially dependent intracellular H_2O_2 concentration in the cytosol. In this model, it is assumed that the peroxisomes are well dispersed in the cytosol and result in a pseudo-homogeneous reaction approximation throughout a spherical volume. The area between the inner dashed lines represent the control volume used in Eqn (3.1). The radius of the cell and nucleus are denoted as r_c and r_n , respectively.

In determining an appropriate set of boundary conditions, it is assumed that in the nucleus ($r_n \geq r \geq 0$), $R_i = 0$. Thus, at the nucleus wall, the flux of H_2O_2 is zero. At the plasma membrane wall, the diffusive flux into the cell is equivalent to the mass flux across the membrane into the cell. Thus, the boundary conditions can be written as

$$r = r_c \quad -\varphi_{plm} D_{ij} \frac{dC_{in}}{dr} = m_{plm} [\varphi_{plm} C_{ext} - C_{in}] \quad \text{Boundary Condition 1}$$

$$r = r_n \quad \frac{dC_{in}}{dr} = 0 \quad \text{Boundary Condition 2}$$

The dimensionless form of this problem can provide tremendous insight and allows one to compare appropriate dimensionless groups across cell lines. Defining a dimensionless concentration (θ) and radius (η),

$$\theta \equiv \frac{C_{in}}{\varphi_{plm} C_{ext}}, \quad \eta \equiv \frac{r}{r_c}$$

Subsequently, $\frac{d\theta}{dC_{in}} = \frac{1}{\varphi_{plm} C_{ext}}$; thus, $\varphi_{plm} C_{ext} d\theta = dC_{in}$. Similarly, $\frac{d\eta}{dr} = \frac{1}{r_c}$; thus,

$$r_c d\eta = dr$$

Redefining in dimensionless form we obtain,

$$\frac{\varphi_{plm} C_{ext} d\theta}{dt} = \frac{D_{ij}}{(r_c \eta)^2} \frac{d}{d\eta} \left((r_c \eta)^2 \frac{\varphi_{plm} C_{ext} d\theta}{r_c d\eta} \right) - k_2^* \rho_p \varphi_{plm} C_{ext} \theta \quad (3.18)$$

Simplifying,

$$\frac{d\theta}{dt} = \frac{D_{ij}}{r_c^2} \frac{1}{\eta^2} \frac{d}{d\eta} \left(\eta^2 \frac{d\theta}{d\eta} \right) - k_2^* \rho_p \theta \quad (3.19)$$

We see the Thiele modulus of the cell emerge,

$$\phi_c = \sqrt{\frac{k_2^* \rho_p r_c^2}{D_{ij}}} \quad (3.20)$$

Here we are interested in species i being H_2O_2 and fluid j being the cytosol. Since the cytosol is composed of 80% H_2O we use the diffusion coefficient of H_2O_2 in H_2O . Our dimensionless equation then reduces further,

$$\frac{d\theta}{dt} = \frac{1}{\eta^2} \frac{d}{d\eta} \left(\eta^2 \frac{d\theta}{d\eta} \right) - \phi_c^2 \theta \quad (3.21)$$

When C_{ext} is constant, the system is assumed to reach steady-state when $t \gg t^*$. Assuming the diffusion coefficient for H_2O_2 in water is $1.4 \times 10^{-9} m^2 s^{-1}$ [66], for a typical cell radius of $10 \mu m$, $t^* = 7.2 \times 10^{-2} s$. All studies satisfy this condition so Eqn (3.20) reduces to,

$$\frac{1}{\eta^2} \frac{d}{d\eta} \left(\eta^2 \frac{d\theta}{d\eta} \right) = \phi_c^2 \theta \quad (3.22)$$

Redefining our boundary conditions in dimensionless, for convenience we define a dimensionless variable lambda (λ), $\lambda = \frac{r}{r_n}$. Thus $r = r_n \lambda$ and previously $r = r_c \eta$;

therefore, $r_n \lambda = r_c \eta$ and at $\eta = 1$ then $\lambda = \frac{r_c}{r_n}$. Addressing the most conservative solution

we will go to the center of the cell $r_c = 0$

$$r = r_c \quad -\varphi_{plm} D_{ij} \frac{dC_{in}}{dr} = m_{plm} [\varphi_{plm} C_{ext} - C_{in}]$$

Making dimensionless

$$\eta = 1 \quad -\varphi_{plm} D_{ij} \frac{\varphi_{plm} C_{ext} d\theta}{r_c d\eta} = m_{plm} [\varphi_{plm} C_{ext} - \varphi_{plm} C_{ext} \theta]$$

$$\frac{-\varphi_{plm}^2 D_{ij} C_{ext} d\theta}{r_c d\eta} = [m_{plm} \varphi_{plm} C_{ext} - m_{plm} \varphi_{plm} C_{ext} \theta]$$

$$-\frac{d\theta}{d\eta} = \frac{m_{plm} \varphi_{plm} C_{ext} r_c}{\varphi_{plm}^2 D_{ij} C_{ext}} - \frac{m_{plm} \varphi_{plm} C_{ext} \theta r_c}{\varphi_{plm}^2 D_{ij} C_{ext}}$$

$$\eta = 1 \quad -\frac{d\theta}{d\eta} = \frac{m_{plm}r_c}{\underbrace{\varphi_{plm}D_{ij}}_{Bi_c}}(1 - \theta) \quad \text{Boundary Condition 1}$$

$$r_c = 0 \quad \eta = 1 \quad \lambda = 0 \quad \frac{d\theta(\lambda)}{d\eta} = 0 \quad \text{Boundary Condition 2}$$

Now that we have successfully transformed both our equation and boundary conditions to dimensionless form, we can solve for theta. Since we are determining whether spatial contributions may exist, we are interested in obtaining the concentration profile in the radial direction (θ_η). So to write the the equation more descriptively we can use θ_η (the concentration at eta).

$$\frac{1}{\eta^2} \frac{d}{d\eta} \left(\eta^2 \frac{d\theta_\eta}{d\eta} \right) = \phi_c^2 \theta_\eta \quad (3.23)$$

With boundary conditions,

$$\lambda = 0 \quad \frac{d\theta(\lambda)}{d\eta} = 0 \quad (3.24)$$

$$\eta = 1 \quad -\frac{d\theta}{d\eta} = Bi_c(1 - \theta_\eta) \quad (3.25)$$

During the process of making the boundary conditions dimensionless, we see another useful dimensionless parameter emerge, the Biot number of the cell which describes the ratio of the membrane permeability to the diffusion of species i in the volume of interest, here the cytosolic region. To solve, we let $g = \eta\theta$ or written another way, $\theta = \frac{g}{\eta}$

$$\frac{d\theta}{d\eta} = \frac{1}{\eta} \frac{dg}{d\eta} - \frac{g}{\eta^2} \quad (3.26)$$

Then,

$$\frac{1}{\eta^2} \frac{d}{d\eta} \left(\eta^2 \left\{ \frac{1}{\eta} \frac{dg}{d\eta} - \frac{g}{\eta^2} \right\} \right) = \phi_c^2 \theta_\eta \quad (3.27)$$

$$\frac{1}{\eta^2} \frac{d}{d\eta} \left(\eta \frac{dg}{d\eta} - g \right) = \phi_c^2 \theta_\eta \quad (3.28)$$

$$\frac{1}{\eta^2} \left[\frac{d\eta}{d\eta} \frac{dg}{d\eta} + \eta \frac{d^2g}{d\eta^2} - \frac{dg}{d\eta} \right] = \phi_c^2 \theta_\eta \quad (3.29)$$

Simplifying,

$$\frac{1}{\eta^2} \left[\eta \frac{d^2g}{d\eta^2} \right] = \phi_c^2 \theta_\eta \quad (3.30)$$

$$\frac{1}{\eta} \frac{d^2g}{d\eta^2} = \phi_c^2 \theta_\eta \quad (3.31)$$

Knowing $\theta_\eta = \frac{g}{\eta}$ we obtain,

$$\frac{1}{\eta} \frac{d^2g}{d\eta^2} = \phi_c^2 \frac{g}{\eta} \quad (3.32)$$

Thus,

$$\frac{d^2g}{d\eta^2} = \phi_c^2 g \quad (3.33)$$

Because this is a linear differential equation with constant coefficients we know the general solution will follow $g = Ae^{B\eta}$. We begin by guessing this as the solution,

$$g = Ae^{B\eta} \text{ then, } \frac{dg}{d\eta} = BAe^{B\eta} \text{ and } \frac{d^2g}{d\eta^2} = B^2 Ae^{B\eta}$$

Here we see $B^2 = \phi_c^2$ thus $B = \pm \phi_c$

Resulting in the solution of the form,

$$g = C_1 e^{\phi_c \eta} + C_2 e^{-\phi_c \eta} \quad (3.34)$$

Where C_1 and C_2 are arbitrary constants solved for later with the boundary conditions.

Since g is defined as $g = \eta\theta$ we see,

$$\eta\theta = C_1 e^{\phi_c \eta} + C_2 e^{-\phi_c \eta} \quad (3.35)$$

And,

$$\theta = \frac{C_1 e^{\phi_c \eta} + C_2 e^{-\phi_c \eta}}{\eta} \quad (3.36)$$

Using the boundary conditions to solve for the constants (C_1 and C_2) we see the general solution presented in this form proves difficult. Taking advantage of hyperbolic functions and understanding that $\cosh(x) = \frac{e^x + e^{-x}}{2}$ and $\sinh(x) = \frac{e^x - e^{-x}}{2}$, we can improve our guess for the general solution to be instead,

$$\theta = \frac{C_1 \sinh(\phi_c \eta) + C_2 \cosh(\phi_c \eta)}{\eta} \quad (3.37)$$

Evaluating at the boundary condition

$$\eta = 0 \quad \frac{d\theta}{d\eta} = 0 \quad (3.38)$$

$$\frac{d\theta}{d\eta} = \frac{\phi_c C_1 \sinh(\phi \eta) + \phi_c C_2 \cosh(\phi \eta)}{\eta} - \frac{C_1 \sinh(\phi_c \eta) + C_2 \cosh(\phi_c \eta)}{\eta^2} \quad (3.39)$$

$$\frac{d\theta}{d\eta} = \frac{\eta[\phi_c C_1 \sinh(\phi \eta) + \phi_c C_2 \cosh(\phi \eta)] - [C_1 \sinh(\phi_c \eta) + C_2 \cosh(\phi_c \eta)]}{\eta^2} \quad (3.40)$$

Thus at this boundary,

$$0 = \frac{0[\phi_c C_1 \sinh(0) + \phi_c C_2 \cosh(0)] - [C_1 \sinh(0) + C_2 \cosh(0)]}{(0)^2} \quad (3.41)$$

$$C_2 = 0 \quad (3.42)$$

Resulting in,

$$\theta = \frac{C_1 \sinh(\phi_c \eta)}{\eta} \quad (3.43)$$

However, if we evaluate the limit as η approaches zero we see,

$$\lim_{\eta \rightarrow 0} \theta = \frac{C_1 \sinh(0)}{0} = \frac{0}{0} \quad (3.44)$$

Because we do not know if this should be considered 1, 0, ∞ , or if it does not exist we are able to further analyze whether a finite constant can be determined through the use of L'Hôpital's rule.

$$\lim_{\eta \rightarrow 0} \frac{C_1 \sinh(\phi_c \eta)}{\eta} = \lim_{\eta \rightarrow 0} \frac{\frac{d}{d\eta}(C_1 \sinh(\phi_c \eta))}{\frac{d}{d\eta}(\eta)} \quad (3.45)$$

$$\lim_{\eta \rightarrow 0} \frac{\phi_c C_1 \cosh(\phi_c \eta)}{1} = \phi_c C_1 \quad (3.46)$$

Now that ϕC_1 is confirmed to be a finite number we can solve

$$\theta = \frac{C_1 \sinh(\phi_c \eta)}{\eta} \quad (3.47)$$

At the boundary condition

$$\eta = 1 \quad \frac{d\theta}{d\eta} = Bi_c (1 - \theta_\eta) \quad (3.48)$$

We see,

$$\frac{\eta[\phi_c C_1 \cosh(\phi_c \eta)] - [C_1 \sinh(\phi_c \eta)]}{\eta^2} = Bi_c (1 - \theta_\eta) \quad (3.49)$$

Since $\theta_\eta = \frac{C_1 \sinh(\phi_c \eta)}{\eta}$

$$\frac{C_1[\phi_c \eta \cosh(\phi_c \eta) - \sinh(\phi_c \eta)]}{\eta^2} = Bi_c \left(1 - \frac{C_1 \sinh(\phi_c \eta)}{\eta}\right) \quad (3.50)$$

At $\eta = 1$,

$$C_1[\phi_c \cosh(\phi_c) - \sinh(\phi_c)] = Bi_c - Bi_c C_1 \sinh(\phi_c) \quad (3.51)$$

$$C_1[\phi_c \cosh(\phi_c) - \sinh(\phi_c)] + Bi_c C_1 \sinh(\phi_c) = Bi_c \quad (3.52)$$

$$C_1[\phi_c \cosh(\phi_c) - \sinh(\phi_c) + Bi_c \sinh(\phi_c)] = Bi_c \quad (3.53)$$

$$C_1 = \frac{Bi_c}{[\phi_c \cosh(\phi_c) - \sinh(\phi_c) + Bi_c \sinh(\phi_c)]} \quad (3.54)$$

$$C_1 = \frac{Bi_c}{[\phi_c \cosh(\phi_c) + \sinh(\phi_c)(Bi_c - 1)]} \quad (3.55)$$

Now that we know the value of C_1 we can replace it in

$$\theta = \frac{C_1 \sinh(\phi_c \eta)}{\eta} \quad (3.56)$$

Thus resulting in,

$$\theta = \frac{Bi_c}{[\phi_c \cosh(\phi_c) + \sinh(\phi_c)(Bi_c - 1)]} \frac{\sinh(\phi_c \eta)}{\eta} \quad (3.57)$$

Or simply,

$$\theta = \frac{Bi_c \sinh(\phi_c \eta)}{\eta [\phi_c \cosh(\phi_c) + \sinh(\phi_c)(Bi_c - 1)]} \quad (3.58)$$

Boxed in red, is the concentration profile in the radial direction from the plasma membrane ($\eta = 1$) to the center of the cell ($\eta = 0$). This conservative solution where $\lambda = 0$ is sufficient for determining whether spatial dependency is significant within the cytosol. The spatial independency is valid provided,

$$\theta_{\eta=0} / \theta_{\eta=1} = \frac{\phi_c}{\sinh(\phi_c)} \approx 1. \quad (3.59)$$

The more general solution for arbitrary θ can be found as follows,

$$\frac{d}{d\eta} \left(\frac{d\theta}{d\eta} \right) = \phi^2 \theta \quad (3.60)$$

$$\phi^2 = \frac{k_{obs} r_c^2}{D_{ij}} \quad (3.26)$$

$$\left. \frac{d\theta}{d\eta} \right|_{\eta=1} = \frac{m_{plm} r_c}{\varphi_c D_{ij}} [1 - \theta|_{\eta=1}] \quad (3.61)$$

Let,

$$Bi = \frac{m_{plm} r_c}{\varphi_c D_{ij}} [1 - \theta|_{\eta=1}] \quad (3.62)$$

And,

$$\left. \frac{d\theta}{d\eta} \right|_{\eta=\lambda} = 0 \quad (3.63)$$

$$\lambda = \frac{r_n}{r_c} \quad (6.64)$$

Solved in Mathematica to obtain:

$$\theta = \frac{Bi e^{\sqrt{\phi^2 - \sqrt{\phi^2} x} (-e^{2\sqrt{\phi^2} \lambda} + e^{2\sqrt{\phi^2} x} + \sqrt{\phi^2} e^{2\sqrt{\phi^2} \lambda} \lambda + \sqrt{\phi^2} e^{2\sqrt{\phi^2} x} \lambda)}{(-e^{2\sqrt{\phi^2} + \sqrt{\phi^2} e^{2\sqrt{\phi^2} + Bi e^{2\sqrt{\phi^2} + e^{2\sqrt{\phi^2} \lambda} + \sqrt{\phi^2} e^{2\sqrt{\phi^2} \lambda} - Bi e^{2\sqrt{\phi^2} + \phi^2 e^{2\sqrt{\phi^2} \lambda - \sqrt{\phi^2} e^{2\sqrt{\phi^2} \lambda} + \sqrt{\phi^2} Bi e^{2\sqrt{\phi^2} \lambda - \phi^2 e^{2\sqrt{\phi^2} \lambda - \sqrt{\phi^2} e^{2\sqrt{\phi^2} \lambda} + \sqrt{\phi^2} Bi e^{2\sqrt{\phi^2} \lambda} x)} \quad (3.65)$$

Eqn (3.65) is the more general solution, but again Eqn (3.58) is sufficient in determining the concentration profile inside the cell as it is the more conservative solution.

3.4.2 Pseudo steady-state assumption

The assumption that C_{ext} is constant is valid for an infinite source approximation (relatively large volumes). For studies that require a finite V_{ext} however, this approximation is reasonable provided the time for the steady-state is substantially less than the process overall time constant. A conservative overall time constant can be determined by reviewing Eqn (3.4) and assuming $C_{in} \approx 0$. Making dimensionless by defining the dimensionless concentration as $\theta_{ext} = \frac{C_{ext}(t)}{C_{ext0}}$ and the time constant is t over the characteristic time,

$\tau_x \equiv \frac{t}{t_x}$ we are left with,

$$\frac{d\theta_{ext}}{d\tau_x} = -\theta_{ext} \quad (3.24)$$

Then the process overall time constant, can be written as

$$t_x \equiv \frac{V_{ext}}{\varphi_{plm} m_{plm} A_{cell} n_{cell}}. \quad (3.25)$$

Thus, the steady-state approximation provides a reasonable approximation when the final time for the study, t_f is such that $t_f \ll t_x$.

3.4.3 Estimation of average external H₂O₂ for clonogenic assay

When t_f is not much less than τ , the external concentration in the sample volume can reduce with time. For a matter of dosing, the timed-average external concentration, \bar{C}_{ext} , can be used to represent the dosing concentration during the study. This value can be determined by solving for $C_{ext}(t)$ using Eqn (3.4 – 3.6) and numerically determining

$$\bar{C}_{ext} = \frac{1}{t_f} \int_0^{t_f} C_{ext}(t) dt. \quad (3.26).$$

CHAPTER 4. EXPERIMENTAL APPROACH FOR DETERMINING INTRACELLULAR H₂O₂ DURING THERAPY

4.1 Determining appropriate parameters to calculate θ_{ss}

The cellular properties that could influence θ_{ss} include membrane permeabilities, catalase concentration as well as the cell and peroxisome geometry and peroxisome number density. Thus, each of the parameters in Eqn (3.7) were experimentally determined to obtain the calculated θ_{ss} value for each cell line.

The cell-specific radius (μm) and cell volume (pL) were obtained using an automated cell counter (Moxi Z Mini Automated Cell Counter, ORFLO Technologies, Ketchum, ID, USA). Using the radii information generated from the instrument, the cell area was calculated (A_{cell}).

Confocal microscopy is used to obtain z-stack images of the cells to obtain both peroxisome information (V_p, A_p, n_p) as well as information on the cell nucleus; the latter is necessary to determine the volume of the cell not occupied by the nucleus (V_{in}).

H₂O₂ consumption studies using extracted catalase free in solution were conducted to obtain the cell-specific catalase concentration of each cell under investigation.

These results were coupled with confocal images providing cell-specific peroxisomes counts (n_p) and peroxisome volumes (V_p) to determine the catalase concentration per peroxisome (C_{cat_p}).

The two membrane permeabilities, m_{plm} and m_p , were determined as regressed parameters from modeling the transient H_2O_2 uptake experimental data from independent studies using intact cells and isolated intact peroxisomes.

4.2 Materials and Methods

4.2.1 Cells and Reagents

Pancreatic H6c7 cells (HPV16-E6E7) [50] were established by transduction of HPV16-E6E7 genes into a primary culture of normal pancreatic duct epithelial cells and cultured in keratinocyte SFM (KSFM, Invitrogen, Carlsbad, CA) with supplements: human recombinant epidermal growth factor and bovine pituitary extract (Life Technologies, Carlsbad, CA, USA). Pancreatic adenocarcinoma MIA PaCa-2 cells (American Type Culture Collection Manassas, VA, USA) were cultured in Dulbecco's Modified Eagle's Medium (DMEM, American Type Culture Collection Manassas, VA, USA) with 10% fetal bovine serum (FBS, ThermoFisher Scientific, Lafayette, CO, USA). Glioblastoma U-87 MG cells (American Type Culture Collection Manassas, VA, USA) were cultured in Eagle's Minimum Essential Medium (EMEM, American Type Culture Collection Manassas, VA, USA) with 10% fetal bovine serum (FBS, ThermoFisher Scientific, Lafayette, CO, USA). Glioblastoma T98G cells (American Type Culture Collection

Manassas, VA) were cultured in Eagle's Minimum Essential Medium (EMEM American Type Culture Collection Manassas, VA, USA) with 10% fetal bovine serum (FBS, ThermoFisher Scientific, Lafayette, CO, USA). Glioblastoma LN-229 (American Type Culture Collection Manassas, VA, USA) were cultured in Dulbecco's Modified Eagle's Medium (DMEM, American Type Culture Collection Manassas, VA, USA) with 5% fetal bovine serum (FBS, ThermoFisher Scientific, Lafayette, CO, USA). All cells were maintained at incubation of 37°C and supplied with 5% CO₂ and 1% penicillin streptomycin (Life Technologies, Carlsbad, CA, USA).

4.2.2 Clonogenic Assessment

Glioblastoma Cells (2.5×10^4) were seeded in 6-well culture (Corning, Union City, CA, USA) treated dishes and exposed to appropriate H₂O₂ doses 48 h later. H₂O₂ exposures of (0 - 90 μ M) were diluted in the appropriate culture media and cells were exposed for 1 h at 37°C. After exposure, the diluted media was removed, cells were trypsinized and counted with the Moxi Z Mini Automated Cell Counter and re-plated at 100 cells mL⁻¹ in triplicates with appropriate media in 6-well culture treated dishes. Plates were incubated for two weeks at 37°C, 5% CO₂ and colonies formed between 10 to 14 d at 37°C. Following a two-week incubation period, the colonies were fixed with 70% ethanol and stained with Coomassie Brilliant Blue R-250 (1610436; BioRad, Hercules, CA). Colonies with more than 50 cells were counted using a Counter-Pen (3133; Traceable Products, Webster, TX). The plating efficiency (PE) and surviving fraction (SF) were determined; PE = (colonies counted/cells plated) x 100 and SF = (PE of treated sample/PE of control) x 100 [53, 54]. Statistical significance between each H₂O₂ exposure dose and cell types or cell

modification was determined through ANOVA (Single Factor). P-values less than 0.05 were accepted as indicating a statistical significant difference. Error bars displayed represent the standard error (SE). Data were analyzed and plotted using Excel-2007 (Microsoft; Redmond, WA), and SigmaPlot (Systat Software Inc; San Jose, CA, USA) software. Clonogenic results for pancreatic cells were determined previously [58].

4.2.3 Confocal Imaging: peroxisomes and cell nucleus

Cells were seeded on glass cover slips (ThermoFisher Scientific, Lafayette, CO, USA) in complete growth medium and incubated at 37 °C, 5 % CO₂ for 48 h to allow 70% confluency to be reached. Adhered cells were transduced with 50 particles per cell (PPC) of CellLight Regents BacMam 2.0 (C10604, ThermoFisher Scientific, Lafayette, CO, USA) and mixed gently to allow peroxisome tagging. GFP transduced cells were incubated at 37 °C, 5 % CO₂ for 48 h before fixing with paraformaldehyde (4% PFA) for 15 min. PFA was removed by three 5-min 1x PBS washes. Glass coverslips containing GFP-tagged peroxisome cells were mounted on microscope slides (ThermoFisher Scientific, Lafayette, CO, USA). NucBlue Live Cell Stain ReadyProbes reagent (R37605; Life Technologies, Carlsbad, CA, USA) was added to stain the nucleus of cells. Z-stack images were taken with the Lecia SP5 confocal microscope (Lecia, Solms, Germany) and analyzed using ImageJ (NIH). Z-stack images were taken to visualize the entire cell and peroxisomes were counted per slice for each cell line. ImageJ (NIH) was used to measure 3 radii measurements for each peroxisome. In addition, ImageJ (NIH) was used to measure 3 peroxisome-to-peroxisome distances spanning the cell.

The latter values provide insight to whether peroxisomes are near the cell membrane or perinuclear. Lastly, ImageJ (NIH) was used to calculate the nucleus volume by combining the z-stacks images of the analyzed particle outlining the nucleus in each plane.

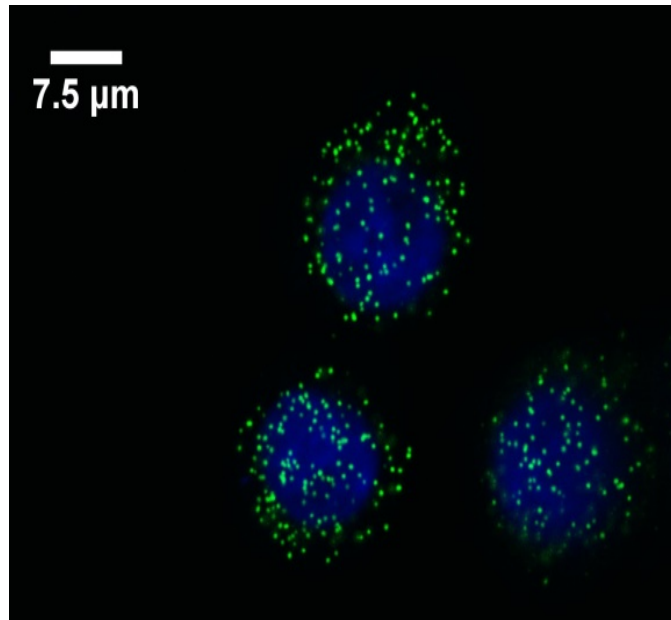


Fig 4.1. An example image of normal pancreatic (H6c7) cells taken from a series of z-stack images using the Leica SP5 confocal microscope to identify peroxisomes per cell. The image displays the nucleus (blue) and peroxisomes (green). Peroxisomes were counted in each z-stack slice to obtain the number of peroxisomes per cell. Additionally, measurements for peroxisome-to-peroxisome across the cell confirmed that the peroxisomes are not perinuclear but are indeed well mixed throughout the cell. For example, the average value for peroxisome-to-peroxisome for the MIA PaCa-2 cells provides a value of $18.5 \times 10^{-6} m$, thus suggesting a cell radius of $9.25 \times 10^{-6} m$. This value falls within the radius of the MIA PaCa-2 cell provided by the Moxi^Z automated cell counter (refer to Table 5.1); thus, peroxisomes are located throughout the cell including near the cell plasma membrane. Another verification for future confirmation would be to conduct three stains consisting of the nucleus, peroxisomes and the plasma membrane wall.

4.2.4 Determining catalase concentration

Catalase concentration, C_{cat_p} , was measured in each cell lysates¹ using a spectrophotometric-based assay [67]. Cells were harvested at a density of $(1.0 - 5.0) \times 10^6$ cells in PBS (3 mL) using a cell scraper (Fisher Scientific, Pittsburgh, PA, USA). The cell count was determined using a MoxiZ Mini Automated Cell Counter to provide the number of cells used in the assay. Scraped cells were centrifuged (Marathon 8K Centrifuge) at 1000 rpm for 5 min. Cells were re-suspended in PBS (1 mL) and transferred to an Eppendorf tube (Fisher Scientific, Pittsburgh, PA, USA) and subsequently centrifuged (Marathon 8K Centrifuge) 2x at 1000 rpm for 5 min. Following the last spin, PBS (1 mL) was layered on top of the pellet and placed in the freezer (-80 °C) for 24 h. Cells were then sonicated (Qsonica, Newtown, CT, USA) 4x for 10 sec intervals with 30 sec breaks at 100% amplitude to fully lyse the cells. It was assumed that the catalase is fully released from sonication and well dispersed into the suspension of the lysate. The cell lysate was further diluted in 50 mM phosphate buffer (pH 7.0), placed in a quartz cuvette (Thorlabs, Newton, NJ, USA) and, 30 mM H₂O₂ (Sigma-Aldrich, St. Louis, MO, USA) was added. The H₂O₂ consumption was followed by the decay in absorbance (@240 nm) over time. Absorbance was measured every 10 s for a total of 25 min. The slope of the logarithmic curve (ln[H₂O₂ absorbance] vs. time (s)) provided the observed rate (k_{obs}) of H₂O₂ consumption. Using the catalytic rate constant per monomer [64], $k_2 = 1.7 \times 10^7 M^{-1} s^{-1}$, and the known number of cells in the chamber (n_{cell}), k_{obs} was used to calculate the active catalase

¹ The catalase concentration regarding the H6c7 cells were kindly provided by our collaborators Dr. Garry R. Buettner and Dr. Claire M. Doskey. All other cell lines were conducted in our lab.

molecules per cell. Acknowledging catalase as a tetramer, the number of tetramers per cell was $\frac{1}{4}$ the monomer count. Subsequently, the confocal images provided the number and volume of peroxisomes for each cell and thus allows $C_{cat_p} = \left[\frac{Cat_{cell}}{V_p n_p} \right]$ to be determined. The error in C_{cat_p} was determined by propagating error associated with Cat_{cell} , the number of peroxisomes per cell, n_p , and the volume of the peroxisome V_p .

4.2.5 Peroxisome isolation

Peroxisomes were extracted from cells using a fractionation centrifugation method. The series of centrifugations were adjusted from the protocol provided by Sigma-Aldrich (Peroxisome Isolation kit, PEROX1, Sigma-Aldrich, St. Louis, MO, USA). Cells were seeded into HyperFlask M cell culture vessels (13700420, Corning, Union City, CA, USA) and incubated at 37 °C until 100% confluency was reached (2×10^8 cells). Cells were harvested using accutase (25-058-CI, Sigma-Aldrich, St. Louis, MO, USA)(50 mL) and PBS (50 mL) was added to increase the volume to extract all cells from the HyperFlask. Accutase was quenched using FBS (100 mL) and the cell suspension (200 mL) was transferred and subsequently centrifuged (Marathon 8K Centrifuge, Beckman Coulter, Brea, CA, USA) 3x at 2,364 rpm (250 x g) for 5 min at room temperature. The supernatant was discarded and cells were re-suspended in 15 mL PBS between spins. Before the final spin, the number of cells were determined using a Moxi Z Mini Automated Cell Counter. A packed cell volume (PCV) (1 – 3 mL), resulting from the third spin, was re-suspended in ice-cold (4°C) 1x peroxisome extraction buffer (PEB) (4 – 5 mL) (7247, Sigma-Aldrich, St. Louis, MO, USA) containing protease inhibitor cocktail 1% (v/v)(P8340, Sigma-

Aldrich, St. Louis, MO, USA). The suspension was transferred to a 7 ml Dounce glass tissue grinder (T0566, Sigma-Aldrich, St. Louis, MO, USA) and a clearance pestle (P1235, Sigma-Aldrich, St. Louis, MO, USA) was used to cause 80 – 85% breakage (~7 strokes). Cell aliquots were stained using Trypan Blue (Sigma-Aldrich, St. Louis, MO, USA) every 5 strokes and counted (dilution factor of 5) using a hemocytometer to monitor breakage. After sufficient cell breakage, cells were centrifuged (Optima ultracentrifuge, Beckman Coulter, Brea, CA, USA) at 3,400 rpm (500 x g) (Type 90 Ti rotor) for 10 min at 4°C. The supernatant was transferred to ice while the pellet was re-suspended in 1x PEB (4 – 5 ml) and subsequently centrifuged at 3,400 rpm (500 x g) for 10 min at 4°C. The supernatants were combined in a new tube and spun at 8,400 rpm (6,000 x g) for 10 min at 4°C. The supernatant was transferred to a new tube and centrifuged at 15,000 rpm (20,000 x g) for 15 min at 4°C. The supernatant was discarded and the pellet re-suspended in ice cold (4°C) 1x PEB. Cells were centrifuged at 4,200 rpm (1500 x g) for 10 min at 4°C to result in a crude peroxisome fraction (CPF). The CPF (1.2 mL) was diluted in the Optiprep density gradient (1.69 mL) (D1556, Sigma-Aldrich, St. Louis, MO, USA) and 1x Optiprep dilution buffer (1.61 mL) (O4889, Sigma-Aldrich, St. Louis, MO, USA). The CPF (4 mL) was then layered between a 27.5% (2 mL) and 20% (2 mL) Optiprep density gradient (D1556, Sigma-Aldrich, St. Louis, MO, USA). The sample was centrifuged at 34,163 rpm (100,000 x g) for 1.5 h at 4°C. Samples following the final centrifugation, if stored, remained in the 4°C for a maximum of 24 h before studies were conducted.

4.2.6 Determining peroxisome membrane permeability

The rate of H₂O₂ uptake for intact peroxisomes extracted from all cells were measured in a similar fluorescent based manner as described previously by Wagner et al. [51]. The adjusted protocol measures the change in extracellular H₂O₂ over time, which decays exponentially representing a pseudo-first order behavior of the intracellular catalase reaction. The technique is a highly sensitive fluorescent method capable of detecting low concentrations of H₂O₂, below 0.5 μM. Isolated peroxisomes (specific to each case were diluted in 50 mM phosphate buffer (pH 7.0), placed into a reaction chamber (6 mL). The reaction chamber (roughly (7 – 12) × 10⁸ peroxisomes) is initiated by the addition of an extracellular bolus of 30 mM H₂O₂ (Sigma-Aldrich, St. Louis, MO, USA) and aliquots (30 μL, chosen to prevent >10% of total volume from being removed) were taken at specified time points (0, 2, 8, 10, 12, 14, 16, 18, 20, and 25 min). Aliquots were transferred, in duplicates, to designated wells of 96-well culture (Corning, Union City, CA, USA) dish. The wells (F2-F11, G2-G11) contained phosphate buffer (30 μL) and a quenching solution (60 μL) comprised of 20 mL phosphate buffer (pH 7.0), 20 μL 1M 4-(2-hydroxyethyl)-1-piperazineethansulfonic acid (HEPES) (pH 7.2 – 7.5) (ThermoFisher Scientific, Lafayette, CO, USA), 10 mg NaHCO₃ (3mM) (ThermoFisher Scientific, Lafayette, CO, USA), 5 mg 4-hydroxyphenylacetic acid (*p*HPA) (Sigma-Aldrich, St. Louis, MO, USA), and 2 mg HRP (horse radish peroxidase Type 1) (Sigma-Aldrich, St. Louis, MO, USA). The stopping solution was used to terminate peroxisome uptake at the desired time point. The quenching solution prevents any remaining H₂O₂ from entering the peroxisome as H₂O₂ instead activates HRP which in turn oxidizes *p*HPA resulting in the fluorescent *p*HPA

dimer. The fluorescent signal is representative of the H_2O_2 concentration in each well and is further detected via the Tecan F200 (Tecan US, Morrisville, NC) plate reader with an excitation at 340 nm (bandwidth 20 nm) and monitoring an emission at 430 nm (bandwidth 20 nm) from above the wells. Additionally, designated wells (B2 – B11, C2 – C11, D2 – D11) contained standard solutions (60 μL) having ten different final concentrations of H_2O_2 (4, 3.6, 3.2, 2.8, 2.4, 2, 1.6, 1.2, 0.8, 0.4 mM) after the addition of the stopping solution (60 μL), completing a final volume of 120 μL . The number of peroxisomes in the reaction chamber were determined after knowing the peroxisome count per cell (see Section 4.3) and determining the number of cells using a Moxi Z Mini Automated Cell Counter used during the peroxisome extraction. The transient data provided from this observed decay in H_2O_2 over time and knowing the number of peroxisomes (n_p) and total volume of extracellular media (V_{ext}) allows for the regression for the peroxisome membrane permeability (m_p). Statistical significance between m_p was determined through ANOVA (Single Factor) and the presented errors are the standard deviations. The m_p across cell lines were all non-significant from one another except for H6c7 cells. P-values less than 0.05 were accepted as indicating a statistical significant difference. Data were analyzed and plotted using Excel-2007 (Microsoft; Redmond, WA), and SigmaPlot (Systat Software Inc; San Jose, CA, USA) software.

4.2.7 H₂O₂ uptake study (whole cell intact): to regress for m_{plm}

The rate of H₂O₂ uptake for each cell line² were measured, in the same manner as described previously by Wagner et al. [51]. This assay provides an extracellular H₂O₂ removal rate, on a per cell basis. The assay measures the change in extracellular H₂O₂ over time, which decays exponentially representing a pseudo-first order behavior of the intracellular catalase reaction. The technique is a highly sensitive fluorescent method capable of detecting low concentrations of H₂O₂, below 0.5 μM. Briefly, cells were seeded in 96-well culture (Corning, Union City, CA, USA) treated dishes and incubated 48 h prior to the assay at 37°C, 5% CO₂; 90% confluency was reached. An extracellular bolus of 20 μM H₂O₂ (Sigma-Aldrich, St. Louis, MO, USA) was introduced in 5 min intervals to defined wells containing cells. A quenching solution comprised of 20 mL 1x HBSS (ThermoFisher Scientific, Lafayette, CO, USA), 20 μL 1M 4(-2-hydroxyethyl)-1-piperazineethansulfonic acid (HEPES) (pH 7.2–7.5) (ThermoFisher Scientific, Lafayette, CO, USA), 10 mg NaHCO₃ (3mM) (ThermoFisher Scientific, Lafayette, CO, USA), 5 mg 4-hydroxyphenylacetic acid (pHPA) (Sigma-Aldrich, St. Louis, MO, USA), and 2 mg HRP (horse radish peroxidase Type 1) (Sigma-Aldrich, St. Louis, MO, USA) was used to terminate the assay. The quenching solution prevents any remaining H₂O₂ from entering the cell as H₂O₂ instead activates HRP which in turn oxidizes pHPA resulting in the fluorescent pHPA dimer. The fluorescent signal is representative of the H₂O₂ concentration in each well and is further detected via the Tecan F200 plate reader with an excitation at

² The rate of uptake for the H6c7 cells were kindly provided by our collaborators Dr. Garry R. Buettner and Dr. Claire M. Doskey to remain consistent with the provided catalase concentration for this cell line.

340 nm (bandwidth 20 nm) and monitoring an emission at 430 nm (bandwidth 20 nm) from above the wells. Wells containing cells were trypsinized and the number of cells were determined using a Moxi Z Mini Automated Cell Counter. The transient data provided from this observed decay in H_2O_2 over time and knowing the number of cells (n_{cells}) and total volume of extracellular media (V_{ext}) allows for the regression for the plasma membrane permeability (m_{plm}). Statistical significance between m_{plm} was determined through ANOVA (Single Factor) and the presented errors are the standard deviations. Cells were counted at the end of the experiment. P-values less than 0.05 were accepted as indicating a statistical significant difference. Data were analyzed and plotted using Excel-2007 (Microsoft; Redmond, WA), and SigmaPlot (Systat Software Inc; San Jose, CA, USA) software.

CHAPTER 5. CELL-SPECIFIC PARAMETERS AND RESULTING INTRACELLULAR H₂O₂

5.1 Parameters used for determining θ_{ss}

Table 5.1 summarizes the parameters used for each of the cell lines used. Cell physical properties were similar however, there is a substantial range in both the catalase concentration within the peroxisomes and membrane permeability. The peroxisome catalase concentration ranges from $(7.98 \pm 5.69) \times 10^{-6} M$ to $(10.8 \pm 6.3) \times 10^{-5} M$ for the MIA PaCa-2 to the U-87 MG, respectively. There is also a wide range in plasma membrane permeability going from $(2.23 \pm 1.72) \times 10^{-6} m s^{-1}$ to $(7.14 \pm 2.72) \times 10^{-6} m s^{-1}$ for the siAQP3 MIA PaCa-2 to the unmodified MIA PaCa-2 cell lines, respectively. The respective P-value comparisons for these cell lines are presented in Table 5.2 The peroxisome membrane permeability ranged from $(0.38 \pm 0.17) \times 10^{-5} m s^{-1}$ for the normal H6c7 cell line to $(2.13 \pm 1.21) \times 10^{-5} m s^{-1}$ for MIA PaCa-2. The peroxisome membrane permeability across cell lines were not significantly different from one another, except the H6c7 cells which had a $P < 0.05$ across for each cell type.

Another mentionable note is that while large variations are not present across cell types in regards to the cell and nucleus volumes independently, it is important to recognize that the cytosolic volume (intracellular volume not occupied by the nucleus) results from the subtraction of these two values and thus leads to potential error in the calculated θ_{ss} value. Here the Moxi Z Mini Automated Cell Counter was used to obtain the cell-specific volume

[ranging from $(2.8 - 4.36) \times 10^{-15} \text{ m}^3$] which is based on a spherical assumption, yet the volume of the nucleus (ranging from $(1.4 - 2.3) \times 10^{-15} \text{ m}^3$) was obtained via confocal z-stack images analyzed in ImageJ and is ellipsoidal. Subtracting the spheroid nucleus from the spherical cell volume has the potential to lead to error within not only this parameter but also the concentration within this region. A variation in the radial direction is on the order of r^3 , and thus could lead to dramatic differences in catalase concentration within the volume of interest. This is later evaluated within the sensitivity analysis of θ_{ss} to the calculated intracellular Volume V_{in} .

There is not a large variation across cell lines in regards to the peroxisome counts, the range falls between 211 - 374 peroxisomes per cell for U-87 and H6c7 respectively. It is safe to assume that the cells were transduced/transfected efficiently and uniformly across cell types and that all peroxisomes within the cells were fluorescently detected.

The other parameters did not display a large variation across cell types. The volume of the peroxisomes range from $(5.8 \pm 1.2) \times 10^{-20} \text{ m}^3$ for LN-229 cells to $(1.87 \pm 1.59) \times 10^{-19} \text{ m}^3$ for H6c7. The area of the peroxisomes range from $(8.1 \pm 4.0) \times 10^{-13} \text{ m}^2$ for LN-229 cells to $(1.5 \pm 0.82) \times 10^{-12} \text{ m}^2$ to T98G cells. And the catalase monomers per cell range from $(128,000 \pm 37,200)$ for MIA PaCa-2 cells to $(875,000 \pm 152,000)$ for U-87 cells. Or this value may also be represented as the catalase concentration per peroxisome $(7.98 \pm 5.69) \times 10^{-6} \text{ M}$ for MIA PaCa-2 and $(1.08 \pm 0.63) \times 10^{-4} \text{ M}$ for U-87 cells.

The combined variability of these parameters could significantly alter the dimensionless intracellular H_2O_2 concentration, θ_{ss} , during dosing to ultimately effect the surviving fraction.

Table 5.1. Summary of Cellular Parameters by Cell Type

Variable	Variable (Units)	MIA PaCa-2	MIA PaCa-2 SiAQP3	H6c7 Cells	Reference/Notes
Cell Radius	(m)	$(8.29 \pm 1.13) \times 10^{-6}$	$(8.29 \pm 1.13) \times 10^{-6}$	$(8.74 \pm 0.14) \times 10^{-6}$	Moxi ^Z N = 3
Cell Area	$A_{cell} (m^2)$	$(0.87 \pm 0.27) \times 10^{-9}$	$(0.87 \pm 0.27) \times 10^{-9}$	$(0.97 \pm 0.03) \times 10^{-9}$	Calculated
Cell Volume	$V_{cell} (m^3)$	$(2.52 \pm 0.98) \times 10^{-15}$	$(2.52 \pm 0.98) \times 10^{-15}$	$(2.8 \pm 0.13) \times 10^{-15}$	Moxi ^Z N = 3
Nucleus Volume	(m^3)	$(1.67 \pm 0.15) \times 10^{-15}$	$(1.67 \pm 0.15) \times 10^{-15}$	$(1.43 \pm 0.16) \times 10^{-15}$	Dapi Confocal N = 4/5
Cell Volume without Cell Nucleus	(m^3)	8.5×10^{-16}	8.5×10^{-16}	1.4×10^{-15}	Calculated
Plasma Membrane Partitioning Coefficient	φ_{plm}	1	1	1	Assumption
Number peroxisomes	n_p	(310 ± 115)	(310 ± 115)	(374 ± 117)	GFP Confocal N = 6
Peroxisome Volume	$V_p (m^3)$	$(8.59 \pm 4.85) \times 10^{-20}$	$(8.59 \pm 4.85) \times 10^{-20}$	$(1.87 \pm 1.59) \times 10^{-19}$	Spherical Estimation GFP Confocal N = 6
Peroxisome Area	$A_p (m^2)$	$(9.12 \pm 3.41) \times 10^{-13}$	$(9.12 \pm 3.41) \times 10^{-13}$	$(1.49 \pm 0.81) \times 10^{-12}$	GFP Confocal N = 6
Active Catalase Monomers	--	$(128,000 \pm 37,200)$	$(128,000 \pm 37,200)$	$(399,000 \pm 23,900)$	Catalase free in solution studies
Catalase Concentration in Peroxisome	$[C_{cat}]_p (M)$	$(7.98 \pm 5.69) \times 10^{-6}$	$(7.98 \pm 5.69) \times 10^{-6}$	$(9.48 \pm 8.61) \times 10^{-6}$	Propagated error
Catalase Rate per peroxisome	$k_p (s^{-1})$	136	136	161	Calculated
Catalase Concentration in Cell	$[C_{cat}]_{cell} (mol m^3)$	$(8.45 \pm 4.11) \times 10^{-8}$	$(8.45 \pm 4.11) \times 10^{-8}$	$(2.37 \pm 0.18) \times 10^{-7}$	Propagated error
Catalase Rate Constant per Monomer	$k_{chance} (M^{-1} s^{-1})$	1.7×10^7	1.7×10^7	1.7×10^7	[64]
Plasma Membrane Permeability	$m_{plm} (m s^{-1})$	$(7.14 \pm 2.72) \times 10^{-6}$	$(2.23 \pm 1.72) \times 10^{-6}$	$(2.56 \pm 0.79) \times 10^{-6}$	Regressed
Peroxisome Membrane Permeability	$m_p (m s^{-1})$	$(2.13 \pm 1.21) \times 10^{-5}$	$(2.13 \pm 1.21) \times 10^{-5}$	$(0.38 \pm 0.17) \times 10^{-5}$	Regressed
Peroxisome Membrane Partition Coefficient	φ_p	1	1	1	Assumption

Variable	Variable (Units)	U-87	T98G	LN-229	Reference/Notes
Cell Radius	(m)	$(9.49 \pm 0.20) \times 10^{-6}$	$(10.1 \pm 0.50) \times 10^{-6}$	$(8.22 \pm 1.37) \times 10^{-6}$	Moxi ^Z N = 3
Cell Area	$A_{cell} (m^2)$	$(1.13 \pm 0.05) \times 10^{-9}$	$(1.29 \pm 0.12) \times 10^{-9}$	$(8.79 \pm 2.35) \times 10^{-10}$	Calculated
Cell Volume	$V_{cell} (m^3)$	$(3.58 \pm 0.23) \times 10^{-15}$	$(4.36 \pm 0.64) \times 10^{-15}$	$(2.52 \pm 1.17) \times 10^{-15}$	Moxi ^Z N = 3
Nucleus Volume	(m^3)	$(1.43 \pm 0.26) \times 10^{-15}$	$(1.79 \pm 0.28) \times 10^{-15}$	$(2.34 \pm 0.11) \times 10^{-15}$	Dapi Confocal N = 3
Cell Volume without Cell Nucleus	(m^3)	2.2×10^{-15}	2.6×10^{-15}	1.8×10^{-16}	Calculated
Plasma Membrane Partitioning Coefficient	φ_{plm}	1	1	1	Assumption
Number peroxisomes	n_p	(211 ± 24)	(231 ± 74)	(296 ± 77)	GFP Confocal N = 4
Peroxisome Volume	$V_p (m^3)$	$(6.4 \pm 3.5) \times 10^{-20}$	$(9.2 \pm 5.6) \times 10^{-20}$	$(5.8 \pm 1.2) \times 10^{-20}$	Spherical Estimation GFP Confocal N = 4
Peroxisome Area	$A_p (m^2)$	$(9.4 \pm 4.1) \times 10^{-13}$	$(1.5 \pm 0.82) \times 10^{-12}$	$(8.1 \pm 4.0) \times 10^{-13}$	GFP Confocal N = 4
Active Catalase Monomers	--	$(875,000 \pm 152,000)$	$(794,000 \pm 51,000)$	$(439,000 \pm 48,000)$	Catalase free in solution studies
Catalase Concentration in Peroxisome	$[C_{cat}]_p (M)$	$(1.08 \pm 0.63) \times 10^{-4}$	$(6.21 \pm 4.29) \times 10^{-5}$	$(4.25 \pm 1.49) \times 10^{-5}$	Propagated error
Catalase Rate per Peroxisome	$k_p (s^{-1})$	1.83×10^3	1.05×10^3	7.22×10^2	Calculated
Catalase Concentration in Cell	$[C_{cat}]_{cell} (mol m^3)$	$(4.06 \pm 0.75) \times 10^{-7}$	$(3.02 \pm 0.49) \times 10^{-7}$	$(2.89 \pm 1.38) \times 10^{-7}$	Propagated error
Catalase Rate Constant per Monomer	$k_{chance} (M^{-1} s^{-1})$	1.7×10^7	1.7×10^7	1.7×10^7	[64]
Plasma Membrane Permeability	$m_{plm} (m s^{-1})$	$(2.52 \pm 1.02) \times 10^{-6}$ (N = 3)	$(5.70 \pm 1.53) \times 10^{-6}$ (N = 3)	$(3.03 \pm 0.67) \times 10^{-6}$ (N = 4)	Regressed for N = 3/3/4
Peroxisome Membrane Permeability	$m_p (m s^{-1})$	$(1.55 \pm 0.79) \times 10^{-5}$ (N = 4)	$(1.87 \pm 1.22) \times 10^{-5}$ (N = 3)	$(1.94 \pm 0.87) \times 10^{-5}$ (N = 3)	Regressed for N = 4/3/3
Peroxisome Membrane Partition Coefficient	φ_p	1	1	1	Assumption

Table 5.2: Significance between reported m_{plm} values

Cell Type	P- Value
H6c7 MIA PaCa-2	P < 0.0001
MIA PaCa-2 MIA PaCa-2 siAQP3	P < 0.001
LN-229 MIA PaCa-2	P < 0.001
MIA PaCa-2 siAQP3 T98G	P < 0.05
T98G H6c7	P < 0.001
T98G LN229	P < 0.001

5.2 θ_{ss} and its validation of lumped parameter assumption

Eqn (3.19) was used to determine the spatial independence of the intracellular concentration profile. All cell lines showed reasonable spatial independence. Table 5.3 summarizes the Biot and Thiele modulus used in this estimate.

Table 5.3: Parameters Used to Verify Spatial Independence of θ_{ss}

	Cell Type	Bi_c	ϕ_c	$\theta_{\eta=0}/\theta_{\eta=1}$
Pancreatic Cells	MIA PaCa-2 Unmodified	0.04	0.360	0.98
	MIA PaCa-2 siAQP3	0.01	0.360	0.98
	H6c7	0.02	0.572	0.95
Glioblastoma Cells	U-87	0.02	0.271	0.99
	T98G	0.04	0.364	0.98
	LN-229	0.02	0.948	0.86

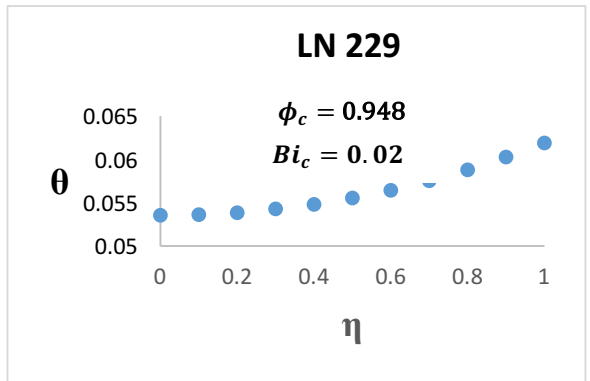
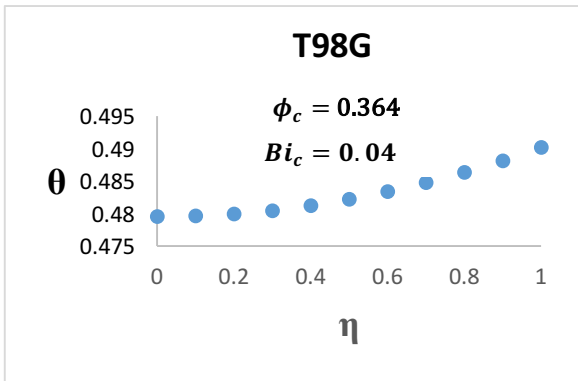
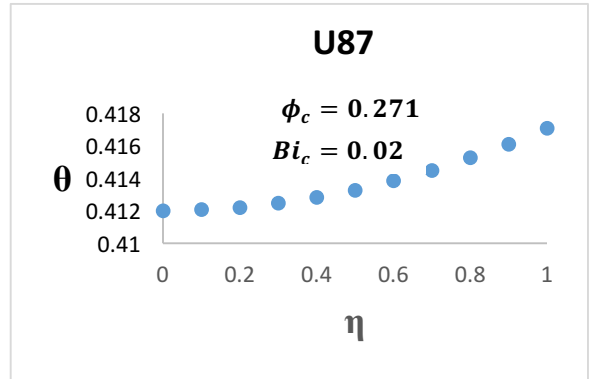
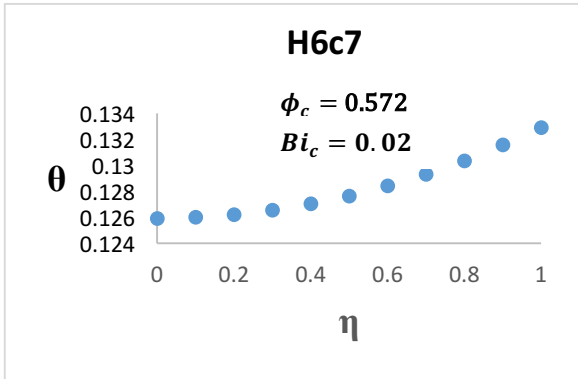
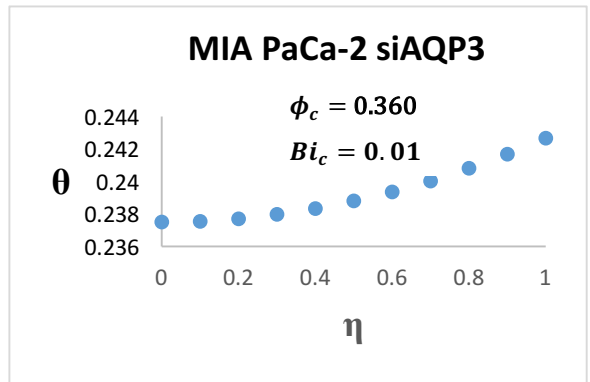
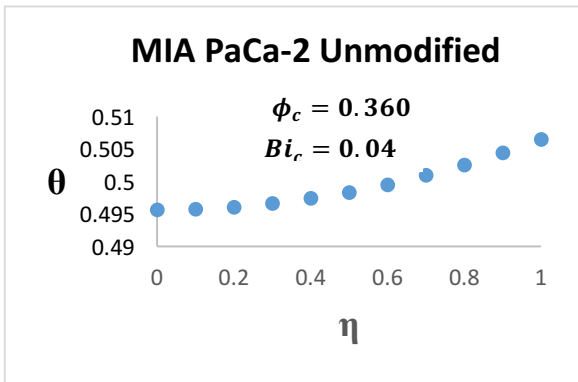


Fig 5.1 Displays each cell line and the spatial dependency for H₂O₂ inside the cell. Spatial variations within the cytosolic space may be ignored. As H₂O₂ travels from the plasma membrane, $\eta = 1$, to the center of the cell, $\eta = 0$, there is no depreciable drop in H₂O₂ concentration. We also see this presented in Table 5.3 where $\theta_{\eta=0}/\theta_{\eta=1}$ is about equal to 1. The largest drop in intracellular H₂O₂ is less than 20% thus allowing the spatial contributions to be considered negligible. The largest change in intracellular H₂O₂ concentration is a 15% reduction at the center for the LN-229 cells.

5.3 Extracellular concentration during dosing

It has been argued that dose exposures are more appropriately presented in terms of concentration per cell [52], i.e. nmol cell^{-1} . This acts to serve as a more informative dosing metric for cell culture, as often times variations seen in experimental results arise as these systems are cell density dependent. In addition to the dependency in cell density, the chamber volume is also of concern. As explained above, section 2.4.3, consideration must be taken when using a confined V_{ext} because of the opportunity for a concentration to decrease in the confined chamber over time. A change in C_{ext} would result in inappropriate use of the steady-state model, as this requires the C_{ext} to be constant. For this reason, the average external concentration was chosen to be displayed and Fig 5 demonstrates the linear relationship between the two forms of representation. Interestingly, while a linear relationship is present between the concentration per cell vs. average C_{ext} (\bar{C}_{ext}), there is also scaling differences amongst cell types. Therefore, it is suggested here that to increase the accuracy in replication of the clonogenic experiment using a given cell line, then the \bar{C}_{ext} outside the cell during the clonogenic experiment should be used rather than the concentration per cell.

Given the external volume during the clonogenic assay, the cell-specific parameters (Table 5.1) and taking advantage of the system of ordinary equations (3.4) - (3.6), the change in the external H_2O_2 concentration C_{ext} over time may be obtained. Using this transient information, Eqn (3.21) is used to calculate the average external H_2O_2 concentration (\bar{C}_{ext}) for each experimental case and cell type (Appendix VI).

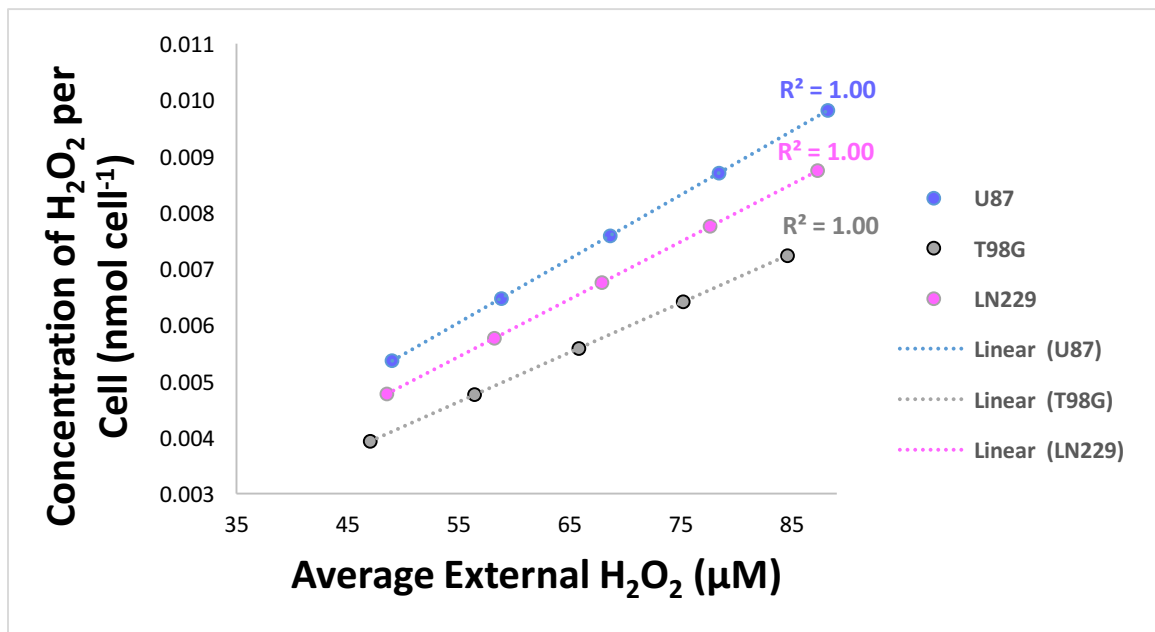


Fig 5.2 The calculated average external H₂O₂ concentration directly correlates with the representation of concentration of H₂O₂ per cell. The calculated average external H₂O₂ for the clonogenic study allows direct quantification for the cell-specific study and further allows replication for future studies. The glioblastoma cells were used as an example for our clonogenic studies. Further, while a linear relationship exists, it is also acknowledged that this scales in a cell-specific manner.

5.4 Calculated θ_{ss} and C_{in}

The steady-state model is used to quantify the intracellular H_2O_2 concentration, which depends on the known and quantified values: peroxisome membrane permeability of H_2O_2 , area of the peroxisome, rate of catalase consumption of H_2O_2 , volume of the peroxisome, plasma membrane permeability as well as the area of the cell and is given by Eqn (3.7) above.

Using the values provided in Table 5.1 we can calculate the θ_{ss} as a function of an average external concentration of H_2O_2 (\bar{C}_{ext}) experienced by the cells during the clonogenic assay. Table 5.4 displays the initial external H_2O_2 concentration (C_{ext}) exposure for each pancreatic and glioblastoma cell line. We quantify the intracellular concentration of each cell line (C_{in}) during the clonogenic assessment when exposed to varying concentrations of H_2O_2 and calculating the resulting \bar{C}_{ext} . Table 5.4 displays the normalized internal concentration $\left(\theta_{ss} = \frac{C_{in}}{\varphi_{plm}\bar{C}_{ext}}\right)$ values which are achieved during the specified clonogenic exposure, \bar{C}_{ext} .

Cell Type		C_{ext} (μM)	\bar{C}_{ext} (μM)	θ_{ss}	C_{in} (μM)	Clonogenic Response
Pancreatic Cells	MIA PaCa-2 Unmodified	0	0	0.73 ± 0.17	0	1 ± 0.28
		50	43		31 ± 7	0.4 ± 0.13
		60	51		37 ± 9	0.41 ± 0.08
		70	60		43 ± 10	0.28 ± 0.06
		80	68		50 ± 12	0.12 ± 0.06
		90	77		56 ± 13	0.07 ± 0.02
	MIA PaCa-2 siAQP3	0	0	0.45 ± 0.28	0	1 ± 0.02
		50	44		20 ± 12	0.35 ± 0.05
		60	53		24 ± 15	0.49 ± 0.13
		70	62		28 ± 17	0.32 ± 0.11
		80	70		32 ± 20	0.31 ± 0.09
		90	79		36 ± 22	0.17 ± 0.08
	H6c7	0	0	0.58 ± 0.19	0	1 ± 0.09
		50	44		26 ± 8	0.99 ± 0.14
		60	53		31 ± 10	1 ± 0.12
		70	62		36 ± 12	0.92 ± 0.11
		80	70		41 ± 13	0.94 ± 0.07
		90	79		46 ± 15	0.89 ± 0.09
Glioblastoma Cells	U-87	0	0	0.51 ± 0.18	0	1 ± 0.1
		50	49		25 ± 9	0.6 ± 0.1
		60	59		30 ± 11	1 ± 0.1
		70	69		35 ± 12	0.76 ± 0.08
		80	78		40 ± 14	0.96 ± 0.13
		90	88		45 ± 16	0.89 ± 0.09
	T98G	0	0	0.59 ± 0.20	0	1 ± 0.14
		50	47		28 ± 9	1 ± 0.14
		60	56		33 ± 11	0.99 ± 0.15
		70	66		39 ± 13	0.91 ± 0.08
		80	75		44 ± 15	0.69 ± 0.07
		90	85		49 ± 17	0.82 ± 0.07
	LN-229	0	0	0.44 ± 0.16	0	1 ± 0.14
		50	49		21 ± 8	0 ± 0.02
		60	58		26 ± 9	0.15 ± 0.09
		70	68		30 ± 11	0.32 ± 0.27
		80	78		34 ± 12	0.42 ± 0.22
		90	87		38 ± 14	0.4 ± 0.04

Table 5.4. Displays the initial concentration dosing (C_{ext}) during the clonogenic assay, the resulting average external H_2O_2 concentration (\bar{C}_{ext}) for the hour of exposure for that cell line, the calculated θ_{ss} ratio of the internal H_2O_2 concentration given any known average external H_2O_2 concentration, the calculated internal H_2O_2 concentration (C_{in}) at each dose exposure, and finally the clonogenic response for each cell pancreatic and glioblastoma cells. The error presented for θ_{ss} is the propagated error. The error in C_{in} is the standard deviation representing the range in intracellular H_2O_2 concentration based from the calculated θ_{ss} for each dose exposure. The error in the clonogenic response (surviving fraction) represent the standard error (SE).

5.5 Sensitivity of internal H₂O₂ to each parameter

Sensitivity analysis is used to understand the contribution of each parameter on the intracellular H₂O₂ accumulation, and further provides insight to which parameter would be best used as a target for modulating this therapy.

The resulting localized sensitivity, after applying Eqn (3.9 – 3.16) for each cell line is presented in Table 5.5

Cell Type	$s_{\theta, m_{plm}}$	$s_{\theta, A_{cell}}$	s_{θ, m_p}	s_{θ, A_p}	$s_{\theta, c_{cat_p}}$	s_{θ, V_p}	s_{θ, n_p}	$s_{\theta, V_{cell}}$
MIA PaCa-2 Unmodified	2×10^{-1}	2×10^{-1}	-7.3×10^{-2}	-7.3×10^{-2}	-1.2×10^{-1}	-1.2×10^{-1}	-2×10^{-1}	-1×10^{-1}
MIA PaCa-2 siAQP3	2.5×10^{-1}	2.5×10^{-1}	-9.3×10^{-2}	-9.3×10^{-2}	-1.6×10^{-1}	-1.6×10^{-1}	-2.5×10^{-1}	-1.9×10^{-1}
H6c7	2.4×10^{-1}	2.4×10^{-1}	-2.1×10^{-1}	-2.1×10^{-1}	-3.9×10^{-2}	-3.9×10^{-2}	-2.4×10^{-1}	-6.5×10^{-2}
U-87	2.5×10^{-1}	2.5×10^{-1}	-2.2×10^{-1}	-2.2×10^{-1}	-2.8×10^{-2}	-2.8×10^{-2}	-2.5×10^{-1}	-4.2×10^{-2}
T98G	2.4×10^{-1}	2.4×10^{-1}	-1.9×10^{-1}	-1.9×10^{-1}	-5.4×10^{-2}	-5.4×10^{-2}	-2.4×10^{-1}	-7.6×10^{-2}
LN-229	2.5×10^{-1}	2.5×10^{-1}	-1.8×10^{-1}	-1.8×10^{-1}	-6.7×10^{-2}	-6.7×10^{-2}	-2.4×10^{-1}	1.4×10^{-1}

It can be seen in Table 5.5 that the intracellular H_2O_2 concentration is sensitive to change in all three parameters m_{plm} , C_{cat_p} , and m_p . Further, the calculated cytosolic volume (V_{cell}) also contributes to changes in the intracellular H_2O_2 concentration. Figure 6 displays surface plots for the sensitivity of θ_{ss} when one parameter is fixed and the other two vary across ranges presented by all 5 cell types in this study. Using the cell-specific parameters displayed in Table 5.1, sensitivity surface plots were generated in MATLAB to represent the effects of varying either m_{plm} , m_p , C_{cat_p} , and/or V_{cell} and the ranges for each parameter span the values which were determined for the cells in this study. The sensitivity curves provide insight to not only the parameters contributing to changes in θ_{ss} but also the ranges that these parameters would have the most impact.

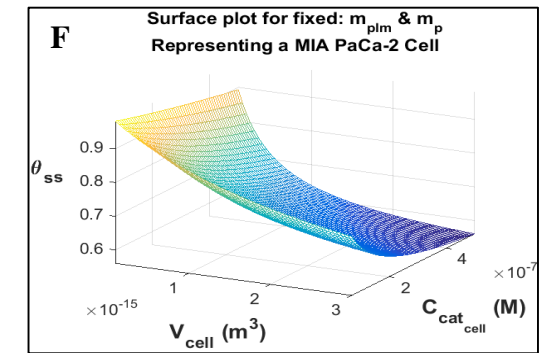
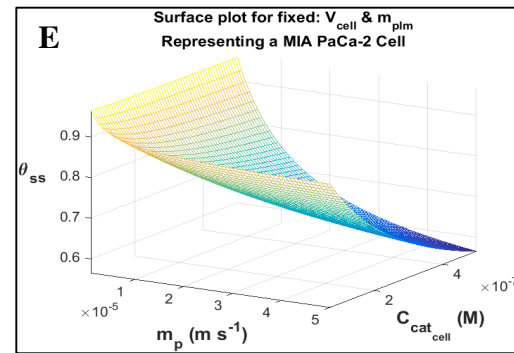
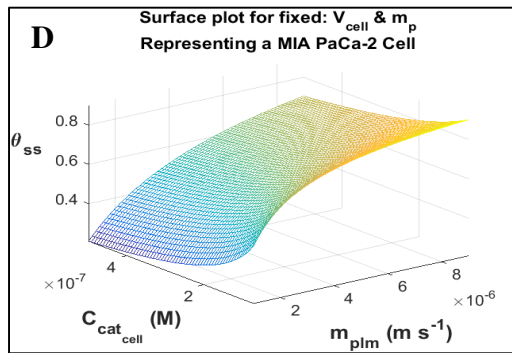
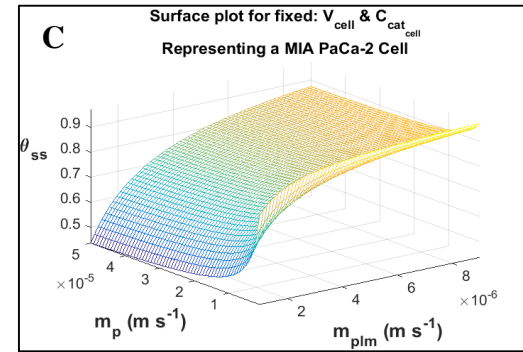
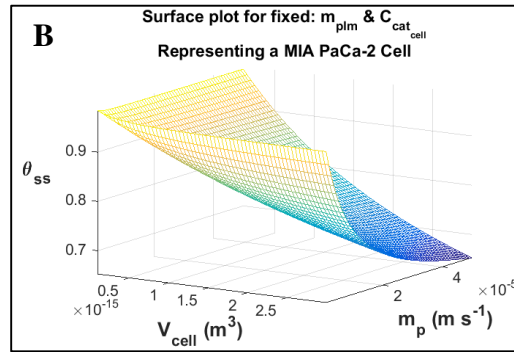
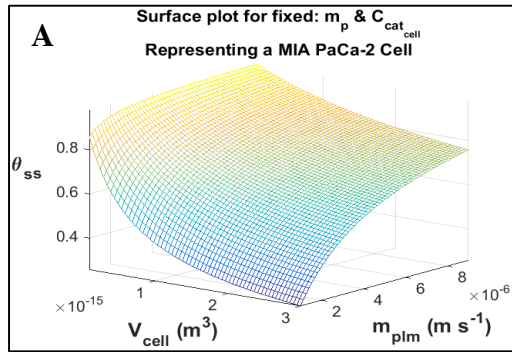


Fig 5.3. Displays surface plots for the internal H₂O₂ concentration (θ_{ss}) of MIA PaCa-2 cells and its variation in relation to altering ranges of either the plasma membrane permeability (m_{plm}), catalase concentration per cell ($C_{cat_{cell}}$) peroxisome membrane permeability (m_p), and/or the volume of the cell not occupied by the nucleus (V_{cell}).

The figures each represent fixing two of the four parameters to the values representing MIA PaCa-2 cells and varying the other two in combinations of $C_{cat_{cell}}$, V_{cell} , m_{plm} , and/or m_p .

A) Fixing $C_{cat_{cell}}$ and m_p , the sensitivity range of m_{plm} falls between $(1 - 9) \times 10^{-6} m s^{-1}$ suggesting that an increase in permeability above this value will not affect the internal H₂O₂ drastically. The sensitivity range for V_{cell} is dramatically sensitive within the range of $(0.1 - 1) \times 10^{-15} m^3$, thus changing the cytosolic volume within this range may result in drastically different C_{in} calculations. **B)** Displays a more prevalent sensitivity of m_p within the range of $(1 - 3) \times 10^{-6} m s^{-1}$. The contribution seen by the V_{cell} has less influence on θ_{ss} even when spanning the range $(0.1 - 3) \times 10^{-15} m^3$ per cell. **C)** Fixing V_{cell} and $C_{cat_{cell}}$ demonstrates very little sensitivity to changes in m_p , except within a narrow region of $(0.1 - 1) \times 10^{-5} m s^{-1}$, m_{plm} on the contrary has a slightly larger range spanning $(1 - 4) \times 10^{-6} m s^{-1}$. **D)** When V_{cell} and m_p are constant, significant changes in θ_{ss} occur with increasing plasma membrane permeability (m_{plm}) to H₂O₂ specifically within the range of $(2 - 8) \times 10^{-6} m s^{-1}$. The $C_{cat_{cell}}$ sensitivity falls within a smaller range between $(0.7 - 2) \times 10^{-7} M$ per cell. **E)** Comparing $C_{cat_{cell}}$ and m_p , for fixed values of V_{cell} and m_{plm} , we see a greater sensitivity in the $C_{cat_{cell}}$ with a steeper decline in θ_{ss} covering the entire range of catalase concentration. Lastly, **F)** provided constant values for

m_{plm} and m_p steep changes in V_{cell} and $C_{cat_{cell}}$ occur. The curves were generated in MATLAB and ranges represent the full range of values expressed by the cells in our study. In Fig 5.3 A) as the volume of the cell increases the intracellular H_2O_2 decreases, as expected as larger volumes promote dilution of the species. The trend for the plasma membrane permeability is also as expected, increasing values leads to an increase in the intracellular concentration. when the peroxisome membrane permeability increases. Fixing $C_{cat_{cell}}$ to a value of 8.45×10^{-8} M and the m_p to a value of 2.13×10^{-5} $m\ s^{-1}$ the sensitivity range of m_{plm} falls between $(1 - 9) \times 10^{-6}$ $m\ s^{-1}$ suggesting that an increase in permeability above this value will not affect the internal H_2O_2 drastically. The sensitivity range for V_{cell} is dramatically sensitive within the range of $(0.1 - 1.5) \times 10^{-15}$ m^3 , thus changing the cytosolic volume within this range may result in altering the intracellular H_2O_2 by a factor of about 2.5, as it θ_{ss} drops from around 0.86 to 0.35 and the smaller m_{plm} range of 3×10^{-6} $m\ s^{-1}$. For larger V_{cell} , 3×10^{-15} m^3 , altering the plasma membrane permeability can affect the intracellular H_2O_2 by a factor of 3. Whereas, for smaller volumes changes in the m_{plm} has less of an effect on θ_{ss} , which changes only by a factor of 1.1. The opposite is also true, where at higher levels of permeability the changes in the V_{cell} also become less sensitive and changes the by only a factor of around 1.1.

B) Represents fixing $C_{cat_{cell}}$ to a value of 8.45×10^{-8} M and the m_{plm} to a value of 7.14×10^{-6} $m\ s^{-1}$. Opposite to increases in m_{plm} , θ_{ss} decreases as the peroxisome membrane permeability increases. This is expected as more H_2O_2 transverses across the peroxisome, thus allowing more H_2O_2 to become available for consumption via catalase.

Again larger cytosolic volumes result in lower intracellular H_2O_2 concentrations. Evaluating the surface plot at the larger end of cytosolic volumes, a more prevalent sensitivity in m_p occurs across $(0.1 - 5) \times 10^{-5} \text{ m s}^{-1}$; where it appears most drastic between $(1 - 2) \times 10^{-5} \text{ m s}^{-1}$. Therefore, an increase in permeability above $3 \times 10^{-6} \text{ m s}^{-1}$ will not affect the internal H_2O_2 as dramatically. Further, the variation in m_p becomes less effective at smaller cytosolic volumes where θ_{ss} essentially remains the same. The contribution seen by the V_{cell} has less influence at smaller m_p values on θ_{ss} even when spanning the range $(0.1 - 3) \times 10^{-15} \text{ m}^3$ per cell. The contrary is true at larger m_p values ($5 \times 10^{-5} \text{ m s}^{-1}$), where changes in V_{cell} across the range provided can alter θ_{ss} by a factor of 1.5.

C) Fixing both V_{cell} and $C_{cat_{cell}}$, θ_{ss} is more sensitive to changes in m_{plm} compared to m_p where m_{plm} has a slightly larger range spanning $(1 - 4) \times 10^{-6} \text{ m s}^{-1}$. At the lower end of m_{plm} values $1 \times 10^{-6} \text{ m s}^{-1}$, demonstrates very little sensitivity to changes in m_p , except within a narrow region of $(0.1 - 1) \times 10^{-5} \text{ m s}^{-1}$. Although this may be considered a narrow region, the θ_{ss} has the opportunity to alter by a factor of 1.8. This is much larger compared to higher m_{plm} values $9 \times 10^{-6} \text{ m s}^{-1}$ where the largest change in θ_{ss} over the entire m_p range is a factor of 1.1. At higher m_p ($5 \times 10^{-5} \text{ m s}^{-1}$) values, the variation of m_{plm} can alter θ_{ss} by a factor of 2. Where at smaller m_p ($0.1 \times 10^{-5} \text{ m s}^{-1}$) values the changing m_{plm} only changes θ_{ss} by a factor of 1.2.

D) Shows that θ_{ss} is highly sensitive to changes in m_{plm} and $C_{cat_{cell}}$. As the permeability of the plasma membrane increases so does θ_{ss} . Further, the intracellular H_2O_2 concentration decreases as catalase concentration increases. Interestingly, the catalase concentration is most effective in the range $(1 - 2) \times 10^{-7} M$. When evaluating at the lower m_{plm} range ($1 \times 10^{-6} m s^{-1}$), the largest change in θ_{ss} for changing $C_{cat_{cell}}$ is a factor of 2.5. At the faster m_{plm} end ($9 \times 10^{-6} m s^{-1}$), θ_{ss} can change by a factor of 1.3 spanning the entire range of $C_{cat_{cell}}$. When evaluating m_{plm} , at higher catalase concentrations ($5 \times 10^{-7} M$), θ_{ss} changes by a factor of where 3.5. This is the largest change in θ_{ss} offered so far. At the opposite end, when $C_{cat_{cell}}$ is on the lower end ($0.7 \times 10^{-7} M$), θ_{ss} changes by a factor of 1.8 over the entire range in m_{plm} offered. The intracellular H_2O_2 concentration is highly sensitive to changes in m_{plm} parameter, but also $C_{cat_{cell}}$. Interestingly, the curve does not begin flattening until the permeability is further increased to the higher end around $9 \times 10^{-6} m s^{-1}$, indicating that increasing m_{plm} past this value would no longer effect θ_{ss} . However, we see that within the range of our m_{plm} values provided for our cells, altering this parameter can significantly increase or decrease the intracellular H_2O_2 concentration by 2.5 times.

E) When the plasma membrane permeability and intracellular volume are fixed and m_p and $C_{cat_{cell}}$ are instead altered, we observe results which indicate that θ_{ss} is highly sensitive to changes in catalase concentration compared to changes in peroxisome permeability. Here, decreasing m_p increases θ_{ss} . The latter is expected as less H_2O_2

transverses across the peroxisome and thus less H_2O_2 is then being consumed by catalase. As catalase concentration increases, θ_{ss} decreases. It is evident that altering the catalase concentration in the cellular range we obtain, when m_p is near the faster end, θ_{ss} can alter by a factor of 1.5. In the lower end of m_p , θ_{ss} is relatively unaltered over the entire range of catalase concentration. This implies that at low peroxisome permeability, increasing the catalase activity does little in decreasing the internal H_2O_2 concentration. Which should hold true as less H_2O_2 is available to be consumed by catalase as the rate limiting step clearly becomes transport to the enzyme and not the enzymatic activity. Varying m_p has little effect at lower catalase activity, where θ_{ss} changes by a factor of 1.1. Contrary, at high catalase activity the sensitivity in θ_{ss} is much more dramatic to m_p where it can change by almost a factor of 2. Again, this relationship is not unexpected as at higher catalase activity and higher peroxisome permeability, θ_{ss} is expected to decrease.

F) When m_{plm} and m_p are fixed to a value of 7.14×10^{-6} and $2.13 \times 10^{-5} \text{ m s}^{-1}$, respectively, steep changes in θ_{ss} occur with changes in V_{cell} as well as $C_{cat_{cell}}$. θ_{ss} is sensitive to varying V_{cell} over the entire range of $(0.1 - 3) \times 10^{-15} \text{ m}^3$, given both high and low catalase concentrations. Spanning the available V_{cell} range, θ_{ss} changes by a factor of 1.3 and 1.6 for low and high $C_{cat_{cell}}$, respectively. The $C_{cat_{cell}}$ is sensitive between $(0.7 - 5) \times 10^{-7} \text{ M}$ where at the larger V_{cell} , θ_{ss} can change by a factor of 1.1 and at smaller volumes θ_{ss} alters by a factor of 1.3.

The surface plot curves were generated in MATLAB and all provided ranges represent the range available from the cells investigated in our studies (refer to Table 5.1). These sensitivity curves are all examples using the MIA PaCa-2 unmodified cell type. However, since all cell lines follow the same general trend and one cell line is sufficient as an example for analysis. These plots serve an important use for understanding which parameter adjustment would have the largest contribution to changes in the internal H_2O_2 concentration. We can see that in order to increase the increase the intracellular H_2O_2 concentration, it would be advantageous to adjust catalase and the membrane permeability.

5.6 Clonogenic response vs. extracellular H₂O₂ concentration

Assays designed to determine the clonogenic survival of cells upon exposure to a bolus of H₂O₂ up to initial dose exposure concentration of 90 μM reveal the dose-response for the three cell lines, Fig 5.4. U-87 cells were unaffected by exposure to bolus addition of extracellular H₂O₂ where T98G cells were slightly affected. LN-229 cells demonstrated significant decrease in their surviving fraction when exposed to increased concentrations of H₂O₂ compared to their controls. Upon exposure to therapeutic ranges of H₂O₂, significant differences exist between T98G and LN-229 at initial dosing of 80 μM ($P = 0.06, n = 3$) and 90 μM ($P = 1.4 \times 10^{-6}, n = 3$). Further, U-87 and LN-229 also exhibited significant differences at 80 μM ($P = 6.5 \times 10^{-7}, n = 3$) and 90 μM ($P = 3.7 \times 10^{-5}, n = 3$). These results resemble the trend presented by ascorbate-susceptibility studies [12] and thus confirm the importance of extracellular H₂O₂. As described previously (section 2.4.3), average external H₂O₂ is presented to allow future replication of this study as the H₂O₂ outside the cell decreases over the hour and is cell-dependent.

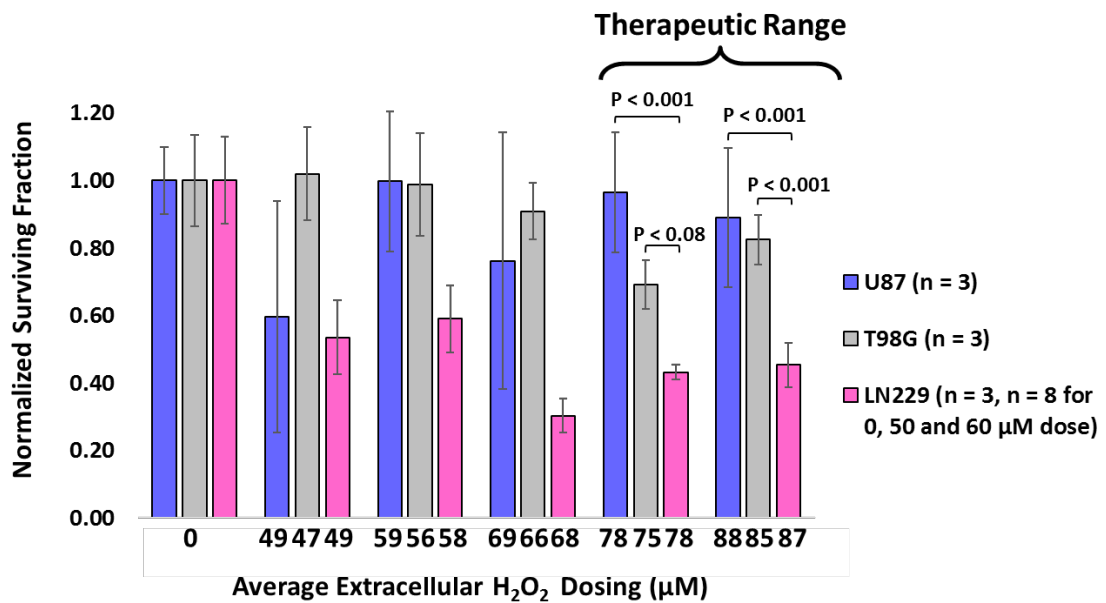
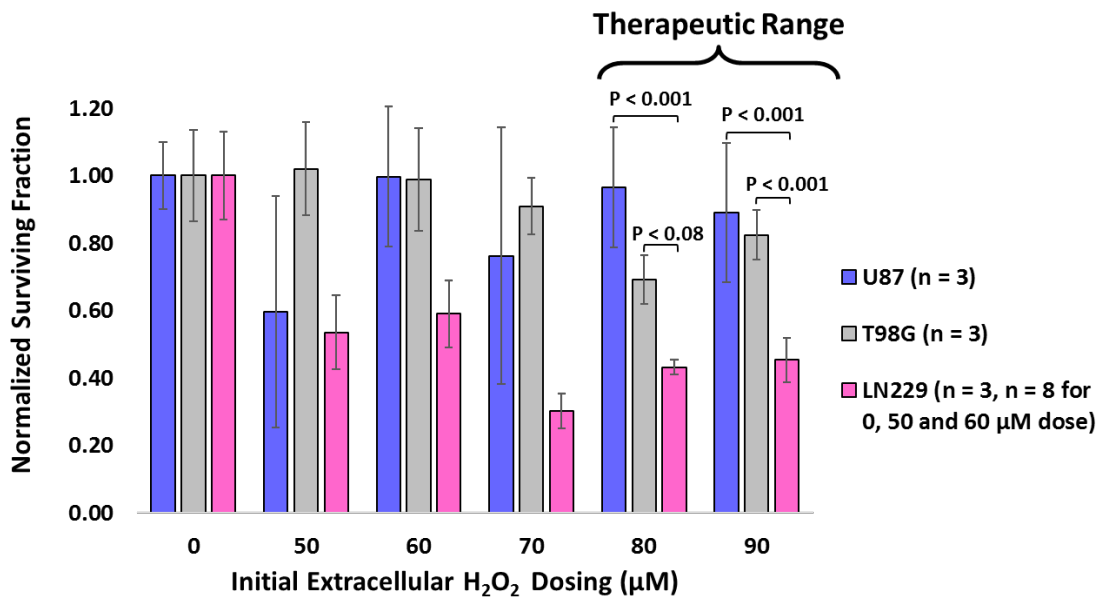


Fig 5.4. Dose response to exposure of bolus H₂O₂ concentrations resemble the response following ascorbate-toxicity studies. Surviving fraction, relative to 0 μM H₂O₂, of U-87 cells are not significantly affected for dosing shown. Surviving fraction, relative to 0 μM H₂O₂, is significantly decreased for LN-229 as compared to U-87 and T98G cells for therapeutic dosing of initial H₂O₂ exposure at 80 μM and 90 μM. Surviving fraction of U-87 cells are not significantly affected for dosing shown. These results confirm the importance of extracellular H₂O₂ in relation to ascorbate-susceptibility. Statistical significance was determined through ANOVA. Error bars displayed represent the standard error (SE).

5.7 Clonogenic response vs. intracellular concentration

While the surviving fraction of cells following bolus addition of H_2O_2 concentrations displayed a dose response as expected, the calculated intracellular H_2O_2 did not follow the expected trend. It would follow that as extracellular H_2O_2 dose increases resulting in a decrease in clonogenic survival, that the intracellular H_2O_2 would in turn also increase. Fig 5.8 does not show this relationship of increasing surviving fraction with decreasing intracellular H_2O_2 concentrations. Instead, it appears that the intracellular H_2O_2 (although high for all cell types) is in actuality handled quite differently depending on the cell type. The non-responding cells (represented by boxes) have a high surviving fraction while also maintaining high levels of intracellular H_2O_2 . The H_2O_2 -susceptible cells also experience high intracellular H_2O_2 concentrations; however, display varying susceptibility. It is difficult to discern whether within the group of H_2O_2 -susceptible cells (triangles) if the surviving fraction decreases as internal H_2O_2 increases. The latter relationship appears to only hold true for the MIA PaCa-2 (blue and green triangles). The calculated intracellular H_2O_2 , displayed in Table 5.4, was calculated for each cell using the average external H_2O_2 concentration for each specific cell line, Fig 5.5.

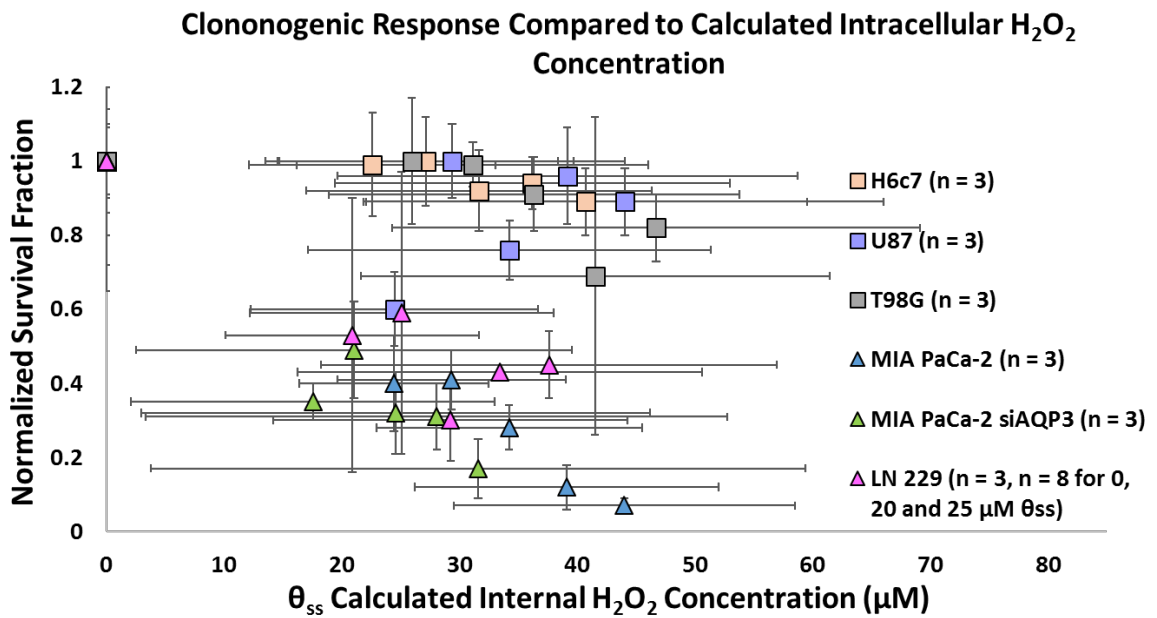


Fig 5.5. Elevated intracellular H₂O₂ concentrations does not necessarily decrease the surviving fraction of cells. The normal and H₂O₂ non-responding cells (squares) have equally high intracellular H₂O₂ concentrations as compared to the H₂O₂-susceptible cells (triangles). These results indicate that the intracellular H₂O₂ concentration is handled differently and is cell-dependent. It can therefore be concluded that there is not a significant H₂O₂ concentration that must be met which is independent of cell type. The vertical error bars represent the standard error from the clonogenic surviving fraction studies. The horizontal error bars represent the propagated error for the calculated intracellular H₂O₂ concentration range at the respective dose.

5.8 Clonogenic response vs. catalase concentration

Interestingly, when the clonogenic response is compared to catalase concentration it appears that a linear trend emerges, Fig 5.6 A and B, at the representative 80 and 90 initial extracellular H₂O₂ dosing. As catalase concentration increases per cell, so does the surviving fraction. This would then imply that catalase concentration of a cell may serve as a predictor to the success of ascorbate therapy. At closer analysis, however, the same catalase concentration from different cell types again displays varying surviving fractions. It would be implied that catalase concentration, if high would improve the clonogenic surviving fraction. This assumption would again lead to the conclusion that the intracellular H₂O₂ is decreasing due to the elevated catalase activity. This is not true as it was seen in Fig 5.8, the cells handle the intracellular H₂O₂ concentrations differently. So, it would hold that elevated catalase concentration may not have the same affect within all cell types. The latter argument is clearly demonstrated in Fig 5.9 B, where there is significant difference at the 90 μM dose between LN-229 (pink) and both U-87 (purple) and T98G (grey) cells. Interestingly, the catalase concentration between LN-229 cells ($2.9 \times 10^{-7} M$) and the T98G cells ($3.02 \times 10^{-7} M$) are not significantly different from each other, yet the clonogenic behavior does alter significantly ($P < 0.001$). Again, implying that catalase concentration is not the only mitigating factor.

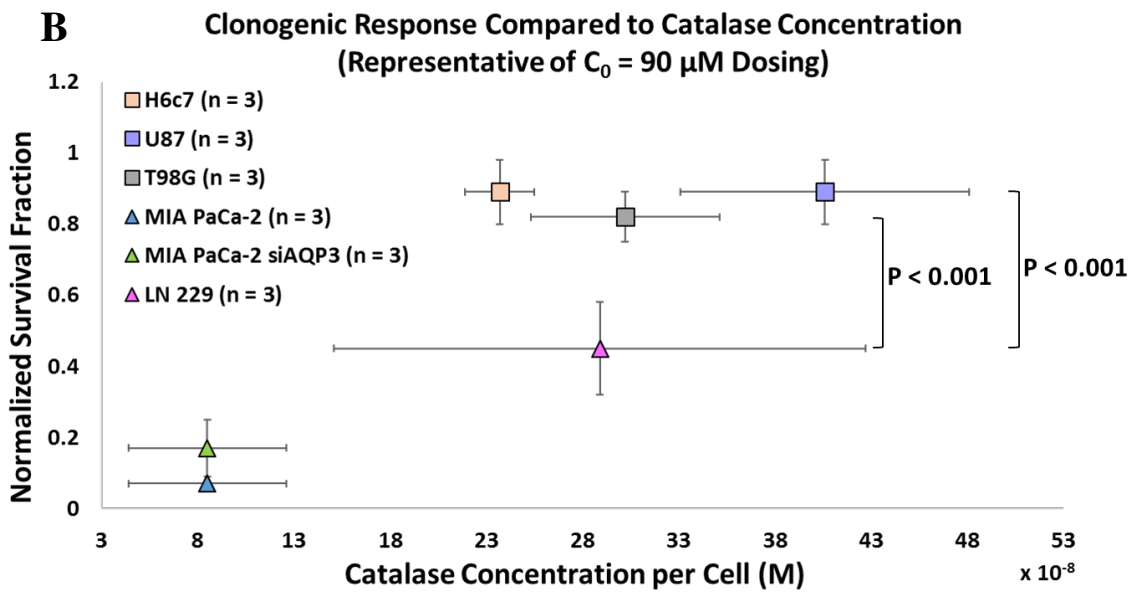
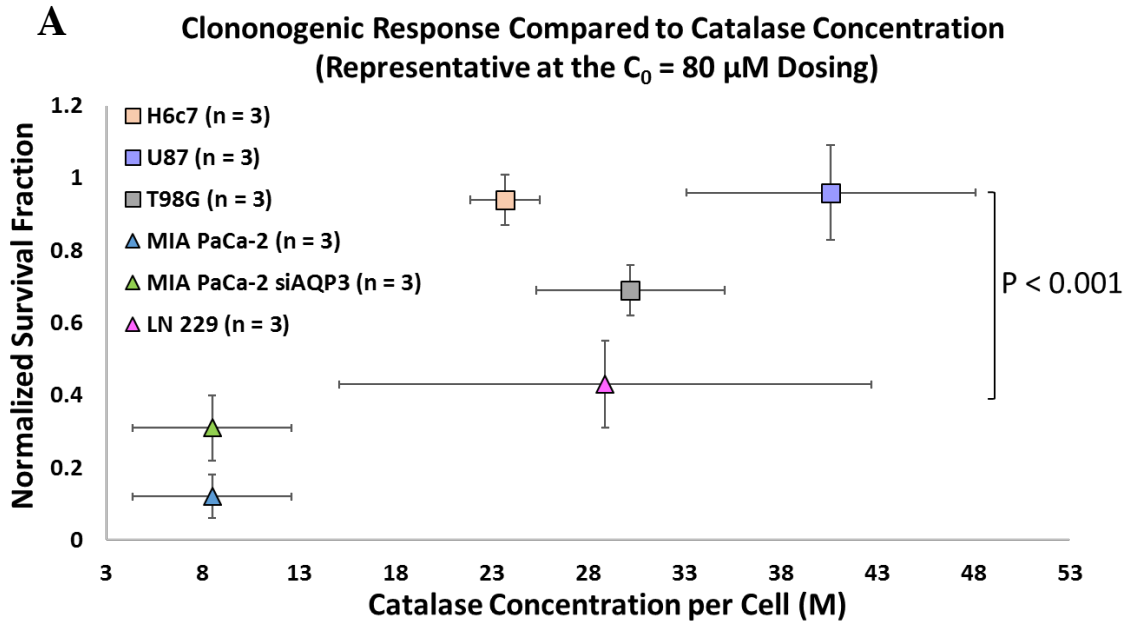
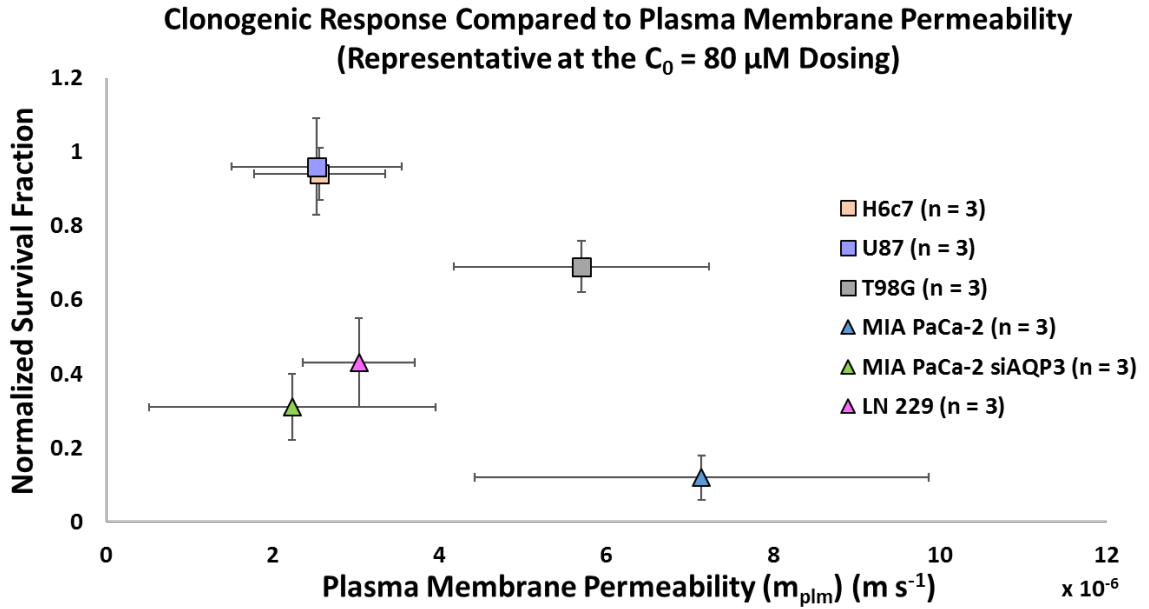


Fig 5.6 A & B. Catalase concentration of the cell does not dictate the surviving fraction. Increasing catalase concentration appears to have a linear relationship with increasing surviving fraction of the cell, at the 80 and 90 μM dosing. The H_2O_2 non-responding cells (squares) reveal having higher catalase activity increases the surviving fraction of these cells. While the H_2O_2 -susceptible cells (triangles) experience lower surviving fractions and comparable lower catalase concentrations per cell. This represents the initial dosing of 80 μM . The horizontal error bars represent the standard error in the catalase activity measured for each cell type and is also presented in Table 5.4. Evaluating the catalase concentration between U-87 (purple), T98G (grey) and LN-229 (pink) cells, it become clear that the surviving fraction remains cell-dependent and catalase is not a predictor of how the cell will handle the intracellular H_2O_2 concentration. ANOVA analysis was conducted to confirm there was statistical difference among the groups. A post hoc analysis using a t-Test of Two-Sample Assuming Equal Variances was used to determine the statistical significance amongst the groups. The vertical error bars represent the standard error from the clonogenic surviving fraction studies. ANOVA analysis was conducted to confirm the statistical significance among the groups.

5.9 Clonogenic response vs. plasma membrane permeability

Previously we showed that decreasing the plasma membrane permeability by silencing peroxiporin AQP3 on MIA PaCa-2 cells increased the surviving fraction for this cell type [58]. Fig 5.7 A and B demonstrates, similar to the catalase concentration, that the plasma membrane permeability alone also is not capable of determining the fate of the cell. Plasma membrane permeability between LN-229 cells ($3.03 \times 10^{-6} \text{ m s}^{-1}$) and the U87 cells ($2.52 \times 10^{-6} \text{ m s}^{-1}$) are not significantly different from one another, yet the clonogenic behavior at 80 and 90 μM does alter significantly ($P < 0.001$). While the plasma membrane permeability did demonstrate an effect in our previous work, Fig 5.7 shows that it is again not independent of cell type. Critical intracellular H_2O_2 concentrations are cell-dependent. Although this is true, if we address the permeability from a cell-dependent manner and turn our attention to the MIA PaCa-2 cells, we see a higher internal H_2O_2 concentration for the unmodified cells compared to the siAQP3 cells. Further the plasma membrane permeability between these cell lines was altered by a factor of 3. Recall, section 5.5 Fig 5.3 A, the intracellular H_2O_2 is altered by a factor 1.5 of within the range of permeability of the MIA PaCA-2 unmodified and siAQP3 cells. The comparison between only this cell line is also seen in Fig 5.7 A and B where the MIA unmodified PaCa-2 (blue triangle) cell has a comparably higher plasma membrane permeability yet a lower surviving fraction compared to the siAQP3 MIA PaCa-2 cells (green triangles). Table 5.4 also shows the calculated internal H_2O_2 for this cell line decreases a factor of 2 for the siAQP3 MIA PaCa-2 cell.

A



B

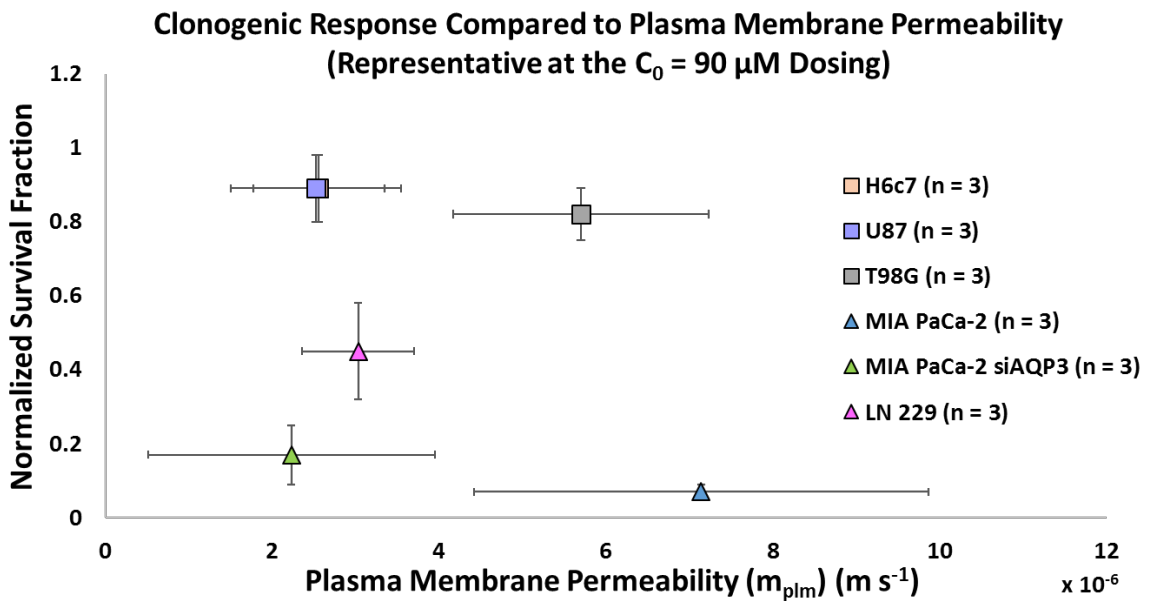


Fig 5.7 A & B. Plasma membrane permeability is not a predictor in cell surviving fraction. The H₂O₂ non-responding cells (squares) have comparable plasma membrane permeability yet significantly different surviving fractions. It can be seen the LN-229 cells (pink triangles) have a similar permeability to both U-87 and H6c7 cells, yet only the LN-229 cells experience a decrease in their surviving fraction. This represents the initial dosing of 80 and 90 μM. The horizontal error bars represent the standard error in the plasma membrane permeability measured for each cell type and is also presented in Table 5.2. The vertical error bars represent the standard error from the clonogenic surviving fraction studies. ANOVA analysis was conducted to confirm the statistical significance among the groups.

5.10 Clonogenic response vs. peroxisome membrane permeability

Lastly, the peroxisome membrane permeability shows no correlation to the surviving fraction of cells. All cell lines have similar peroxisome H₂O₂ permeability, with no significant difference, except the H6c7 cell lines, Fig 5.8 A and B. While the permeability of this membrane does not vary, the clonogenic response is quite different depending on cell line. Further, despite H6c7 cells having a slower permeability, the clonogenic survival of this cell line is much higher than the susceptible cells (triangles). It is clear from these plots, that the peroxisome membrane permeability has the least effect on dictating whether the cell will respond to therapeutic H₂O₂. Further, this parameter also does not vary across cancer cell types.

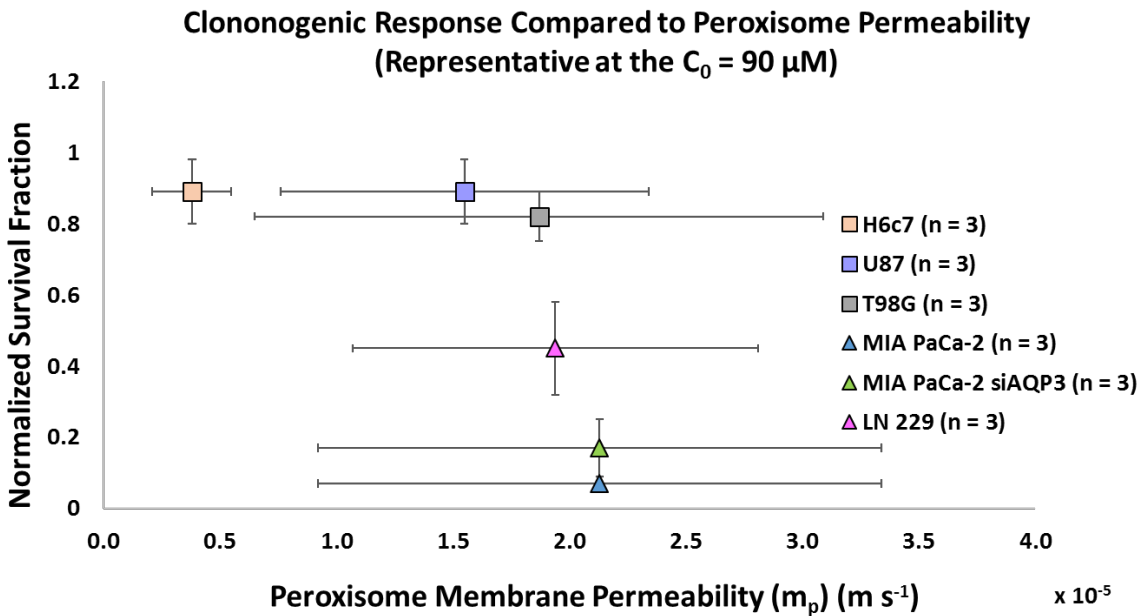
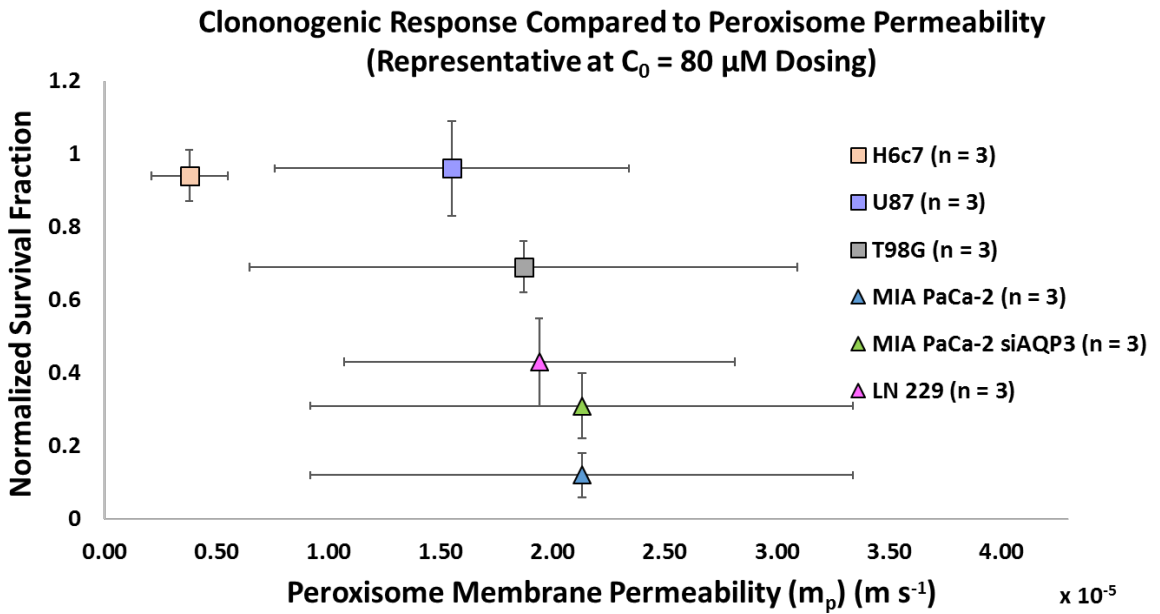


Fig 5.8 A & B. Peroxisome membrane permeability also does not indicate whether the surviving fraction will increase or decrease. U-87 cells and LN-229 do not have statistically different plasma membrane permeability yet they do have statistically significant surviving fractions. Thus, these results indicate that permeability is not a useful parameter for predicting the surviving fraction. The vertical error bars represent the standard error from the clonogenic surviving fraction studies. ANOVA analysis was conducted to confirm the statistical significance among the groups. The horizontal error bars represent the standard error in the peroxisome membrane permeability measured for each cell type.

5.12 Conclusion

This work once again reiterates that toxicity via extracellular H_2O_2 dosing is indeed an important factor when considering the mechanism behind ascorbate therapy. We have illuminated that the complexity behind ascorbate therapy is more intricate than simply linking ascorbate-susceptibility to a quantifiable intracellular H_2O_2 concentration. The variations in catalase concentration and permeability clearly have combined effects on the surviving fraction of a cell. Neither catalase activity nor the cell membrane permeability characteristics have the potential to serve as a predictor for the success of ascorbate therapy independently.

There exist numerous additional factors which may alter the effects of internal H_2O_2 of these cells. One avenue for further exploration is the free labile iron within cells [46]. It has also been suggested that intracellular H_2O_2 is activated in the presence of catalytic transition metals generating significant hydroxyl radical ($\text{HO}\cdot$) [46], which serves to substantially increase DNA damage. Perhaps furthering this model to include catalytic iron variations amongst cells and its effects on $\text{HO}\cdot$ production would aid in defining the critical concentration of internal H_2O_2 needed to produce the toxic $\text{HO}\cdot$.

Although there is not a critical intracellular H_2O_2 concentration independent of cell type, understanding the contributions of each of cell-specific parameter lends itself to the opportunity of insight for future cellular targets and ability to improve the efficacy of this therapy for cancer cells that are currently less susceptible.

CHAPTER 6. ON CATALASE LATENCY: A MATHEMATICAL INTERPRETATION

6.1 Introduction

Catalase concentration varies widely across cell lines. Catalase is known to exhibit lower activity in tumor cells; where catalase expression ranges on the order of 10-100 fold times more for normal cells when compared to tumor cells [41]. Other empirical studies have shown more than a 50% decrease in steady-state catalase activity for tumor cells [12]. This variation in catalase activity across cell lines could significantly affect the removal of H_2O_2 , making tumor cells more susceptible to ascorbate mediated cell-death, as their capability to remove H_2O_2 is greatly hindered. Catalase, in contrast to the other removal enzymes, is responsible for irreversibly consuming intracellular H_2O_2 when in the presence of high concentrations [12, 17]. The latter justifies the focus on catalase, in regards to P-AscH⁻, as the primary intracellular reaction to remove the accumulating H_2O_2 .

Catalase is entrapped within peroxisomes thus requiring H_2O_2 to transport across an additional membrane. De Duve in the 1950s described the change in observed catalase activity of enzymes in free solution versus enzymes entrapped inside a compartment, i.e. the peroxisome, in terms of latency [61, 68]. Latency of an enzyme occurs in the presence of a membrane as the diffusion of the substrate, H_2O_2 , to the catalase becomes limited [61]. Although this is true, what was attempting to be described is the membrane characteristics to the transport of the substrate across, or more correctly the mass transfer of H_2O_2 . When

addressing the two compartments containing H_2O_2 (cytosol and peroxisome), it is clear that the consumption inside the peroxisome, via catalase, serves as the driving force for H_2O_2 to diffuse down its concentration gradient. The magnitude of the gradient depends on two aspects, the catalase activity removing H_2O_2 as well as the permeability of H_2O_2 across the membrane. Therefore, encompassed within this concept of latency is the flux of H_2O_2 across the membrane which depends on diffusion of H_2O_2 and the concentration gradient; described mathematically as $J = -D\nabla C \approx m_{\text{H}_2\text{O}_2} \Delta C$. The flux may be approximated to be described by a mass transfer coefficient and instead the change in concentration.

It is therefore of interest to obtain the rate of H_2O_2 transport across peroxisome membranes and thus experimental data is used to observe rates when peroxisome is intact and extract the peroxisome mass transfer coefficient for H_2O_2 (refer to section 4.2.6). Using readily available catalase activity or rate of H_2O_2 consumption measured for lysed cells (catalase in free solution, refer to section 4.2.4), the cell-specific catalase activity is obtained.

Previous work conducted by Antunes and Cadenas (2000) [61], experimentally determined catalase activity for Jurkat T-cells for cases where peroxisome membranes are intact and disrupted. They were interested in mathematically modeling the intracellular concentration of H_2O_2 primarily because of its critical significance in the homeostasis of the cellular redox environment, function as a signaling model, cell development etc. They address latency to estimate the H_2O_2 gradients developed in Jurkat T-cells, to provide the first method for H_2O_2 quantification.

Here we develop a mathematical model for latency and address the most significant factors. We further provide a systematic method for calculating the peroxisome membrane permeability (refer to section 4.2.6) and demonstrate the importance of latency in regards to P-AscH therapy. Unfortunately, there is no quantification to date on the effects of this latency term.

6.2 Mathematical Methods

6.2.1 Latency in the peroxisome

The latency of the catalytic reaction is the result of i) mass transfer resistance due to the peroxisome membrane and, 2) a reduction in catalytic effectiveness. The mass transfer resistance is related to the peroxisome membrane permeability to H_2O_2 , m_p . Because the reaction of catalase is a second order reaction dependent on both catalase concentration and H_2O_2 concentration, then local H_2O_2 becomes a concern. Comparing catalase free in solution versus the catalase confined in the peroxisome and given the same initial H_2O_2 , we see a difference in the overall reactivity of catalase in these different volumes. The reaction effectiveness is directly related to the geometry of the peroxisome organelle where catalase is confined or entrapped. As H_2O_2 permeates the peroxisome membrane, it is converted/consumed by the catalase closer to the surface of the peroxisome. As the remaining H_2O_2 continues to diffuse into the organelle, the H_2O_2 concentration lowers. Since the reaction rate is a function of the local H_2O_2 concentration, the overall reactivity of the catalase in the peroxisome is reduced compared to the same concentration of catalase

in a volume exposed at the same initial concentration of H_2O_2 . This concept of effectiveness is illustrated in Fig 6.1.

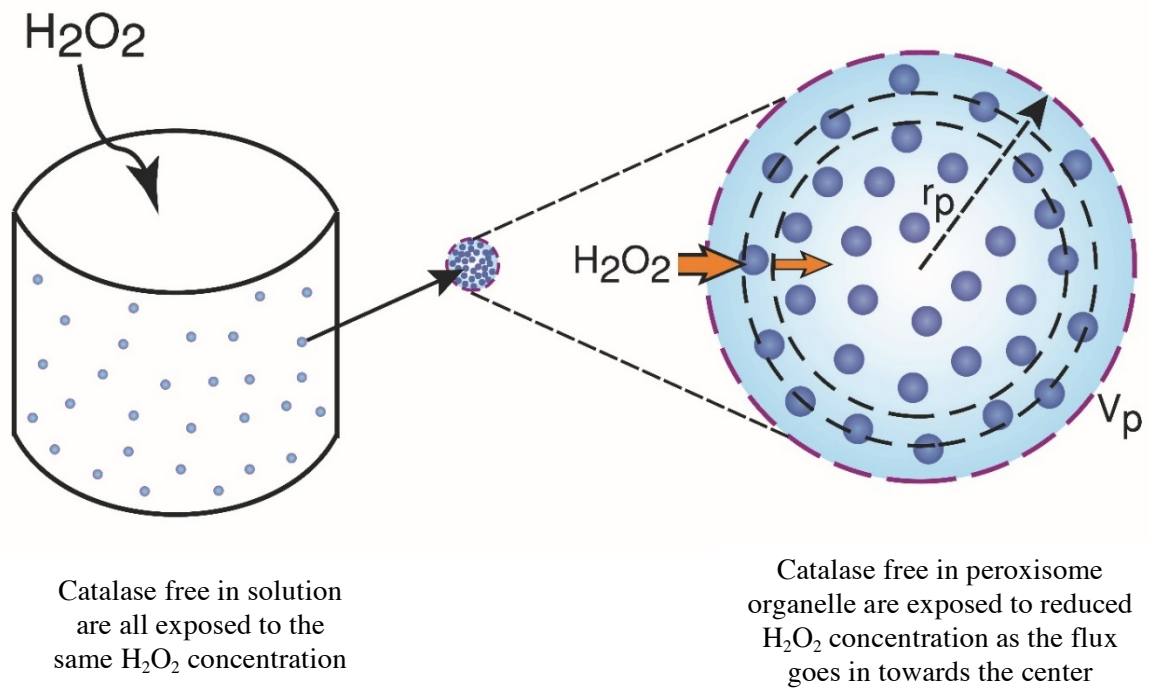


Fig 6.1. The latency of the catalase in the peroxisome is associated with the permeability of the peroxisome membrane wall, m_p and the effectiveness of the catalase overall within the peroxisome. With respect to effectiveness, the catalase in solution represented on the left-hand side of the figure, all have access to the same concentration of H_2O_2 in the well-mixed system. However, within the peroxisome, the catalase near the surface of the organelle react to a higher concentration of H_2O_2 than the catalase near the center. This is depicted by the larger H_2O_2 arrow in the outer dashed surface compared to the smaller arrow for the inner dashed line. Since the overall reaction rate is a linear function of the concentration of H_2O_2 (C_p), the reaction rate of the catalase near the center is reduced. The effectiveness factor takes this into consideration.

The overall reaction rate in the peroxisome is

$$R_i = -k_2 C_{cat_p} C_p(r) \quad (6.1)$$

The catalase rate consumption of H_2O_2 is a second order reaction which depends on the concentration of H_2O_2 (C_p) and catalase (C_{cat_p}) in the peroxisome. Catalase is a tetramer with monomer activity well known to be $1.7 \times 10^{-7} M^{-1} s^{-1}$ from the work of Britton Chance in 1943 [64], denoted here as k_2 .

The volume average reaction rate is

$$\bar{R}_i = \frac{\int_{V_p} -k_2 C_{cat_p} C_p(r) dV_p}{\int_{V_p} dV_p} = \frac{1}{V_p} \int_{V_p} -k_2 C_{cat_p} C_p(r) dV_p \quad (6.2)$$

Where V_p denotes the volume of the peroxisome. Since the volume of the peroxisome is assumed to take a spherical geometry, we have $V_p = \frac{4}{3} \pi r^3$.

The overall latency of the catalase due to its presence in the peroxisome can be directly calculated. This includes taking the volume average of the radial concentration of H_2O_2 through the spherically-modelled peroxisome at steady state, and comparing the overall reaction rate to the reaction rate if all catalase were directly in solution. Assuming again the pseudo-homogeneous reaction, we begin with the conservation of mass for a dilute species with 1-D diffusion in the peroxisome radial direction only and thus the governing equation would be,

$$D_{ij} \frac{1}{r^2} \frac{d}{dr} \left(r^2 \frac{dC_p}{dr} \right) = R_i. \quad (6.3)$$

Here, R_i represents the catalase reaction inside the peroxisome $R_i = -k_2 C_{cat_p} C_p(r)$

$$D_{ij} \frac{1}{r^2} \frac{d}{dr} \left(r^2 \frac{dC_p}{dr} \right) = -k_2 C_{cat} C_p. \quad (6.4)$$

In determining the appropriate boundary conditions, the flux balance at the peroxisome membrane wall equals the diffusive flux in the peroxisome to the membrane permeability flux model. The H_2O_2 is consumed in the peroxisome and as H_2O_2 travels towards the center of the peroxisome, less H_2O_2 is present.

$$r = r_p \quad -\varphi_p D_{ij} \frac{dC_p}{dr} = m_p [\varphi_p C_{in} - C_p] \quad \text{Boundary Condition 1} \quad (6.5)$$

$$r = 0 \quad \frac{dC_p}{dr} = 0 \quad \text{Boundary Condition 2} \quad (6.6)$$

Making dimensionless by letting theta (θ) describe the concentrations and ksi (ξ) describing the radial direction,

$$\theta = \frac{C_p}{\varphi_p C_{in}}, \quad \xi = \frac{r}{r_p}$$

So,

$$\frac{d\theta}{dC_p} = \frac{1}{\varphi_p C_{in}}$$

thus, $\varphi_p C_{in} d\theta = dC_p$. Similarly,

$$\frac{d\xi}{dr} = \frac{1}{r_p}$$

and $r_p d\xi = dr$. Redefining in dimensionless form we obtain,

$$\frac{\varphi_p C_{in} d\theta}{dt} = \frac{D_{ij}}{(r_p \xi)^2} \frac{d}{r_p d\xi} \left((r_p \xi)^2 \frac{\varphi_p C_{in} d\theta}{r_p d\xi} \right) - k_2 C_{cat_p} \varphi_p C_{in} \theta \quad (6.7)$$

Simplifying,

$$\frac{d\theta}{dt} = \frac{D_{ij}}{r_p^2} \frac{1}{\xi^2} \frac{d}{d\xi} \left(\xi^2 \frac{d\theta}{d\xi} \right) - k_2 C_{cat_p} \theta \quad (6.8)$$

We see the Thiele modulus of the peroxisome emerge,

$$\phi_p = \sqrt{\frac{k_2 C_{cat_p} r_p^2}{D_{ij}}} \quad (6.9)$$

Here we are interested in species i , H_2O_2 , travelling through fluid j , the fluid within the peroxisome. The fluid inside the peroxisome is similar to cytosol and we therefore again use the diffusion coefficient of H_2O_2 in H_2O as $1.4 \times 10^{-9} m^2 s^{-1}$ [66]. Our dimensionless equation then reduces further,

$$\frac{d\theta}{dt} = \frac{1}{\xi^2} \frac{d}{d\xi} \left(\xi^2 \frac{d\theta}{d\xi} \right) - \phi_p^2 \theta \quad (6.10)$$

Again, we are interested at steady-state,

$$\frac{1}{\xi^2} \frac{d}{d\xi} \left(\xi^2 \frac{d\theta}{d\xi} \right) = \phi_p^2 \theta \quad (6.11)$$

Redefining our boundary conditions in dimensionless form

$$r = r_p \quad -\varphi_p D_{ij} \frac{dC_p}{dr} = m_p [\varphi_p C_{in} - C_p] \quad (6.12)$$

Making dimensionless

$$\xi = 1 \quad -\varphi_p D_{ij} \frac{\varphi_p C_{in} d\theta}{r_p d\xi} = m_p [\varphi_p C_{in} - \varphi_p C_{in} \theta] \quad (6.13)$$

$$\frac{-\varphi_p^2 D_{ij} C_{in} d\theta}{r_p d\xi} = [m_p \varphi_p C_{in} - m_p \varphi_p C_{in} \theta] \quad (6.14)$$

$$-\frac{d\theta}{d\xi} = \frac{m_p \varphi_p C_{in} r_p}{\varphi_p^2 D_{ij} C_{in}} - \frac{m_p \varphi_p C_{in} \theta r_p}{\varphi_p^2 D_{ij} C_{in}} \quad (6.15)$$

$$\xi = 1 \quad -\frac{d\theta}{d\xi} = \frac{m_p r_p}{\underbrace{\varphi_p D_{ij}}_{Bi_p}} (1 - \theta) \quad \text{Boundary Condition (6.16)}$$

$$r_p = 0 \quad \xi = 0 \quad \frac{d\theta}{d\xi} = 0 \quad \text{Boundary Condition 2 (6.17)}$$

Now that we have successfully transformed both our equation and boundary conditions to dimensionless form, we can solve for theta inside the peroxisome. We are interested in obtaining the concentration profile in the radial direction (θ_ξ). So to write the equation more descriptively we can use θ_ξ (the concentration at and peroxisome radial position, ksi).

$$\frac{1}{\xi^2} \frac{d}{d\xi} \left(\xi^2 \frac{d\theta_\xi}{d\xi} \right) = \phi_p^2 \theta_\xi \quad (6.18)$$

With boundary conditions,

$$\xi = 0 \quad \frac{d\theta}{d\xi} = 0 \quad (6.19)$$

$$\xi = 1 \quad -\frac{d\theta}{d\xi} = Bi_p(1 - \theta_\xi) \quad (6.20)$$

During the process of making the boundary conditions dimensionless, another useful dimensionless parameter emerges, the peroxisome Biot number (Bi_p). The Biot number describes the ratio of the membrane permeability to the diffusion of species i in the volume of interest, here that being the peroxisome region.

To solve, we let $g = \xi\theta_\xi$ or written another way, $\theta_\xi = \frac{g}{\xi}$

$$\frac{d\theta}{d\xi} = \frac{1}{\xi} \frac{dg}{d\xi} - \frac{g}{\xi^2} \quad (6.21)$$

Then,

$$\frac{1}{\xi^2} \frac{d}{d\xi} \left(\xi^2 \left\{ \frac{1}{\xi} \frac{dg}{d\xi} - \frac{g}{\xi} \right\} \right) = \phi_p^2 \theta_\xi \quad (6.22)$$

$$\frac{1}{\xi^2} \frac{d}{d\xi} \left(\xi \frac{dg}{d\xi} - g \right) = \phi_p^2 \theta_\xi \quad (6.23)$$

$$\frac{1}{\xi^2} \left[\frac{d\xi}{d\xi} \frac{dg}{d\xi} + \xi \frac{d^2g}{d\xi^2} - \frac{dg}{d\xi} \right] = \phi_p^2 \theta_\xi \quad (6.24)$$

Simplifying,

$$\frac{1}{\xi^2} \left[\xi \frac{d^2g}{d\xi^2} \right] = \phi_p^2 \theta_\xi \quad (6.25)$$

$$\frac{1}{\xi} \frac{d^2g}{d\xi^2} = \phi_p^2 \theta_\xi \quad (6.26)$$

Knowing $\theta_\xi = \frac{g}{\xi}$ we obtain,

$$\frac{1}{\xi} \frac{d^2 g}{d\xi^2} = \phi_p^2 \frac{g}{\xi} \quad (6.27)$$

Thus,

$$\frac{d^2 g}{d\xi^2} = \phi_p^2 g \quad (6.28)$$

Because this is a linear differential equation with constant coefficients we know the general solution will follow $g = Ae^{B\xi}$. We begin by guessing this as the solution, $g = Ae^{B\xi}$ then, $\frac{dg}{d\xi} = BAe^{B\xi}$ and $\frac{d^2 g}{d\xi^2} = B^2 Ae^{B\xi}$. It becomes clear $B^2 = \phi_p^2$ thus $B = \pm \phi_p$ resulting in the solution of the form, $g = C_1 e^{\phi_p \xi} + C_2 e^{-\phi_p \xi}$. Where C_1 and C_2 are, arbitrary constants solved for later using the boundary conditions. Since g is defined as $g = \xi \theta_\xi$ we can re-write the general solution as,

$$\xi \theta_\xi = C_1 e^{\phi_p \xi} + C_2 e^{-\phi_p \xi} \quad (6.29)$$

And obtain,

$$\theta_\xi = \frac{C_1 e^{\phi_p \xi} + C_2 e^{-\phi_p \xi}}{\xi} \quad (6.30)$$

Using the boundary conditions to solve for the constants (C_1 and C_2) we see this form for the general solution, similar to the lumped parameter validation, proves again difficult. For simplicity, we are able to take advantage of hyperbolic functions and understanding that

$\cosh(x) = \frac{e^x + e^{-x}}{2}$ and $\sinh(x) = \frac{e^x - e^{-x}}{2}$, we can improve our guess for the general solution to be instead,

$$\theta_\xi = \frac{C_1 \sinh(\phi_p \xi) + C_2 \cosh(\phi_p \xi)}{\xi} \quad (6.31)$$

Evaluating at the boundary condition

$$\xi = 0 \quad \frac{d\theta}{d\xi} = 0 \quad (6.32)$$

$$\frac{d\theta}{d\xi} = \frac{\phi_p C_1 \sinh(\phi_p \xi) + \phi_p C_2 \cosh(\phi_p \xi)}{\xi} - \frac{C_1 \sinh(\phi_p \xi) + C_2 \cosh(\phi_p \xi)}{\xi^2} \quad (6.33)$$

$$\frac{d\theta}{d\xi} = \frac{\xi[\phi_p C_1 \sinh(\phi_p \xi) + \phi_p C_2 \cosh(\phi_p \xi)] - [C_1 \sinh(\phi_p \xi) + C_2 \cosh(\phi_p \xi)]}{\xi^2} \quad (6.34)$$

Thus, at this boundary,

$$0 = \frac{0[\phi_p C_1 \sinh(0) + \phi_p C_2 \cosh(0)] - [C_1 \sinh(0) + C_2 \cosh(0)]}{(0)^2} \quad (6.35)$$

$$C_2 = 0$$

Resulting in,

$$\theta_\xi = \frac{C_1 \sinh(\phi_p \xi)}{\xi} \quad (6.36)$$

However, if we evaluate the limit as ξ approaches zero we see,

$$\lim_{\xi \rightarrow 0} \theta_\xi = \frac{C_1 \sinh(0)}{0} = \frac{0}{0} \quad (6.37)$$

We again use L'Hôpital's rule to determine whether a finite constant can be determined.

$$\lim_{\xi \rightarrow 0} \frac{c_1 \sinh(\phi_p \xi)}{\xi} = \lim_{\xi \rightarrow 0} \frac{\frac{d}{d\xi}(c_1 \sinh(\phi_p \xi))}{\frac{d}{d\xi}(\xi)} \quad (6.38)$$

$$\lim_{\xi \rightarrow 0} \frac{\phi_p c_1 \cosh(\phi_p \xi)}{1} = \phi_p c_1 \quad (6.39)$$

Now that $\phi_p c_1$ is confirmed to be a finite number we can solve

$$\theta_\xi = \frac{c_1 \sinh(\phi_p \xi)}{\xi} \quad (6.40)$$

At the boundary condition

$$\xi = 1 \quad \frac{d\theta}{d\xi} = Bi_p (1 - \theta_\xi) \quad (6.41)$$

We see,

$$\frac{\xi[\phi_p c_1 \cosh(\phi_p \xi)] - [c_1 \sinh(\phi_p \xi)]}{\xi^2} = Bi_p (1 - \theta_\xi) \quad (6.42)$$

Since $\theta_\xi = \frac{c_1 \sinh(\phi_p \xi)}{\xi}$

$$\frac{c_1[\phi_p \xi \cosh(\phi_p \xi) - \sinh(\phi_p \xi)]}{\xi^2} = Bi_p \left(1 - \frac{c_1 \sinh(\phi_p \xi)}{\xi}\right) \quad (6.43)$$

At $\xi = 1$,

$$c_1[\phi_p \cosh(\phi_p) - \sinh(\phi_p)] = Bi_p - Bi_p c_1 \sinh(\phi_p) \quad (6.44)$$

$$C_1[\phi \cosh(\phi_p) - \sinh(\phi_p)] + Bi_p C_1 \sinh(\phi_p) = Bi_p \quad (6.45)$$

$$C_1[\phi_p \cosh(\phi_p) - \sinh(\phi_p) + Bi_p \sinh(\phi_p)] = Bi_p \quad (6.46)$$

$$C_1 = \frac{Bi_p}{[\phi_p \cosh(\phi_p) - \sinh(\phi_p) + Bi_p \sinh(\phi_p)]} \quad (6.47)$$

$$C_1 = \frac{Bi_p}{[\phi_p \cosh(\phi_p) + \sinh(\phi_p)(Bi_p - 1)]} \quad (6.48)$$

Now that we know the value of C_1 we can replace it in

$$\theta_\xi = \frac{C_1 \sinh(\phi_p \xi)}{\xi} \quad (6.49)$$

Resulting in,

$$\theta_\xi = \frac{Bi_p}{[\phi_p \cosh(\phi_p) + \sinh(\phi_p)(Bi_p - 1)]} \frac{\sinh(\phi_p \xi)}{\xi} \quad (6.50)$$

Or simply,

$$\theta_\xi = \frac{Bi_p \sinh(\phi_p \xi)}{\xi [\phi_p \cosh(\phi_p) + \sinh(\phi_p)(Bi_p - 1)]} \quad (6.51)$$

The overall effectiveness can be determined by taking the ratio of the average reaction rate in the peroxisome (\bar{R}_i), Eqn 6.2, to the reaction rate if all catalase were directly exposed to the solution, denoted as R_{ext} . Defining the effectiveness factor or latency factor as

$$\eta_{eff} = \frac{\bar{R}_i}{R_{ext}} = \frac{\int -k_2 C_{cat_p} C_p(r) dV}{\int -k_2 C_{cat_p} \phi_p C_{ext} dV} \quad (6.52)$$

$$\eta_{eff} = \frac{\int C_p(r) dV}{\int \phi_p C_{ext} dV} \quad (6.53)$$

Recall, $\theta = \frac{C_p}{\phi_p C_{ext}}$ thus reducing Eqn (6.53) to,

$$\eta_{eff} = \frac{\int \theta dV}{\int dV} \quad (6.54)$$

$$\eta_{eff} = \frac{\int \theta dV}{V_p} \quad (6.55)$$

$$\eta_{eff} = \frac{1}{V_p} \int_0^{r_p} \theta dV \quad (6.56)$$

Since the volume of the peroxisome is assumed to be spherical, $V_p = \frac{4}{3} \pi r_p^3$ thus,

$$dV_p = 4\pi r_p^2 dr,$$

$$\eta_{eff} = \frac{1}{\frac{4}{3} \pi r_p^3} \int_0^{r_p} \theta 4\pi r^2 dr \quad (6.57)$$

Since $r = \xi r_p$ and $\xi = \frac{r}{r_p}$ where $\frac{d\xi}{dr} = \frac{1}{r_p}$ thus $dr = r_p d\xi$ then Eqn (6.57) becomes,

$$\eta_{eff} = \frac{1}{\frac{4}{3} \pi r_p^3} \int_0^{r_p} \theta 4\pi (\xi r_p)^2 r_p d\xi \quad (6.58)$$

$$\eta_{eff} = \frac{4\pi r_p^3}{\frac{4}{3} \pi r_p^3} \int_0^{r_p} \theta \xi^2 d\xi \quad (6.59)$$

Simplifying Eqn (6.59) further we obtain,

$$\eta_{eff} = \frac{\bar{R}_i}{R_{ext}} = 3 \int_0^1 \theta_\xi \xi^2 d\xi, \quad (6.60)$$

where \bar{R}_i is the average volume reaction rate across the peroxisome and R_{ext} is the reaction rate for the case where all the catalase enzymes are directly exposed to the solution.

Now that we have the relationship for the effectiveness factor (η_{eff}) and the concentration profile (θ_ξ) in the peroxisome, we can use integration by parts to integrate and obtain a solution for η_{eff} . Therefore replacing Eqn (6.51) into Eqn (6.60) we obtain Eqn (6.61)

$$\eta_{eff} = 3 \int_0^1 \frac{Bi_p \sinh(\phi_p \xi)}{\xi [\phi_p \cosh(\phi_p) + (Bi_p - 1) \sinh(\phi_p)]} \xi^2 d\xi \quad (6.61)$$

$$\eta_{eff} = 3 \int_0^1 \frac{Bi_p \sinh(\phi_p \xi) \xi}{[\phi_p \cosh(\phi_p) + (Bi_p - 1) \sinh(\phi_p)]} d\xi \quad (6.62)$$

Pulling out the constants,

$$\eta_{eff} = \frac{3Bi_p}{[\phi_p \cosh(\phi_p) + (Bi_p - 1) \sinh(\phi_p)]} \int_0^1 \sinh(\phi_p \xi) \xi d\xi \quad (6.63)$$

Here we must use integration by parts (IBP),

$$\eta_{eff} = \frac{3Bi_p}{[\phi_p \cosh(\phi_p) + (Bi_p - 1) \sinh(\phi_p)]} \left[uv \Big|_0^1 - \int_0^1 v du \right] \quad (6.64)$$

To carry out IBP let,

$$u = \xi$$

$$dv = \sinh(\phi_p \xi) d\xi$$

$$du = d\xi$$

$$v = \frac{\cosh(\phi_p \xi)}{\phi_p}$$

Solving,

$$\eta_{eff} = \frac{3Bi_p}{[\phi_p \cosh(\phi_p) + (Bi_p - 1) \sinh(\phi_p)]} \left[\xi \frac{\cosh(\phi_p \xi)}{\phi_p} \Big|_0^1 - \int_0^1 \frac{\cosh(\phi_p \xi)}{\phi_p} d\xi \right] \quad (6.65)$$

$$\eta_{eff} = \frac{3Bi_p}{[\phi_p \cosh(\phi_p) + (Bi_p - 1) \sinh(\phi_p)]} \left[\xi \frac{\cosh(\phi_p \xi)}{\phi_p} \Big|_0^1 - \frac{1}{\phi_p} \int_0^1 \cosh(\phi_p \xi) d\xi \right] \quad (6.66)$$

$$\eta_{eff} = \frac{3Bi_p}{[\phi_p \cosh(\phi_p) + (Bi_p - 1) \sinh(\phi_p)]} \left[\xi \frac{\cosh(\phi_p \xi)}{\phi_p} \Big|_0^1 - \frac{1}{\phi_p} \frac{\sinh(\phi_p \xi)}{\phi_p} \Big|_0^1 \right] \quad (6.67)$$

$$\eta_{eff} = \frac{3Bi_p}{[\phi_p \cosh(\phi_p) + (Bi_p - 1) \sinh(\phi_p)]} \left[\eta \frac{\cosh(\phi_p \eta)}{\phi_p} \Big|_0^1 - \frac{1}{\phi_p} \frac{\sinh(\phi_p \xi)}{\phi_p} \Big|_0^1 \right] \quad (6.68)$$

$$\eta_{eff} = \frac{3Bi_p}{[\phi_p \cosh(\phi_p) + (Bi_p - 1) \sinh(\phi_p)]} \left[\frac{\cosh(\phi_p)}{\phi_p} - \frac{1}{\phi_p} \frac{\sinh(\phi_p)}{\phi_p} \right] \quad (6.69)$$

$$\eta_{eff} = \frac{3Bi_p}{[\phi_p \cosh(\phi_p) + (Bi_p - 1) \sinh(\phi_p)]} \left[\frac{\cosh(\phi_p)}{\phi_p} - \frac{\sinh(\phi_p)}{\phi_p^2} \right] \quad (6.70)$$

$$\eta_{eff} = \frac{3Bi_p \cosh(\phi_p)}{[\phi_p \cosh(\phi_p) + (Bi_p - 1) \sinh(\phi_p)] \phi_p} - \frac{3Bi_p \sinh(\phi_p)}{[\phi_p \cosh(\phi_p) + (Bi_p - 1) \sinh(\phi_p)] \phi_p^2} \quad (6.71)$$

$$\eta_{eff} = \frac{3Bi_p \cosh(\phi_p) \phi_p}{[\phi_p \cosh(\phi_p) + (Bi_p - 1) \sinh(\phi_p)] \phi_p^2} - \frac{3Bi_p \sinh(\phi_p)}{[\phi_p \cosh(\phi_p) + (Bi_p - 1) \sinh(\phi_p)] \phi_p^2} \quad (6.72)$$

$$\eta_{eff} = \frac{3Bi_p \cosh(\phi_p) \phi_p - 3Bi_p \sinh(\phi_p)}{[\phi_p \cosh(\phi_p) + (Bi_p - 1) \sinh(\phi_p)] \phi_p^2} \quad (6.73)$$

$$\eta_{eff} = \frac{3Bi_p (\phi_p \cosh(\phi_p) - \sinh(\phi_p))}{\phi_p^2 [\phi_p \cosh(\phi_p) + (Bi_p - 1) \sinh(\phi_p)]} \quad (6.74)$$

Thus, it becomes clear that,

$$\eta_{eff} = \frac{3Bi_p}{\phi_p^2} \left[\frac{\phi_p \cosh(\phi_p) - \sinh(\phi_p)}{[\phi_p \cosh(\phi_p) - \sinh(\phi_p) + Bi_p \sinh(\phi_p)]} \right] \quad (6.75)$$

Further, defining latency (χ) as the ratio of reduction in effectiveness to the maximum potential for the catalase reaction, we obtain

$$\chi \equiv \frac{R_{ext} - \bar{R}_i}{R_{ext}} = 1 - \frac{3Bi_p}{\phi_p^2} \left[\frac{\phi_p \cosh(\phi_p) - \sinh(\phi_p)}{\phi_p \cosh(\phi_p) - \sinh(\phi_p) + Bi_p \sinh(\phi_p)} \right] \quad (6.76)$$

Therefore, latency is

$$\chi = 1 - \eta_{eff} \quad (6.78)$$

Eqn (6.78) can be used to determine the latency of any enzymatic reaction associated with an organelle provided the membrane permeability, enzyme activity, diffusivity and organelle average radius are known.

Table 6.1 Parameters used for calculating cell Thiele modulus using observed H₂O₂ decay for intact peroxisome

Cell Line	$k_{obs_p}(s^{-1})$	$k_{obs_p}(s^{-1})$	n_p^*	k_2'	k_2'	Average k_2'	ϕ_c
U-87 (Case 1)	$(6.02 \pm 0.07) \times 10^{-4}$	$(5.05 \pm 0.11) \times 10^{-4}$	$(1.56 \pm 0.30) \times 10^8$	2.31×10^{-17}	1.94×10^{-17}	$(2.13 \pm 0.26) \times 10^{-17}$	0.366
U-87 (Case 2)	$(4.56 \pm 1.40) \times 10^{-4}$	$(4.69 \pm 0.08) \times 10^{-4}$	$(2.72 \pm 0.43) \times 10^8$	1.01×10^{-17}	1.04×10^{-17}	$(1.02 \pm 0.02) \times 10^{-17}$	0.254
U-87 (Case 3)	$(3.99 \pm 0.21) \times 10^{-4}$	$(4.50 \pm 0.33) \times 10^{-4}$	$(2.90 \pm 0.16) \times 10^8$	8.25×10^{-18}	9.31×10^{-18}	$(8.78 \pm 0.75) \times 10^{-18}$	0.235
U-87 (Case 4)	$(7.52 \pm 0.32) \times 10^{-4}$	$(7.29 \pm 0.78) \times 10^{-4}$	$(5.32 \pm 0.65) \times 10^8$	8.48×10^{-18}	8.22×10^{-18}	$(8.35 \pm 0.18) \times 10^{-18}$	0.229
T98G (Case 1)	$(7.07 \pm 0.19) \times 10^{-4}$	$(6.76 \pm 0.11) \times 10^{-4}$	$(1.23 \pm 0.21) \times 10^8$	3.45×10^{-17}	3.30×10^{-17}	$(3.37 \pm 0.11) \times 10^{-17}$	0.474
T98G (Case 2)	$(7.94 \pm 0.08) \times 10^{-4}$	$(6.91 \pm 0.53) \times 10^{-4}$	$(3.91 \pm 0.54) \times 10^8$	1.22×10^{-17}	1.06×10^{-17}	$(1.14 \pm 0.11) \times 10^{-17}$	0.275
T98G (Case 3)	$(5.43 \pm 0.45) \times 10^{-4}$	$(5.67 \pm 0.13) \times 10^{-4}$	$(1.88 \pm 0.23) \times 10^8$	1.73×10^{-17}	1.81×10^{-17}	$(1.77 \pm 0.05) \times 10^{-17}$	0.344
LN-229 (Case 1)	$(1.62 \pm 0.05) \times 10^{-3}$	$(1.53 \pm 0.02) \times 10^{-3}$	$(5.94 \pm 1.21) \times 10^8$	1.63×10^{-17}	1.54×10^{-17}	$(1.59 \pm 0.06) \times 10^{-17}$	1.16
LN-229 (Case 2)	$(1.18 \pm 0.07) \times 10^{-3}$	$(1.11 \pm 0.03) \times 10^{-3}$	$(7.28 \pm 0.50) \times 10^8$	9.72×10^{-18}	9.17×10^{-18}	$(9.45 \pm 0.39) \times 10^{-18}$	0.90
LN-229 (Case 3)	$(5.96 \pm 1.61) \times 10^{-4}$	$(8.54 \pm 0.70) \times 10^{-4}$	$(6.12 \pm 0.66) \times 10^8$	5.85×10^{-18}	8.37×10^{-18}	$(7.11 \pm 1.79) \times 10^{-18}$	0.78
MIA PaCa-2 (Case 1)	$(8.34 \pm 0.91) \times 10^{-4}$	$(8.81 \pm 1.70) \times 10^{-4}$	$(6.08 \pm 0.09) \times 10^8$	8.23×10^{-18}	8.69×10^{-18}	$(8.46 \pm 0.33) \times 10^{-18}$	0.401
MIA PaCa-2 (Case 2)	$(1.32 \pm 0.04) \times 10^{-3}$	$(1.43 \pm 0.03) \times 10^{-3}$	$(2.13 \pm 0.45) \times 10^9$	3.72×10^{-18}	4.03×10^{-18}	$(3.87 \pm 0.22) \times 10^{-18}$	0.271
MIA PaCa-2 (Case 3)	$(1.96 \pm 0.03) \times 10^{-3}$	$(1.60 \pm 0.06) \times 10^{-3}$	$(1.36 \pm 0.08) \times 10^9$	8.63×10^{-18}	7.06×10^{-18}	$(7.84 \pm 1.11) \times 10^{-18}$	0.386
MIA PaCa-2 (Case 4)	$(7.80 \pm 0.20) \times 10^{-4}$	$(7.47 \pm 0.95) \times 10^{-4}$	$(5.91 \pm 0.03) \times 10^8$	7.91×10^{-18}	7.59×10^{-18}	$(7.75 \pm 0.23) \times 10^{-18}$	0.383
H6c7 (Case 1)	$(2.42 \pm 0.14) \times 10^{-3}$	$(2.07 \pm 0.05) \times 10^{-3}$	$(2.99 \pm 0.03) \times 10^8$	4.86×10^{-17}	4.15×10^{-17}	$(4.50 \pm 0.50) \times 10^{-17}$	0.819
H6c7 (Case 2)	$(7.99 \pm 0.17) \times 10^{-4}$	$(7.76 \pm 0.57) \times 10^{-4}$	$(7.61 \pm 0.08) \times 10^8$	6.30×10^{-18}	6.12×10^{-18}	$(6.21 \pm 0.13) \times 10^{-18}$	0.304
H6c7 (Case 3)	$(7.21 \pm 0.91) \times 10^{-4}$	$(7.33 \pm 1.13) \times 10^{-4}$	$(1.86 \pm 0.01) \times 10^9$	2.33×10^{-17}	2.36×10^{-17}	$(2.34 \pm 0.03) \times 10^{-17}$	0.591

Table 6.1 displays the calculated Thiele modulus of the cell using the observed H_2O_2 uptake when the peroxisomes remained intact $k_{obs_p} (s^{-1})$. Recall from Chapter 3, Thiele modulus for the cell is described as $\phi_c \equiv \sqrt{k_2^* \rho_p r_c^2 / D_{ij}}$. Thus, the table shows the number of peroxisomes in the chamber, n_p^* , and the volume of the chamber, V_{ext}^* , are known which allows for k_2^* to be calculated. k_2^* is obtains the following relationship $\frac{k_{obs_p}}{(n_p^*/V_{ext}^*)}$ and is further explained in Appendix VII. Thus multiplying k_2^* by ρ_p (density of peroxisomes of the cell) we can obtain the Thiele modulus. For clarification, the $\rho_p = n_p/V_{in}$ which is the number of peroxisomes for the given cell divided by the volume of that cell that is not occupied by the nucleus.

6.2.2 Latency

Using the cell-specific parameters previously determined (Chapter 5) we calculate the Biot number, Thiele modulus, effectiveness and latency of the peroxisome specific for each cell respectively, Table 6.2.

The Biot number for the peroxisome (Bi_p) was obtained using the cell-specific peroxisome membrane mass transfer coefficient (m_p), the radius of the peroxisome (r_p), and the diffusion of H_2O_2 in water was taken as $1.4 \times 10^{-9} m^2 s^{-1}$ [66].

The Bi_p indicates whether the concentration inside the peroxisome will vary significantly in space while mass is transferring across the peroxisome membrane. The resulting range

across the cell lines for the Bi_p falls between 0.001 – 0.005 and are not significantly different from one another. Further, these small Bi_p declare that the concentration is uniformly distributed throughout the peroxisome organelle. The (m_p) values across the cell lines do not vary significantly from one another and contributes to the similar Bi_p across cell lines to arise.

The Thiele modulus for the peroxisome (ϕ_p) provides information on how quickly the H_2O_2 diffuses inside the peroxisome to the center before it is consumed. This dimensionless parameter is important for understanding whether spatial contributions should be considered or if the compartment can be considered well-mixed. Here we have

$$\phi_p = \sqrt{k_2 C_{cat_p} r_p^2 / D_{ij}},$$

where the ranges fall between 0.085 – 0.317 for MIA PaCa-2

unmodified to U-87 cells respectively. With a Thieles modulus $\ll 1$, it is safe to assume that spatial contributions may be ignored and that H_2O_2 diffuses to the center of the peroxisome before being consumed. Thus, there is not a large gradient of H_2O_2 from the wall to the center and instead the H_2O_2 diffuses everywhere allowing for the well-mixed assumption.

The effectiveness factor (η_{eff}) indicates how effective the peroxisome organelle is in terms of its efficiency to consume H_2O_2 . The effectiveness of the catalase inside the peroxisome ranges from 0.08 – 0.64, for the U-87 to MIA PaCa-2 cell respectively. There is more of a distribution across the cell lines in respect to the effectiveness factor. It appears that

certain cells have a more efficient catalytic activity than others. The variation in this parameter likely arises from the peroxisome volume variations across the cell lines. The size of the peroxisome will directly affect the catalase activity. If the peroxisome is confined to smaller regions, then its effectiveness would increase and vice versa the catalase would become less efficient as the space increases. Another factor is the Thiele modulus, we see it is larger for U-87, thus meaning the reaction is increased and causing more of a gradient to occur inside the peroxisome than with the MIA PaCa-2 which has a much lower Thiele modulus.

Cell Type	η_{eff}	Bi_p	ϕ_p	χ
MIA PaCa-2 Unmodified	0.64	0.004	0.085	0.36
MIA PaCa-2 siAQP3	0.64	0.004	0.085	0.36
H6c7	0.12	0.001	0.118	0.88
U-87	0.08	0.003	0.317	0.92
T98G	0.13	0.005	0.303	0.87
LN-229	0.24	0.004	0.184	0.76

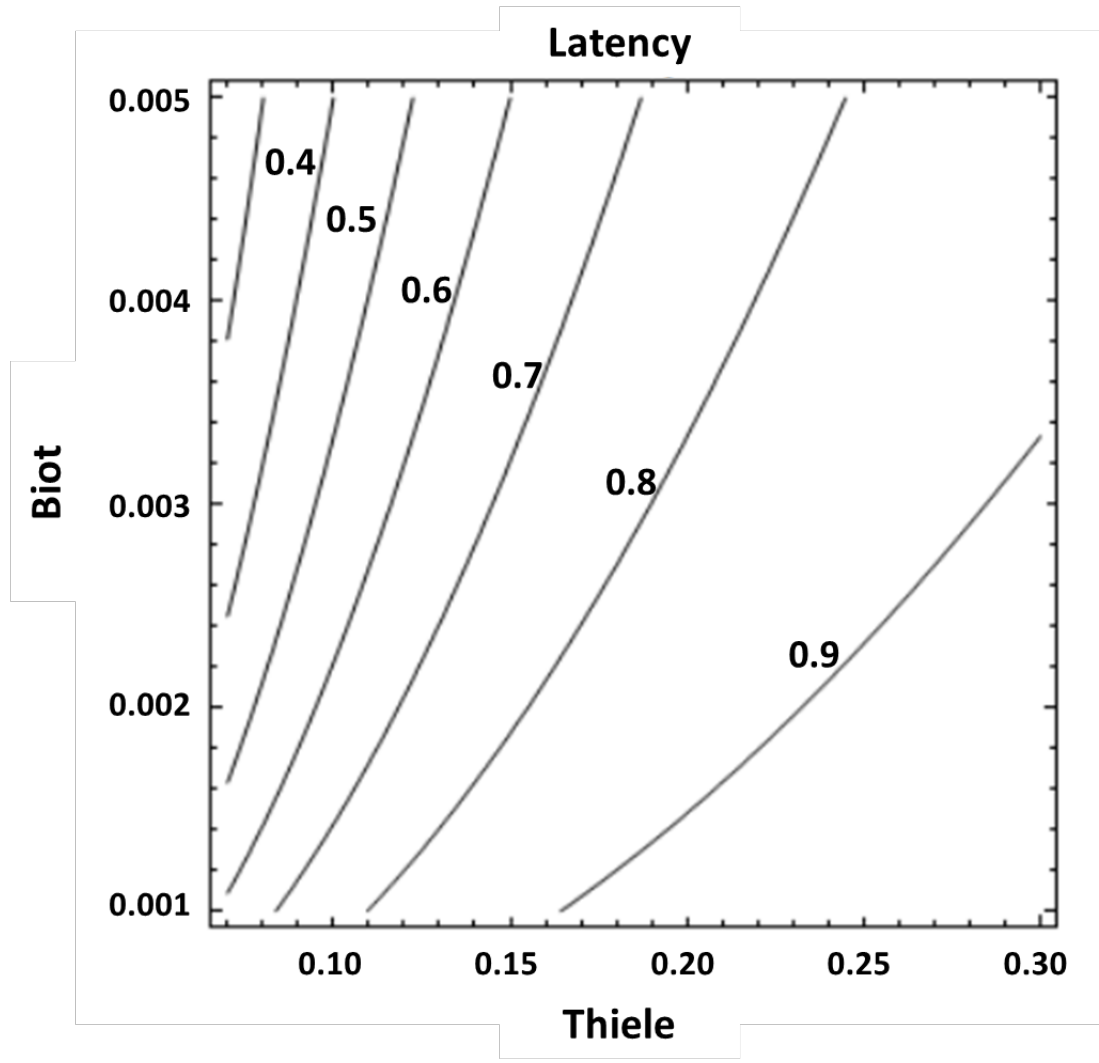


Figure 6.2. Displays the overall Latency (χ), by representing the relationship between the Bi_p and the ϕ_p . Comparing Table 6.2 with this curve, we see for example U-87 cells have a Biot number of 0.003 and a Thiele modulus for the peroxisome membrane measuring 0.32 resulting in a latency of 0.87, if we reflect to the curve presented here we see the same values presented.

6.3 Conclusion

Here we have presented a model that quantifies latency based on known cell-specific parameters. We successfully calculated the effectiveness factor, where latency is $1 - \eta_{eff}$.

CHAPTER 7. CONCLUSION AND IMPACT

This work once again reiterates that toxicity via extracellular H_2O_2 dosing is indeed an important factor when considering the mechanism behind P-AscH⁻. We have illuminated that the complexity behind ascorbate therapy is more intricate than simply linking ascorbate-susceptibility to a quantifiable intracellular H_2O_2 concentration. The variations in catalase concentration and permeability clearly have combined effects on the surviving fraction of a cell. Neither catalase activity nor the cell membrane permeability characteristics have the potential to serve as a predictor for the success of ascorbate therapy independently. Although this is true, if we address the permeability from a cell-dependent manner, for instance the MIA PaCa-2 cells have a higher intracellular H_2O_2 concentration for the unmodified cells compared to the siAQP3 cells. Further the plasma membrane between these cell lines was altered by a factor of 3. While it is undeniable that a critical H_2O_2 concentration independent of cell-type is not a plausible answer, H_2O_2 may be indicative on a cell-specific manner.

Thus, evaluating cells individually and understanding the contributions of each of cell-specific parameter (sensitivity analysis) lends itself the opportunity of insight for future cellular targets and ability to improve the efficacy of this therapy for cancer cells that are currently less susceptible. For example, certain cancer drugs, such as gemcitabine, are known to elevate AQP3 expression for some cancer cells [55]. Interestingly, not only is gemcitabine a current pancreatic cancer treatment but P-AscH⁻ has shown to have

synergistic effects and demonstrated itself to be specifically promising as an adjuvant to this drug [3, 6, 27, 32]. This suggests that future use of ascorbate in combination with AQP modulating drugs, specifically peroxiporin modulating, may prove successful in the treatment of cancer.

While the positive combinatorial effects of ascorbate with peroxiporin-modulating drugs is all speculation at the current time, we demonstrated that modification of peroxiporin AQP3 did contribute to H₂O₂ cytotoxicity. Further silencing peroxiporin AQP3 on pancreatic cancer cells displayed a lower membrane permeability, lower resulting intracellular H₂O₂, and increased surviving fraction for this cell line. Further evaluation of peroxiporins is therefore warranted.

Our preliminary work (Appendix V) displays possible variation in peroxiporin expression on glioblastoma cells but further examination of other peroxiporins on other cell types would be a great direction for future work. In this regard, it is of great interest to conduct western blots for all peroxiporins on each of the cell types to further quantify the expression level differences. While we could provide a preliminary look at peroxiporin variation through flow cytometry and immunocytochemistry, evaluating western blots for these cases would aid tremendously in understanding the relationship of peroxiporin expression and H₂O₂ toxicity. Western blot analysis would provide the opportunity for improved

quantification such as specifically addressing the peroxiporin contribution in overall permeability (for example, addressing same cell cases containing silencing modifications). Silencing the additional peroxiporins would also be interesting, such as AQP 8, to evaluate whether the other peroxiporins contribute to the success of ascorbate therapy. In addition to silencing modifications, overexpressing these peroxiporins should also be conducted. It is suspected that overexpression of peroxiporins would increase the intracellular H_2O_2 and result in a decreased clonogenic surviving fraction. When evaluating overexpression affects, our sensitivity analysis would allow the researcher to understand the limit for when overexpressing will no longer change the intracellular H_2O_2 levels etc. Although our cell plasma membrane permeability parameter (m_{plm}) describes the overall permeability and thus encompasses both peroxiporin contribution, it does not discern which peroxiporin nor peroxiporin contribution independently. This could also be clearly demonstrated in the future with continued effort in this area via western blots and peroxiporin modifications (silencing and overexpressing).

In regards to permeability, the cancer lines we evaluated exhibited similar peroxisome membrane permeability (refer to table 5.1). The only cell line that exhibited a significantly different peroxisome membrane permeability was the normal pancreatic cell line (H6c7). It is noted that this is the only normal cell line out of the cells investigated in this work. It was expected that this membrane permeability would not vary across cell lines as there was no indication in literature suggesting property differences in this membrane across cells.

While literature does not propose that this membrane varies across cell lines, it also does not contain any discussion of the presence of porins/AQPs or lack thereof on this membrane. We confirmed for our studies that AQP3 was not present on the peroxisome membrane through ELISAs. While confident AQP3 is not present, we did not confirm that the other porins were not expressed on peroxisome membranes, and thus a full analysis of this membrane may want to be further investigated for confirmation.

Continuing discussion on Table 5.1, some of the obtained values within in this chart have opportunity for improvement. While analysis of confocal microscopy images provided results comparable to literature for information pertaining to the peroxisomes and nucleus of each cell, the error in these values can be significantly reduced by using SEM and TEM. Decreasing the error is important as the calculated intracellular H_2O_2 concentration depends on numerous variables in this chart and the total error is propagated. The resulting propagated error as seen in Fig 5.5 is quite large. Further the size of the nucleus could also be confirmed with these additional techniques. The latter is extremely important as the volume of the cell used for all calculations is the volume that is not occupied by the nucleus. Decreasing the error in this value is of great importance.

We also find that reporting the average external concentration (\bar{C}_{ext}) used during clonogenic assays could improve results across labs. We find that through using \bar{C}_{ext} for dose exposure increases accuracy compared to representing the exposure in terms of

concentration per cell [52]. Both dose representations act to serve as a more informative dosing metric for cell culture, as often, variations seen in experimental results arise as these systems are cell density dependent. However, in addition to issues arising with cell-density dependency are those concerned with chamber volume. For this reason, calculating the \bar{C}_{ext} permits the most accurate concentration exposure over the hour for the clonogenic setup. Further, it was revealed in Fig 5.2 that the external concentration scales in a cell-specific manner and thus \bar{C}_{ext} provides the dose exposure for each cell type. Thus, depending on the cell under investigation, the initial dose introduced may vary and must be calculated to ensure the appropriate external concentration is used for either experimental replication or calculating the resulting intracellular H_2O_2 concentration for the given dose.

Further, using the estimation for the average external H_2O_2 is a precursor to more predictive tool to determine time for treatment. An advanced model can determine treatment times if correlated with growth cellular dynamics. This could be useful if treatment moves to scenarios such as in-home IV methods as could indicate the duration and frequency of therapy.

Moving forward from the quantification of intracellular H_2O_2 , we understand that there exist numerous additional factors which may alter the effects of internal H_2O_2 of these cells. One avenue for further exploration is the free labile iron within cells [46]. It has also been suggested that intracellular H_2O_2 is activated in the presence of catalytic transition

metals generating significant hydroxyl radical ($\text{HO}\cdot$) [46], which serves to substantially increase DNA damage. Perhaps furthering this model to include catalytic iron variations amongst cells and its effects on $\text{HO}\cdot$ production would aid in defining the critical concentration of internal H_2O_2 needed to produce the toxic $\text{HO}\cdot$ on a cell-specific basis.

It has been clearly demonstrated that H_2O_2 , alone, is not the mitigating factor: The results show that even when the intracellular H_2O_2 concentrations was estimated to be the same, the non-cancerous cells exhibited a significantly higher surviving fraction than any of the cancer cells. This is consistent with the recent analysis that the intracellular H_2O_2 , while critical during P-AscH⁻ therapy, is not the only factor in predicting pharmacological ascorbate therapy success. The presented mathematical model provides a quantitative assessment of intracellular H_2O_2 during high P-AscH⁻ that can be improved to understand the efficacy of pharmacological ascorbate therapy.

APPENDIX I: EXAMPLE IMMUNOCYTOCHEMISTRY

STAINING FOR AQP3

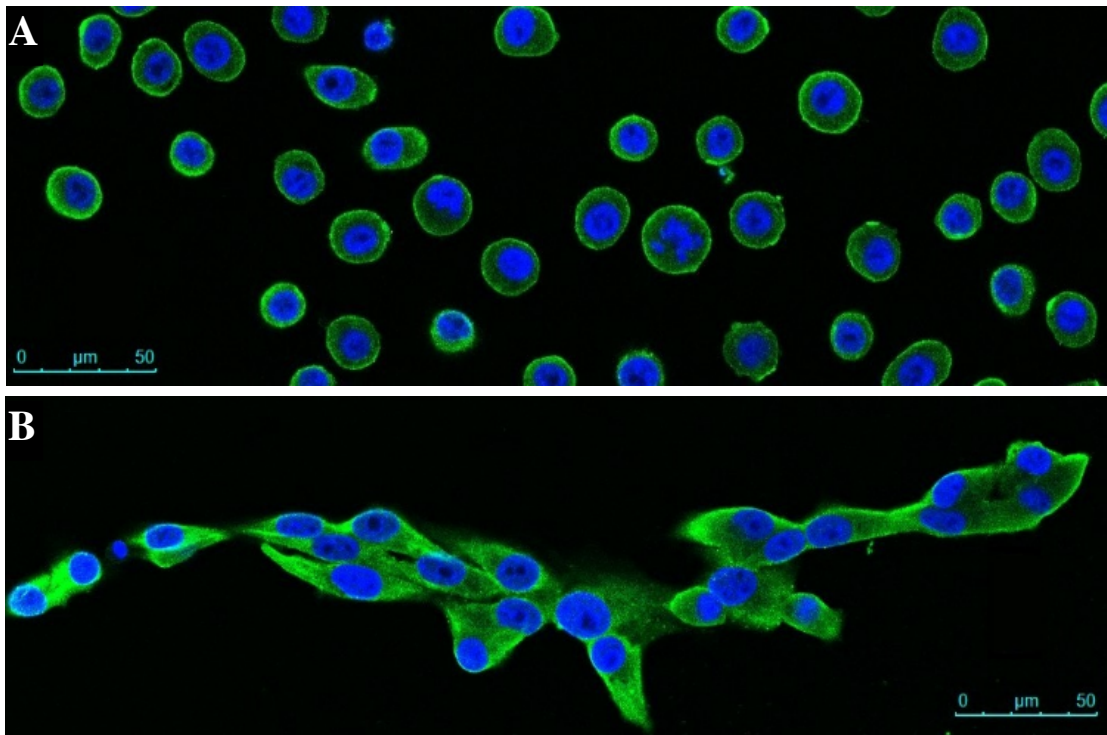


Fig Appendix I. Examples of immunocytochemistry staining for the presence of peroxiporin AQP3 of H6c7 (A) and MIA PaCa-2 (B) pancreatic cells. The nucleus of the cell is indicated in blue, stained with Dapi and the green fluorescence is peroxiporin AQP3. These images were further analyzed for the AQP3 signal intensity per cell using ImageJ. The signal intensities evaluated from immunocytochemistry also allowed for a qualitative measurement for the relative expression levels for each peroxiporin on both cell types. Elevated signal intensities indicate greater presence of these proteins and therefore elevated expression. Images of the immunocytochemistry staining for AQP1, AQP3, and AQP8 in H6c7 and MIA PaCa-2 cell, allow qualitative assessment for AQP expression of each cell type (refer to Fig 2.1)

APPENDIX II: CODE FOR REGRESSION OF PEROXISOME MEMBRANE PERMEABILITY (m_p)

Codes for regression for peroxisome membrane permeability

```
function nonlinfit_of_argus4R  
  
clear; clc  
  
data = xlsread('LN_perox_case3_170504.xlsx'); %Reads in each specific cell file case  
tobs = data(:,1); %Reads the column where the specific time points for that data excel  
reads  
  
yobs = data(:,7); %Reads the column containing the data points  
  
  
b0 = 2*10^-5; %Initial guess for  $m_p$  (if initial guess is too far from the solution, the  
regression may not converge to a solution)  
  
[b_fit,X2,sigma_b,sigma_y,corr,R_sq,cvg_hst]=lm(@panoptes4R,b0,tobs,yobs,1,10^-15)  
%Uses Levenberg-Marquardt regression (lm.m) file that and solves the system of ODEs  
to fit the data to the first curve. The first curve represents the external H2O2 concentration  
over time and is the projected trajectory based on the cell-specific parameters entered  
within the argus4R.m file. The data from the H2O2 uptake (peroxisome intact) study are  
time points that should follow this general trend. Thus, fitting the data to the first curve  
will allow for the regression of the peroxisome membrane mass transfer coefficient.
```



```
y_hat = panoptes4R(tobs,b_fit) % The panoptes file has the argus4R.m file nested within  
it, this allows the series of ODES to be solved while indexing the appropriate values  
based on the actual data points provided.
```

```
lm_plots(tobs,yobs,y_hat,sigma_y,cvg_hst) %The Levenberg-Marquardt file cited below  
the code
```

```
mp = b_fit %The regressed peroxisome mass transfer coefficient is asked to be printed  
for the user
```

```
sigma_mp = sigma_b %The error within the regressed peroxisome mass transfer  
coefficient is printed for the user
```

```
end
```

Levenberg-Marquardt method of regression was used and is nested in this argus4R.m file,
which reads lm.m and was provided by [69]. The curve fitting reads the file
panoptes4R.m

```
function y_hat= panoptes4R(tobs,b,c)
```

```
t0=0; tf=1300;
```

```
tobs=t0:1:tf
```

```
y0=[1 0]; %The initial conditions for outside the peroxisome and inside the peroxisome
```

```
[tobs,y]=ode15s(@argus4R,tobs,y0,[],b); %argus4R contains cell-specific parameters &  
ODE system. The ode solver chosen is ODE15s (for a stiff system)
```

```
y_tmp=y(:,1)
```

disc_values =[1201 1081 961 841 721 601 481 121 1]; %Depending on data set time points used within the experiment, these may be changed. This allows for fitting the data to the projected trajectory curve produces from the system of ODEs presented in the argus4R.m file.

```
y_hat=y_tmp(disc_values)
```

```
end
```

```
function cdot=argus4R(t,y,b)
```

```
Vext=6*10^-6; %6 mL cuvette is the reaction chamber so here it is represented in m^3
```

```
np=6.12*10^8; %(perox/cell)*(ncell) example for U-87. Each case will have the appropriate np in the chamber
```

```
Vp=5.8*10^-20; %Cell-specific peroxisome volume
```

```
Ap=8.1*10^-13; %Cell-specific peroxisome area
```

```
kp=7.22*10^2; %Cell-specific catalase activity per peroxisome. kp = (Ccatp)* k2. Where k2 is the constant determined by Britton Chance, which we denote ask2 = 1.7 x 107 s-1 M-1
```

```
%% cdot below is a system of two ordinary differential equations describing the change in H2O2 1) Outside the peroxisomes in the chamber, 2) Inside one peroxisome
```

```
%Note: b(1) is the parameter being regressed upon and represents mp (the mass transfer coefficient of peroxisome membrane)
```

```
cdot=[(-(b(1)*Ap*np)/Vext)*(y(1)-y(2));((b(1)*Ap)/Vp)*(y(1)-y(2))-((kp)*y(2))];
```

```
end
```

Results for pancreatic peroxisome membrane mass transfer coefficient (m_p)

File name	n_p	Regress m_p ($m s^{-1}$) a	Regress m_p ($m s^{-1}$) b
H6c7_peroxintact_160808_2b	$(2.99 \pm 0.03) \times 10^8$	$(4.05 \pm 0.99) \times 10^{-6}$	$(4.20 \pm 1.05) \times 10^{-6}$
H6c7_peroxintact_160831_2b	$(7.61 \pm 0.08) \times 10^8$	$(5.16 \pm 0.16) \times 10^{-6}$	$(5.86 \pm 0.59) \times 10^{-6}$
H6c7_peroxintact_160915_2b	$(1.86 \pm 0.01) \times 10^9$	$(1.43 \pm 0.23) \times 10^{-6}$	$(2.15 \pm 0.36) \times 10^{-6}$
Average		$(3.81 \pm 1.71) \times 10^{-5}$	

File name	n_p	Regress m_p ($m s^{-1}$) a	Regress m_p ($m s^{-1}$) b
MIA_peroxintact_160726	$(6.08 \pm 0.09) \times 10^8$	$(2.39 \pm 0.37) \times 10^{-5}$	$(2.56 \pm 1.05) \times 10^{-5}$
MIA_peroxintact_160808_2b	$(2.13 \pm 0.45) \times 10^9$	$(5.29 \pm 0.35) \times 10^{-6}$	$(6.07 \pm 0.30) \times 10^{-6}$
MIA_peroxintact_160802_2b	$(1.36 \pm 0.08) \times 10^9$	$(2.95 \pm 0.16) \times 10^{-5}$	$(1.48 \pm 0.17) \times 10^{-5}$
MIA_peroxintact_160831_2b	$(5.91 \pm 0.03) \times 10^8$	$(2.43 \pm 0.22) \times 10^{-5}$	$(4.12 \pm 1.99) \times 10^{-5}$
Average		$(2.13 \pm 1.21) \times 10^{-5}$	

Results for glioblastoma peroxisome membrane mass transfer coefficient (m_p)

File name	n_p	Regress m_p ($m s^{-1}$) a	Regress m_p ($m s^{-1}$) b
U-87_perox_case1_170504	$(1.56 \pm 0.30) \times 10^8$	$(3.12 \pm 0.04) \times 10^{-5}$	$(2.42 \pm 0.06) \times 10^{-5}$
U-87_perox_case2_170504	$(2.72 \pm 0.43) \times 10^8$	$(1.55 \pm 0.38) \times 10^{-5}$	$(1.23 \pm 0.02) \times 10^{-5}$
U-87_perox_case3_170504	$(2.90 \pm 0.16) \times 10^8$	$(9.88 \pm 0.44) \times 10^{-6}$	$(1.01 \pm 0.07) \times 10^{-5}$
U-87_perox_case4_170504	$(5.32 \pm 0.65) \times 10^8$	$(1.03 \pm 0.05) \times 10^{-5}$	$(1.09 \pm 0.13) \times 10^{-5}$
Average		$(1.55 \pm 0.79) \times 10^{-5}$	

File name	n_p	Regress m_p ($m s^{-1}$) a	Regress m_p ($m s^{-1}$) b
T98G_perox_case1_170504	$(1.23 \pm 0.21) \times 10^8$	$(3.39 \pm 0.15) \times 10^{-5}$	$(3.44 \pm 0.09) \times 10^{-5}$
T98G_perox_case2_170504	$(3.91 \pm 0.54) \times 10^8$	$(0.94 \pm 0.01) \times 10^{-5}$	$(0.72 \pm 0.69) \times 10^{-5}$
T98G_perox_case3_170504	$(1.88 \pm 0.23) \times 10^8$	$(1.28 \pm 0.12) \times 10^{-5}$	$(1.44 \pm 0.04) \times 10^{-5}$
Average		$(1.87 \pm 1.22) \times 10^{-5}$	

File name	n_p	Regress m_p ($m s^{-1}$) a	Regress m_p ($m s^{-1}$) b
LN_perox_case1_170504	$(5.94 \pm 1.21) \times 10^8$	$(2.84 \pm 0.05) \times 10^{-5}$	$(3.18 \pm 0.07) \times 10^{-5}$
LN_perox_case2_170504	$(7.28 \pm 0.50) \times 10^8$	$(1.77 \pm 0.05) \times 10^{-5}$	$(1.49 \pm 0.03) \times 10^{-5}$
LN_perox_case3_170504	$(6.12 \pm 0.66) \times 10^8$	$(1.05 \pm 0.06) \times 10^{-5}$	$(1.33 \pm 0.08) \times 10^{-5}$
Average		$(1.94 \pm 0.87) \times 10^{-5}$	

APPENDIX III: CODE FOR REGRESSION OF PLASMA

MEMBRANE PERMEABILITY (m_{plm})

Codes for regression for plasma membrane permeability

```
function cdot=argus24R(t,y,b)
```

```
Vext=3*10^-6; %(clonogenic external volume in m3). 1*10^-7 m3 for 96 well plate
```

```
n=200000; %example number of cells in the well during experiment
```

```
Vin=1.4*10^-15; % Volume of cell not occupied by the nucleus
```

```
Acell=0.97*10^-9; %Area of the cell obtained from MoxiZ
```

```
np=374; % Average # of peroxisomes per cell obtained from GFP images
```

```
Vp=1.87*10^-19; % Volume of a peroxisome obtained using ImageJ from GFP Images
```

```
Ap=1.49*10^-12; %Area of a peroxisome obtained using ImageJ from GFP Images
```

```
kp=161; % Is the first order reaction rate that is based off the cell-specific catalase
```

```
activity per peroxisome. For example,  $kp = C_{cat\_p} * k_2$ . Where  $k_2$  is the constant
```

```
determined by Britton Chance, which we denote  $ask = 1.7 \times 10^7 \text{ s}^{-1} \text{ M}^{-1}$ 
```

```
mp=0.38*10^-5; % Mass Transfer Coefficient for the peroxisome membrane. Regressed
```

```
for using the known catalase concentration per cell obtained from catalase free in solution
```

```
studies. And the code above containing the 2-ODE system of equations
```

```
%% Here, we now have a system of three ordinary differential equations describing the
```

```
change in  $\text{H}_2\text{O}_2$  1) Outside the cells in the chamber, 2) Inside one cell, and 3) Inside one
```

```
peroxisome
```

%Note: b(1) is the parameter being regressed upon and represents m_{plm} (the mass transfer coefficient of plasma membrane)

```
cdot=[(-(b(1)*Acell*n)/Vext)*(y(1)-y(2));((Acell*b(1))/Vin)*(y(1)-y(2))-  
((mp*Ap*np)/(Vin))*(y(2)-y(3));((mp*Ap)/Vp)*(y(2)-y(3))-(kp)*y(3)];  
  
end
```

```
function nonlinfit_of_argus24R  
clear; clc
```

```
data = xlsread('U-87_case5_170603.xlsx'); %Reads in data file
```

```
tobs = data(:,1); %Reads the time points for the data, which are all the values in column 1
```

```
yobs = data(:,4); %Reads the data points, which are all the values in column 4
```

```
b0=5*10^-6; %The initial guess for the plasma membrane permeability (again want a  
guess that is as close to the solution as possible to increase the probability of converging  
to a solution.
```

```
[b_fit,X2,sigma_b,sigma_y,corr,R_sq,cvg_hst]=lm(@panoptes24R,b0,tobs,yobs,1,10^-  
15) %Uses Levenberg-Marquardt regression (lm.m) file that again solves the system of  
ODEs to fit the data to the first curve. The first curve represents the external H2O2  
concentration over time and is the projected trajectory based on the cell-specific  
parameters entered within the argus24R.m file. The data from the H2O2 uptake study are  
time points that should follow this general trend. Thus, fitting the data to the first curve  
will allow for the regression of the plasma membrane mass transfer coefficient.
```

```
y_hat = panoptes24R(tobs,b_fit)
```

```
lm_plots(tobs,yobs,y_hat,sigma_y,cvg_hst)
```

```
mplm = b_fit %The regressed plasma membrane permeability value is asked to be printed
```

```
sigma_mplm = sigma_b %The error in  $m_{plm}$  is asked to be printed
```

```
end
```

```
function y_hat= panoptes24R(tobs,b,c)
```

```
t0=0;tf=2500;
```

```
tobs=t0:1:tf
```

```
y0=[1 0 0];%Initial concentration for outside the cells, inside the cell and inside the  
peroxisome respectively
```

```
[tobs,y]=ode15s(@argus24R,tobs,y0,[],b);%Uses ODE15s solver to read argus24R.m file
```

```
y_tmp=y(:,1)
```

```
disc_values =[2401 2101 1801 1501 1201 901 601 301 121 1]; %Depending on data set  
time points used within the experiment, these may be changed. This allows for fitting the  
data to the projected trajectory curve produces from the system of ODEs presented in the  
argus24R.m file.
```

```
y_hat=y_tmp(disc_values)
```

```
end
```

**Note: This same code is used for determining \bar{C}_{ext} where the variables above are adjusted to match the clonogenic assay set-up and cell-specific parameters for the cell under investigation*

Results for pancreatic plasma membrane mass transfer coefficient (m_{plm})

File name	n_{cells}	Regress m_{plm} ($m s^{-1}$) a	Regress m_{plm} ($m s^{-1}$) b
MIA_case4_052217	28290 \pm 2551	(5.65 \pm 1.32) $\times 10^{-6}$	(8.87 \pm 4.48) $\times 10^{-6}$
MIA_case1_052217_a b	25193 \pm 3232	(1.13 \pm 0.39) $\times 10^{-5}$	(6.08 \pm 0.97) $\times 10^{-6}$
MIA_case6_052217_a b	40570 \pm 5000	(3.49 \pm 1.11) $\times 10^{-6}$	(6.87 \pm 4.59) $\times 10^{-6}$
MIA_case9_052217_a b	39850 \pm 3495	(8.74 \pm 1.79) $\times 10^{-6}$	(6.12 \pm 1.75) $\times 10^{-6}$
Average		(7.14 \pm 2.72) $\times 10^{-6}$	

File name	n_{cells}	Regress m_{plm} ($m s^{-1}$) a	Regress m_{plm} ($m s^{-1}$) b
MIA_si_n_4_161112_3_c2 c3	74150 \pm 7139	(4.41 \pm 0.35) $\times 10^{-7}$	(7.45 \pm 0.64) $\times 10^{-7}$
MIA_si_n_4_161112_3_c5	61240 \pm 8703	(5.99 \pm 1.35) $\times 10^{-6}$	(2.26 \pm 0.43) $\times 10^{-6}$
MIA_si_n_4_161112_3_c6 c7	60690 \pm 5104	(2.77 \pm 0.32) $\times 10^{-6}$	(2.27 \pm 0.37) $\times 10^{-6}$
MIA_si_n_4_161112_3_c8 c9	126029 \pm 41974	(2.11 \pm 0.25) $\times 10^{-6}$	(1.26 \pm 0.21) $\times 10^{-6}$
Average		(2.23 \pm 1.72) $\times 10^{-6}$	

File name	n_{cells}	Regress m_{plm} ($m s^{-1}$) a	Regress m_{plm} ($m s^{-1}$) b	Regress m_{plm} ($m s^{-1}$) c
H6c7_case1_170411_2	39708	(2.78 \pm 0.22) $\times 10^{-6}$	(1.98 \pm 0.13) $\times 10^{-6}$	(1.82 \pm 0.14) $\times 10^{-6}$
H6c7_case2_170411_2	32125	(2.30 \pm 0.32) $\times 10^{-6}$	(2.42 \pm 0.33) $\times 10^{-6}$	(1.76 \pm 0.16) $\times 10^{-6}$
H6c7_case3_170411_2	17600	NA	(3.95 \pm 0.66) $\times 10^{-6}$	(3.45 \pm 0.62) $\times 10^{-6}$
Average		(2.56 \pm 0.79) $\times 10^{-6}$		

Results for glioblastoma plasma membrane mass transfer coefficient (m_{plm})

File name	n_{cells}	Regress m_{plm} ($m s^{-1}$) a	Regress m_{plm} ($m s^{-1}$) b
U-87_case3_170508	$35,264 \pm 6296$	$(1.09 \pm 0.29) \times 10^{-6}$	$(2.83 \pm 0.45) \times 10^{-6}$
U-87_case4_170508	$36,568 \pm 5113$	$(2.67 \pm 0.39) \times 10^{-6}$	$(3.49 \pm 0.24) \times 10^{-6}$
U-87_case5_170603	$32,356 \pm 2427$	$(2.57 \pm 0.30) \times 10^{-6}$	$(2.49 \pm 0.29) \times 10^{-6}$
Average		$(2.52 \pm 0.79) \times 10^{-6}$	

File name	n_{cells}	Regress m_{plm} ($m s^{-1}$) a	Regress m_{plm} ($m s^{-1}$) b
T98G_case2_170508	$20,024 \pm 1,915$	$(8.12 \pm 0.71) \times 10^{-6}$	$(6.57 \pm 1.72) \times 10^{-6}$
T98G_case3_170508	$23,376 \pm 2,295$	$(5.20 \pm 1.12) \times 10^{-6}$	$(6.00 \pm 0.43) \times 10^{-6}$
T98G_case4_170508	$21,712 \pm 3,180$	$(4.14 \pm 0.32) \times 10^{-6}$	$(4.17 \pm 0.23) \times 10^{-6}$
Average		$(5.70 \pm 1.53) \times 10^{-6}$	

File name	n_{cells}	Regress m_{plm} ($m s^{-1}$) a	Regress m_{plm} ($m s^{-1}$) b
LN_case1_170508	$39,848 \pm 4,187$	$(2.31 \pm 0.09) \times 10^{-6}$	$(1.87 \pm 0.18) \times 10^{-6}$
LN_case2_170508	$27,244 \pm 3,352$	$(3.36 \pm 0.13) \times 10^{-6}$	$(2.69 \pm 0.13) \times 10^{-6}$
LN_case3_170508	$39,067 \pm 3,031$	$(3.83 \pm 0.11) \times 10^{-6}$	$(3.33 \pm 0.17) \times 10^{-6}$
LN_case4_170508	$37,552 \pm 10,496$	$(3.53 \pm 0.13) \times 10^{-6}$	$(3.32 \pm 0.13) \times 10^{-6}$
Average		$(3.03 \pm 0.67) \times 10^{-6}$	

APPENDIX IV: EXAMPLE CALCULATION FOR \bar{C}_{ext}

Overview

When t_f is much less than t_x , the external concentration in the sample volume can reduce with time. For a matter of dosing, the timed-average external concentration, \bar{C}_{ext} , can be used to represent the dosing concentration during the study. This value can be determined by solving for $C_{ext}(t)$ using Eqn (4 – 6) and numerically determining

$$\bar{C}_{ext} = \frac{1}{t_f} \int_0^{t_f} C_{ext}(t) dt.$$

Code for generating external H₂O₂ during clonogenic study

This file is titled runargus24R2.m

```
close all; clear all; clc
```

```
y0=[1 0 0]; %Initial values for extracellular environment, inside one cell and inside one peroxisome  
a=0:100:3600; %time span from 0 to 3600 s to see Cext over the hour during the clonogenic study  
b0=[3.03*10^-6];% Initial guess for the mass transfer coefficient being regressed for  
[a,y]=ode15s(@argus24R,a,y0,[],b0); %solves the system of ODE in argus24R which now has the adjusted parameters representing the clonogenic assay study and specific cells used  
disp(num2str([a y])) %displays the numbers so can use to calculate the average external concentration from the time points
```

```
plot(a,y, '--');  
hold on
```

```
a=title({'MIA PaCa-2 Unmodified', 'H2O2 Concentration vs. Time for Each Compartment'});  
l=legend('H2O2 Concentration Outside of Cell','H2O2 Concentration Inside Cell','H2O2 Concentration Inside Peroxisome')  
xl=xlabel('Time (s)'); yl=ylabel('H2O2 Concentration (M)');  
hold on
```

Example results

The following data for $C_{ext}(t)$ for each cell type and experimental case is provided:

MIA PaCa-2			
Time (s)	<i>Normalized C_{ext}</i>	<i>Normalized C_{in}</i>	<i>Normalized C_p</i>
0	1.0000	0.0000	0.0000
100	0.9890	0.7250	0.4528
200	0.9783	0.7172	0.4479
300	0.9678	0.7095	0.4431
400	0.9573	0.7018	0.4382
500	0.9467	0.6941	0.4334
600	0.9366	0.6866	0.4288
700	0.9265	0.6792	0.4241
800	0.9163	0.6718	0.4195
900	0.9064	0.6645	0.4149
1000	0.8966	0.6573	0.4105
1100	0.8869	0.6502	0.4060
1200	0.8771	0.6430	0.4015
1300	0.8675	0.6360	0.3971
1400	0.8580	0.6290	0.3928
1500	0.8486	0.6222	0.3885
1600	0.8393	0.6153	0.3842
1700	0.8301	0.6086	0.3800
1800	0.8210	0.6019	0.3759
1900	0.8120	0.5953	0.3717
2000	0.8031	0.5887	0.3676
2100	0.7942	0.5823	0.3636
2200	0.7855	0.5759	0.3596
2300	0.7769	0.5695	0.3557
2400	0.7683	0.5633	0.3517
2500	0.7599	0.5571	0.3479
2600	0.7515	0.5510	0.3440
2700	0.7433	0.5449	0.3403
2800	0.7351	0.5389	0.3365
2900	0.7270	0.5330	0.3328
3000	0.7190	0.5271	0.3292
3100	0.7111	0.5213	0.3255
3200	0.7033	0.5156	0.3220
3300	0.6956	0.5099	0.3184
3400	0.6879	0.5043	0.3149
3500	0.6804	0.4988	0.3115
3600	0.6729	0.4933	0.3080

Using this transient data provided by the argus24R.m and the runargus24R2.m files, after adjusting appropriately with the parameters representing the clonogenic studies, MATLAB produces the chart printed above. Presented is the normalized concentration values inside each compartment (outside the cell, inside one cell, and inside one peroxisome) at each designated time point. The time points have been conveniently incremented to increase in time steps of 100 s for a total time of 3600 s which is the exposure time (1 h).

Integrating under the curve we are able to get the average external concentration over the 1h exposure. Presented here are the external concentration at each time point, which are further multiplied by the step size (100 s), summed and divided by the total time (3600 s). Since each cell has specific parameters, the change in external H_2O_2 over the hour will be specific to each case. Again, depending on the cell density used for that case, the cell area, permeability characteristics, catalase characteristics etc.

MIA PaCa-2

Time (s)	Normalized C_{ext}	$\Delta t * C_{ext}$
0	1.0000	100
100	0.9890	98.90
200	0.9783	97.83
300	0.9678	96.78
400	0.9573	95.73
500	0.9467	94.67
600	0.9366	93.66
700	0.9265	92.65
800	0.9163	91.63
900	0.9064	90.64
1000	0.8966	89.66
1100	0.8869	88.69
1200	0.8771	87.71
1300	0.8675	86.75
1400	0.8580	85.80
1500	0.8486	84.86
1600	0.8393	83.93
1700	0.8301	83.01
1800	0.8210	82.10
1900	0.8120	81.20
2000	0.8031	80.31
2100	0.7942	79.42
2200	0.7855	78.55
2300	0.7769	77.69
2400	0.7683	76.83
2500	0.7599	75.99
2600	0.7515	75.15
2700	0.7433	74.33
2800	0.7351	73.51
2900	0.7270	72.70
3000	0.7190	71.90
3100	0.7111	71.11
3200	0.7033	70.33
3300	0.6956	69.56
3400	0.6879	68.79
3500	0.6804	68.04
3600	0.6729	67.29
		3057.70

$$C_{ext} = \mathbf{0.85}$$

APPENDIX V: PEROXIPORIN EXPRESSION

Quick preliminary look at the peroxiporin expression, indicates that the proteins vary across cell lines specifically relating back to the pancreatic cells, Fig 2.1. Flow cytometric analysis was used to verify peroxiporin AQP3 and AQP8 expression on the plasma membrane of glioblastoma cells. Interestingly, AQP3 has elevated expression on all three glioblastomas compared to pancreatic cancer cells, where the glioblastomas expression are on the order of 10^4 compared to the pancreatic cancer cells which were on the order of 10^2 . Despite the differences in peroxiporin expression, we see the plasma membrane permeability were high only for MIA PaCa-2 and U-87 cells. Thus the role of peroxiporins expression remains inconclusive.

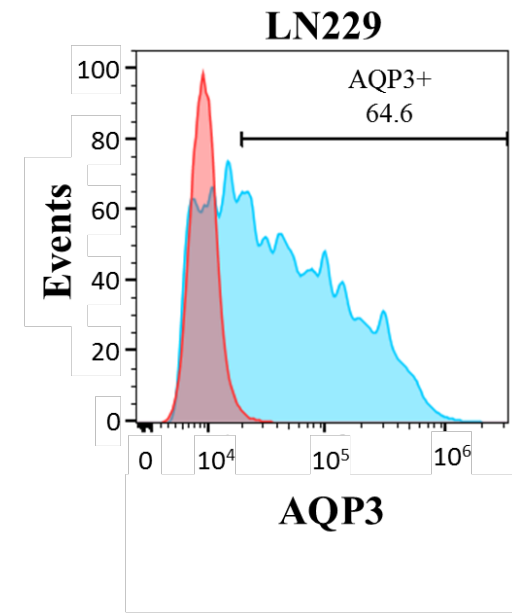
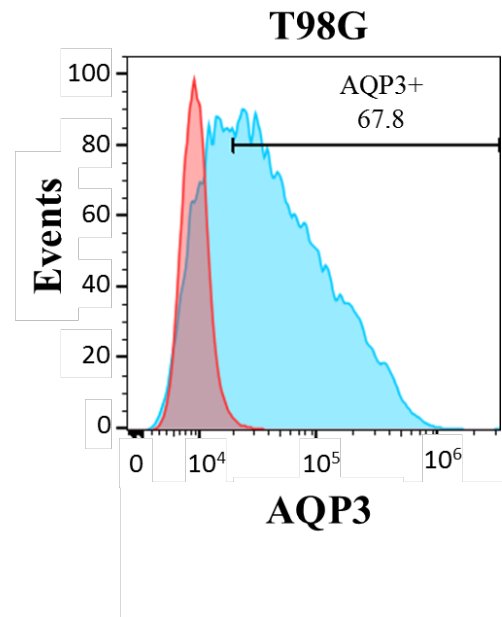
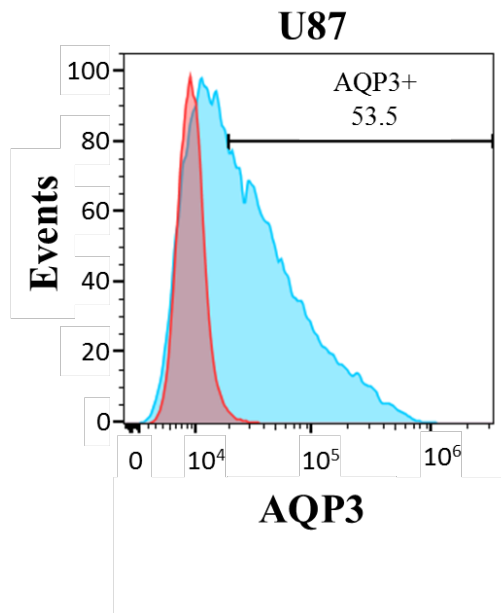


Fig Appendix V.1 Flow cytometry for glioblastoma peroxiporin AQP3. A positive AQP3 signal frequency (blue) of 53.5 for the U-87 cancer cells sampled (23,807 cells), 67.8 for the T98G cancer cells sampled (23,975 cells) and 64.6 for the LN-229 cancer cells sampled (2,449 cells). It is noted there was a low number of cells sampled for the LN-229 case, and thus may not be entirely accurate. The shift in fluorescence between T98G and U-87 cells demonstrates an increase in AQP3 expression for T98G cells by a factor of 3, when comparing the average displayed by the peaks of each curve. This is quite a small shift when comparing to the previous pancreatic cancer data, which displayed a factor of 10 difference in AQP3 for silenced vs. unmodified MIA PaCa-2 cells. Further, the factor of 10 difference in expression resulted in only a small improvement in cell surviving fraction. It may suggest then, that a small factor difference of 3 would have little effect on the surviving fraction. This speculation could only be determined with either silencing or overexpressing the protein on the same cell type and further examining the effects. Unfortunately, we do not have this control and only are able to conclude the silencing of the MIA PaCa-2 cells.

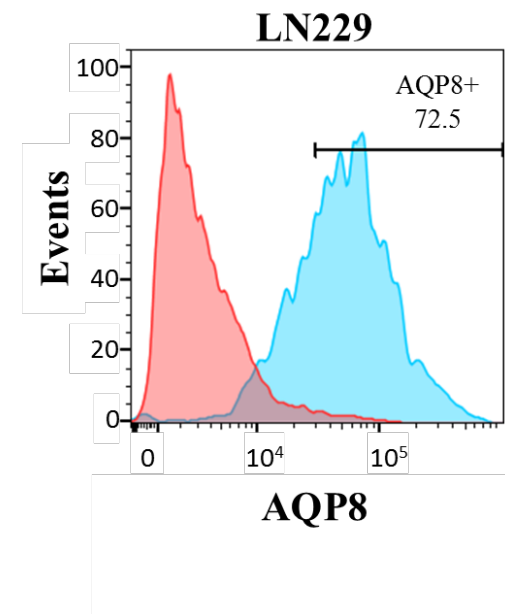
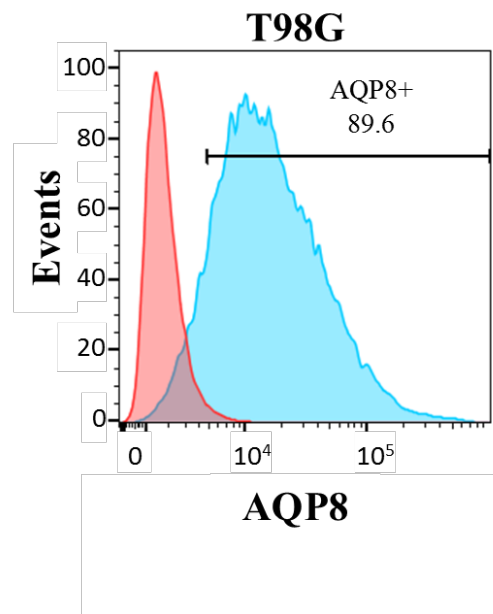
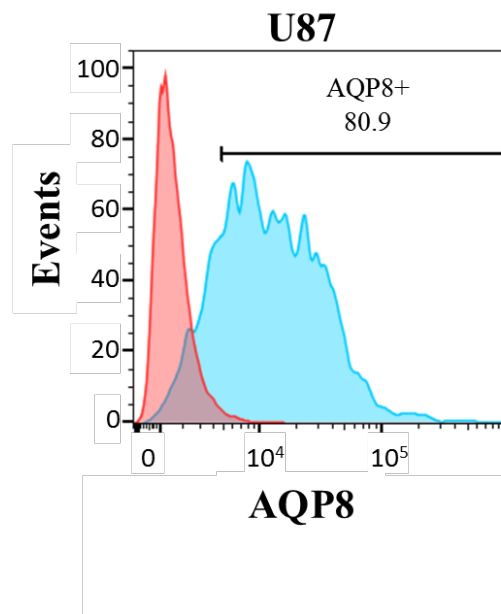


Fig Appendix V.2 Flow cytometry for peroxiporin AQP8 expression on glioblastoma cells. A positive AQP8 signal frequency (blue) of 80.9 for the U-87 cancer cells sampled (2,728 cells), 89.6 for the T98G cancer cells sampled (28,826 cells) and 72.5 for the LN-229 cancer cells sampled (1,895 cells). It is noted there was a low number of cells sampled for the U-87 and LN-229 cases, and thus may not be entirely accurate. All AQP8 expression signals were on the order of 10^4 . Interestingly, the LN-229 cells appear to have the highest AQP8 expression about a factor of 3.5 greater than the T98G. The LN-229 are also more susceptible to therapeutic H_2O_2 , thus it may be a further direction to be researched the role of peroxiporins.

REFERENCES

- ¹ Du J, Martin SM, Levine M, Wagner BA, Buettner GR, Wang SH, *et al.* Mechanisms of ascorbate-induced cytotoxicity in pancreatic cancer. *Clin Cancer Res.* 2010;16(2): 509-520.
- ² Du J, Cieslak JA, Welsh JL, Sibenaller ZA, Allen BG, Wagner BA, *et al.* Pharmacological ascorbate radiosensitizes pancreatic cancer. *Cancer Res.* 2015;75(16): 3314-3326.
- ³ Welsh JL, Wagner BA, Van't Erve TJ, Zehr PS, Berg DJ, Halfdanarson TR, *et al.* Pharmacological ascorbate with gemcitabine for the control of metastatic and node-positive pancreatic cancer (PACMAN): results from a phase I clinical trial. *Cancer Chemoth Pharm.* 2013;71(3): 765-775.
- ⁴ Cieslak JA, J Cullen JJ. Treatment of pancreatic cancer with pharmacological ascorbate. *Curr Pharm Biotechno.* 2015;16(9); 759-770.
- ⁵ National Cancer Institute; National Institutes of Health; University of Iowa. Pharmacological Ascorbate for Lung Cancer. In: *ClinicalTrials.gov* [Internet]. Bethesda (MD): National Library of Medicine (US). 2000 - [cited 2016 Jun 20]. Available from: <https://clinicaltrials.gov/ct2/show/NCT02420314>. NLM Identifier: NCT02420314
- ⁶ Joseph J. Cullen; University of Iowa. Gemcitabine, Ascorbate, Radiation Therapy for Pancreatic Cancer, Phase I. In: *ClinicalTrials.gov* [Internet]. Bethesda (MD): National Library of Medicine (US). 2000 - [cited 2016 Jun 20]. Available from: <https://clinicaltrials.gov/ct2/show/NCT01852890>. NLM Identifier: NCT01852890.
- ⁷ National Cancer Institute; National Institutes of Health; University of Iowa. A Phase I Trial of High-Dose Ascorbate in Glioblastoma Multiforme. In: *ClinicalTrials.gov* [Internet]. Bethesda (MD): National Library of Medicine (US). 2000 - [cited 2016 Jun 20]. Available from: <https://clinicaltrials.gov/ct2/show/NCT01752491>. NLM Identifier: NCT01752491.

-
- ⁸ Holden Comprehensive Cancer Center; University of Iowa. A Phase 2 Trial of High-Dose Ascorbate in Glioblastoma Multiforme. In: ClinicalTrials.gov [Internet]. Bethesda (MD): National Library of Medicine (US). 2000 - [cited 2016 Jun 20]. Available from: <https://clinicaltrials.gov/ct2/show/NCT02344355>. NLM Identifier: NCT02344355.
- ⁹ Ohno S, Ohno Y, Suzuki N, Soma G, Inoue M, "High-dose vitamin C (ascorbic acid) therapy in the treatment of patients with advanced cancer." *Anticancer res* **29**(3):809-815 (2009).
- ¹⁰ Creagan ET, Moertel CG, O'Fallon JR, Schutt AJ, O'Connell MJ, Rubin J, Frytak S, "Failure of high-dose vitamin C (ascorbic acid) therapy to benefit patients with advanced cancer: a controlled trial", *New Engl J Med* **301**(13):687-690 (1979).
- ¹¹ Moertel CG, Fleming TR, Creagan ET, Rubin J, O'Connell MJ, Ames MM, "High-dose vitamin C versus placebo in the treatment of patients with advanced cancer who have had no prior chemotherapy: a randomized double-blind comparison", *New Engl J Med* **312**(3):137-141 (1985).
- ¹² Chen Q, Espey MG, Sun AY, Pooput C, Kirk KL, Krishna MC, *et al.* Pharmacologic doses of ascorbate act as a prooxidant and decrease growth of aggressive tumor xenografts in mice. *Proc Natl Acad Sci USA*. 2008;105(32): 11105-11109.
- ¹³ Buettner GR, Jurkiewicz BA. Catalytic metals, ascorbate and free radicals: combinations to avoid. *Radiat Res*. 1996;145(5): 532-541.
- ¹⁴ Du J, Nelson ES, Simons AL, Olney KE, Moser JC, Schrock HE, *et al.* Regulation of pancreatic cancer growth by superoxide. *Mol Carcinogen*. 2013;52(7): 555-567.
- ¹⁵ Frei B, Lawson S. Vitamin C and cancer revisited. *Proc Natl Acad Sci USA*. 2008;105(32): 11037-11038.
- ¹⁶ Halliwell B. Vitamin C: poison, prophylactic or panacea? *Trends Biochem Sci*. 1999;24(7): 255-259.
- ¹⁷ Du J, Cullen JJ, Buettner GR. Ascorbic acid: chemistry, biology and the treatment of cancer. *BBA-Rev Cancer*. 2012;1826(2): 443-457.

-
- ¹⁸ Heaney ML, Gardner JR, Karasavvas N, Golde DW, Scheinberg DA, Smith EA, O'Connor OA, "Vitamin C antagonizes the cytotoxic effects of antineoplastic drugs", *Cancer Res* **68**(19):8031-8038 (2008).
- ¹⁹ Chen Q, Espey MG, Sun AY, Lee JH, Krishna MC, Shacter E, *et al.* Ascorbate in pharmacologic concentrations selectively generates ascorbate radical and hydrogen peroxide in extracellular fluid in vivo. *Proc Natl Acad Sci USA*. 2007;104(21): 8749-8754.
- ²⁰ Buettner GR. In the absence of catalytic metals ascorbate does not autoxidize at pH 7: ascorbate as a test for catalytic metals. *J Biochem Biophys Meth*. 1988;16(1): 27–40.
- ²¹ Doskey CM, Buranasudja V, Wagner BA, Wilkes JG, Du J, Cullen JJ, *et al.* Tumor cells have decreased ability to metabolize H₂O₂: Implications for pharmacological ascorbate in cancer therapy. *Redox Biology*. 2016;10: 274–284. pmid:27833040
- ²² Chen P, Yu J, Chalmers B, Drisko J, Yang J, Li B, *et al.* Pharmacological ascorbate induces cytotoxicity in prostate cancer cells through ATP depletion and induction of autophagy. *Anticancer Drugs*. 2012;23(4): 437–444. pmid:22205155
- ²³ Chen Q, Espey MG, Krishna MC, Mitchell JB, Corpe CP, Buettner GR, *et al.* Pharmacologic ascorbic acid concentrations selectively kill cancer cells: action as a pro-drug to deliver hydrogen peroxide to tissues. *Proc Natl Acad Sci USA*. 2005;102(32): 13604–13609.
- ²⁴ Rawal M, Schroeder SR, Wagner BA, Cushing CM, Welsh J, Button AM, *et al.* Manganoporphyrins increase ascorbate-induced cytotoxicity by enhancing H₂O₂ generation. *Cancer Res*. 2013;73(16): 5232–5241. pmid:23764544
- ²⁵ Sestili P, Brandi G, Brambilla L, Cattabeni F, Cantoni O. Hydrogen peroxide mediates the killing of U937 tumor cells elicited by pharmacologically attainable concentrations of ascorbic acid: cell death prevention by extracellular catalase or catalase from cocultured erythrocytes or fibroblasts. *J Pharm Exp Ther*. 1996;277(3): 1719–1725.
- ²⁶ Tian J, Peehl DM, Knox SJ. Metalloporphyrin synergizes with ascorbic acid to inhibit cancer cell growth through fenton chemistry. *Cancer Biother Radiopharm*. 2010;25(4): 439–448. pmid:20735206
- ²⁷ Espey MG, Chen P, Chalmers B, Drisko J, Sun AY, Levine M, *et al.* Pharmacologic ascorbate synergizes with gemcitabine in preclinical models of pancreatic cancer. *Free Radic Biol Med*. 2011;50(11): 1610–1619. pmid:21402145

-
- ²⁸ Ranzato E, Biffo S, Burlando B. Selective ascorbate toxicity in malignant *mesothelioma*: a redox Trojan mechanism. *Am J Respir Cell Mol Biol*. 2011;44(1): 108–117. pmid:20203294
- ²⁹ Klingelhoefter C, Kämmerer U, Koospal M, Mühlhng B, Schneider M, Kapp M, et al. Natural resistance to ascorbic acid induced oxidative stress is mainly mediated by catalase activity in human cancer cells and catalase-silencing sensitizes to oxidative stress. *BMC Complement Alter Med*. 2012;12(1): 61.
- ³⁰ Shatzer AN, Espey MG, Chavez M, Tu H, Levine M, Cohen JI. Ascorbic acid kills Epstein-Barr virus positive Burkitt lymphoma cells and Epstein-Barr virus transformed B-cells in vitro, but not in vivo. *Leuk Lymphoma*. 2013;54(5): 1069–1078. pmid:23067008
- ³¹ Ma Y, Chapman J, Levine M, Polireddy K, Drisko J, Chen Q. High-dose parenteral ascorbate enhanced chemosensitivity of ovarian cancer and reduced toxicity of chemotherapy. *Sci Transl Med*. 2014;6(222): 222ra18. pmid:24500406
- ³² Cieslak JA, Strother RK, Rawal M, Du J, Doskey CM, Schroeder SR, et al. Manganoporphyrins and ascorbate enhance gemcitabine cytotoxicity in pancreatic cancer. *Free Radic Biol Med*. 2015;83: 227–237. pmid:25725418
- ³³ Almasalmeh A, Krenc D, Wu B, Beitz E. Structural determinants of the hydrogen peroxide permeability of aquaporins. *FEBS J*. 2014;281(3): 647–656. pmid:24286224
- ³⁴ Sies H. Role of Metabolic H₂O₂ Generation: REDOX SIGNALING AND OXIDATIVE STRESS. *J Biol Chem*. 2014;289(13): 8735–8741. pmid:24515117
- ³⁵ Wu B, Beitz E. Aquaporins with selectivity for unconventional permeants. *Cell Mol Life Sci*. 2007;64(18): 2413–2421. pmid:17571212
- ³⁶ Uhlen M, Oksvold P, Fagerberg L, Lundberg E, Jonasson K, Forsberg M, et al. Towards a knowledge-based human protein atlas. *Nat Biotechnol*. 2010; 28(12): 1248–1250. pmid:21139605
- ³⁷ Verkman AS, Hara-Chikuma M, Papadopoulos MC. Aquaporins—new players in cancer biology. *J Mol Med*. 2008;86(5): 523–529. pmid:18311471
- ³⁸ Ng CF, Schafer FQ, Buettner GR, Rodgers VGJ (2007) The rate of cellular hydrogen peroxide removal shows dependency on GSH: mathematical insight into in vivo H₂O₂ and GPx concentrations. *Free Radic Res* 41(11):1201-1211.

-
- ³⁹ Sasaki K, Bannai S, Makino N. Kinetics of hydrogen peroxide elimination by human umbilical vein endothelial cells in culture. *BBA-Genl Subjects*. 1998;1380(2): 275-288.
- ⁴⁰ Low FM, Hampton MB, Peskin AV, Winterbourn CC. Peroxiredoxin 2 functions as a noncatalytic scavenger of low-level hydrogen peroxide in the erythrocyte. *Blood*. 2007;109(6): 2611-2617.
- ⁴¹ Benade L, Howard T, Burk D. Synergistic killing of Ehrlich ascites carcinoma cells by ascorbate and 3-amino-1, 2, 4,-triazole. *Oncology*. 1969;23(1): 33-43.
- ⁴² Olney KE, Du J, van't Erve TJ, Witmer JR, Sibenaller ZA, Wagner BA, et al. Inhibitors of hydroperoxide metabolism enhance ascorbate-induced cytotoxicity. *Free Radical Res*. 2013; 47(3): 154–163.
- ⁴³ Du, J., Doskey, C.M., Wilkes, J.G., Buettner, G.R. and Cullen, J.J., 2016. 271-Catalase as a Potential Biomarker of Pharmacological Ascorbate Cancer Therapy. *Free Radical Biology and Medicine*, 100, p.S121.
- ⁴⁴ Herst PM, Broadley KW, Harper JL, McConnell MJ. Pharmacological concentrations of ascorbate radiosensitize glioblastoma multiforme primary cells by increasing oxidative DNA damage and inhibiting G2/M arrest. *Free Radic Biol Med*. 2012;52(8): 1486–1493.
- ⁴⁵ Castro ML, McConnell MJ, Herst PM. Radiosensitisation by pharmacological ascorbate in glioblastoma multiforme cells, human glial cells, and HUVECs depends on their antioxidant and DNA repair capabilities and is not cancer specific. *Free Radic Biol Med*. 2014;74: 200–209.
- ⁴⁶ Du J, Wagner BA, Buettner GR, Cullen JJ. Role of labile iron in the toxicity of pharmacological ascorbate. *Free Radical Bio Med*. 2015;84: 289-295.
- ⁴⁷ Chen Q, Espey MG, Sun AY, Lee JH, Krishna MC, Shacter E, *et al*. Ascorbate in pharmacologic concentrations selectively generates ascorbate radical and hydrogen peroxide in extracellular fluid in vivo. *Proc Natl Acad Sci USA*. 2007;104(21): 8749-8754.
- ⁴⁸ Herst PM, Broadley KW, Harper JL, McConnell MJ. Pharmacological concentrations of ascorbate radiosensitize glioblastoma multiforme primary cells by increasing

oxidative DNA damage and inhibiting G2/M arrest. *Free Radic Biol Med.* 2012;52(8): 1486–1493.

- ⁴⁹ Castro ML, McConnell MJ, Herst PM. Radiosensitisation by pharmacological ascorbate in glioblastoma multiforme cells, human glial cells, and HUVECs depends on their antioxidant and DNA repair capabilities and is not cancer specific. *Free Radic Biol Med.* 2014;74: 200–209.
- ⁵⁰ Ouyang H, Mou LJ, Luk C, Liu N, Karaskova J, Squire J, et al. Immortal human pancreatic duct epithelial cell lines with near normal genotype and phenotype. *Am J Pathol.* 2000;157(5): 1623–1631. pmid:11073822
- ⁵¹ Wagner BA, Witmer JR, van't Erve TJ, Buettner GR. An assay for the rate of removal of extracellular hydrogen peroxide by cells. *Redox Biol.* 2013;1(5): 210–217.
- ⁵² Doskey CM, van't Erve TJ, Wagner BA, Buettner GR. Moles of a Substance per Cell Is a Highly Informative Dosing Metric in Cell Culture. *PloS One.* 2015;10(7): e0132572. pmid:26172833
- ⁵³ Franken NAP, Rodermond HM, Stap J, Haveman J, Bree CV. Clonogenic assay of cells in vitro. *Nat Protoc.* 2006;1: 2315–2319. pmid:17406473
- ⁵⁴ Munshi A, Hobbs M, Meyn RE. Clonogenic cell survival assay. Chemosensitivity: Volume 1 *In Vitro Assays.* 2005: 21–28.
- ⁵⁵ Trigueros-Motos L, Pérez-Torras S, Casado FJ, Molina-Arcas M, Pastor-Anglada M. Aquaporin 3 (AQP3) participates in the cytotoxic response to nucleoside-derived drugs. *BMC cancer.* 2012;12(1): 434.
- ⁵⁶ Schoenfeld et al., O₂- and H₂O₂-Mediated Disruption of Fe Metabolism Causes the Differential Susceptibility of NSCLC and GBM Cancer Cells to Pharmacological Ascorbate, *Cancer Cell* (2017), <http://dx.doi.org/10.1016/j.ccell.2017.02.018>
- ⁵⁷ Haber F., Weiss J. (1932) Über die Katalyse des Hydroperoxydes (On the catalysis of hydroperoxide). *Naturwissenschaften.* **20** (51): 948–950.
- ⁵⁸ Erudaitius, D, Huang A, Kazmi S, Buettner GR, Rodgers VGJ (2017) Peroxiporin Expression Is an Important Factor for Cancer Cell Susceptibility to Therapeutic H₂O₂: Implications for Pharmacological Ascorbate Therapy, *PloS ONE* **12**(1): e0170442.

-
- ⁵⁹ Bienert GP, Schjoerring JK, Jahn TP. Membrane transport of hydrogen peroxide. *Biochimica et Biophysica Acta (BBA)-Biomembranes* 2006;1758(8):994-1003.
- ⁶⁰ Miller, Evan W, Dickinson BC, Chang CJ. Aquaporin-3 mediates hydrogen peroxide uptake to regulate downstream intracellular signaling. *Proceedings of the National Academy of Sciences* 2010;107(36):15681-15686.
- ⁶¹ Antunes F, Cadenas E (2000) Estimation of H₂O₂ gradients across biomembranes. *FEBS Lett* 475(2):121-126.
- ⁶² Makino N, Sasaki K, Hashida K, Sakakura Y (2004) A metabolic model describing the H₂O₂ elimination by mammalian cells including H₂O₂ permeation through cytoplasmic and peroxisomal membranes: comparison with experimental data, *Biochimica et Biophysica Acta*, 1673: 149-159.
- ⁶³ Lim JB, Huang BK, Deen WM, Sikes HD (2015) Analysis of the lifetime and spatial localization of hydrogen peroxide generated in the cytosol using a reduced kinetic model, *FRBM*, 89: 47-53.
- ⁶⁴ Chance B (1943) The kinetics of the enzyme-substrate compound of peroxidase, *J Biol Chem* **151**(2):553-577.
- ⁶⁵ Yue H, Brown M, Knowles J, Wang H, Broomhead DS, Kell DB (2006) Insights into the behaviour of systems biology models from dynamic sensitivity and identifiability analysis: a case study of an NF- κ B signalling pathway, *Molecular BioSystems* 2:640-649.
- ⁶⁶ van Stroe-Blezen SAM, Everaerts FM, Janssen LJJ, Tacken RA (1993) Diffusion coefficients of oxygen, hydrogen peroxide and glucose in a hydrogel. *Analytica Chimica Acta*, 273 553-560.
- ⁶⁷ Aebi H. (1984) Catalase in vitro. *Method Enzymol.* 105: 121-126.
- ⁶⁸ De Duve C, Baudhuin P, "Peroxisomes (Microbodies and Related Particles)", *Physiol Rev* **46**:323-357 (1966).
- ⁶⁹ Gavin, H., 2011. The Levenberg-Marquardt method for nonlinear least squares curve-fitting problems.